Dear Topical Editor and Reviewers:

On behalf of my co-authors, we thank you very much for reviewing our manuscript and giving us a lot of useful comments and suggestions. We appreciate the comments on our manuscript entitled "GWL_FCS30: global 30 m wetland map with fine classification system using multi-sourced and time-series remote sensing imagery in 2020" (essd-2022-180).

We have revised the manuscript carefully according to the comments. All the changes were high-lighted (red color) in the manuscript. And the point-by-point response to the comments of the reviewers is also listed below.

Looking forward to hearing from you soon.

Best regards,

Prof. Liangyun Liu

liuly@radi.ac.cn

Institute of Remote Sensing and Digital Earth, Chinese Academy of Sciences

No.9 Dengzhuang South Road, Haidian District, Beijing 100094, China

Response to comments

Paper #: essd-2022-180
Title: GWL_FCS30: global 30 m wetland map with fine classification system using multi-sourced and time-series remote sensing imagery in 2020
Journal: Earth System Science Data

Reviewer #1

In terms of the whole workload, there is no doubt that this paper carried out a lot of data processing and analysis. The submitted MS also has good writing. However, I still have some concerns about the method and accuracy of classification results. My major comments are as below.

Great thanks for the positive comments. The manuscript has been greatly improved based on your and two other reviewers' comments and suggestions.

1. Besides the mangrove, how did you consider other coastal swamp in the classification system?

Great thanks for the comment and this great question. I am sorry we do not consider the coastal swamp in the manuscript because: 1) Ramsar convention only defines the coastal wetlands into: unvegetated tidal flats, saltmarshes, coastal deltas, mangroves, seagrass beds and coral reefs, it can be found that the **coastal tree-related wetlands** only include mangrove forest and **no other coastal swamp**. 2) We currently defined coastal wetlands into mangrove, saltmarsh and tidal flat **because there is almost no global/regional coastal swamp products can be used**. And the coastal wetland system of three subcategories (mangrove, salt marsh and tidal flat) is also widely recognized in many previous studies (Murray et al. 2022, Zhang et al., 2022).

Murray, N. J., Worthington, T. A., Bunting, P., Duce, S., Hagger, V., Lovelock, C. E., ... & Lyons, M. B. (2022). High-resolution mapping of losses and gains of Earth's tidal wetlands. Science, 376(6594), 744-749.

Zhang, Z., Xu, N., Li, Y., & Li, Y. (2022). Sub-continental-scale mapping of tidal wetland composition for East Asia: A novel algorithm integrating satellite tide-level and phenological features. Remote Sensing of Environment, 269, 112799.

2. As mentioned, the wetlands have clear seasonal changes within a year?

Great thanks for the comment. After carefully checking our manuscript, the manuscript didn't state that **the wetland have clear seasonal changes**, instead, we emphasize that the spectra variability of wetlands is simultaneously affected by the **water-level and phenology changes**. Therefore, we use time-series Landsat and Sentinel-1 to generate the lowest and highest water-levels:

The spectral characteristics of the wetlands would quickly change along with the seasonal or daily water levels of the underlying surface. For example, the tidal flat was the status of seawater at the high tidal stage and mud or sand flats at low tidal stages (Wang et al., 2021); therefore, it was necessary to **extract the highest and lowest water-level composites to completely capture these inundated wetlands**. Over the past several years, the time-series compositing strategy has been widely used to capture phenological and cloud-free composites.

Derived the phenological features from time-series Landsat imagery as:

Many studies also demonstrated that a multi-temporal phenology was also essential for classifying the vegetated wetlands and excluding these non-wetland land-cover types (Li et al., 2020; Ludwig et al., 2019). There were usually two options for capturing phenological features from time-series Landsat imagery. These included seasonal-based compositing (Zhang et al., 2021a; Zhang et al., 2022a) and percentile-based compositing (Hansen et al., 2014; Zhang and Roy, 2017; Zhang et al., 2021b). The former used the phenological calendar for selecting time-matched imagery. It then adopted the compositing rule to capture the seasonal features, while the latter directly used the statistical distributions to select various percentiles. Azzari and Lobell (2017) quantitatively analyzed the performance of two compositing methods and found that both of them had similar mapping accuracy for land-cover mapping. Meanwhile, the seasonal-based compositing method needed the prior phenological calendar, while the percentile compositing method did not require any prior knowledge or explicit assumptions regarding the timing of the season; therefore, the percentile compositing method was more suitable to generate phenological features. This study composited time-series Landsat reflectance bands and four spectral indexes into five percentiles (15th, 30th, 50th, 70th and 85th). It should be noted that the minimum and maximum percentiles were excluded because they were usually affected by residual clouds, shadows, and saturated observations.

How did you define the final date for the wetland product?

Great thanks for the comment. The global wetland product is developed for the nominal year of 2020, because the time-series Landsat imagery and Sentinel-1 SAR observations, used in this study, are mainly around 2020. It has been explained in the manuscript as:

First, all available Landsat imagery, including Landsat 7 ETM+ and Landsat 8 OLI missions, **during 2019–2021 was obtained for the nominal year of 2020 via the Google Earth Engine platform** for minimizing the influence of frequent cloud contamination in the tropics and snow and ice in the high latitudes.

The description of Sentinel-1: All the **time-series Sentinel-1 imageries archived on the GEE platform in 2020** in Interferometric Wide Swath mode with a dual-polarization of VV and VH were used.

3. Besides the time-series feature? Did you consider other features

Thanks for the comment. In this study, we used the time-series Landsat imagery to generate the lowest and highest water-level composites and multiple phenological features, used the time-series Sentinel-1 imagery to generate the lowest and highest water-level features, and used the ASTER GDEM to derive elevation, slope and aspect. To intuitively understand all training features, the 77 multisourced training features were listed in a table as:

In summary, a total of 77 multisource training features (listed in Table 3), including 70 optical features from Landsat imagery, 4 SAR features from Sentinel-1 imagery and 3 topographical features from ASTER GDEM.

Table 3. The multisourced and multitemporal training features for wetland mapping.

Data	Derived training features from multisource remote sensing imagery
Landsat	**Water-level features**: the lowest and highest composites with Blue, Green, Red, NIR, SWIR1, SWIR2, LSWI, NDWI, NDVI and EVI bands **Phenological features:** 5th, 30th, 50th, 70th and 85th percentiles with Blue, Green, Red, NIR, SWIR1, SWIR2, LSWI, NDWI, NDVI and EVI bands
Sentinel-1 SAR	**Water-level features**: the lowest and highest composites using 5th and 95th percentiles for VV and VH bands.
ASTER GDEM	**Topographical features**: elevation, slope and aspect.

4. How did you training the model? One model for the global wetland or one model per grid? There are distinctly phenological differences for the different wetland types and even the same wetland type. Please clarify it.

Great thanks for the comment. We used 961 local adaptive classification models in 961 5° × 5° geographical tiles after considering the phenological differences for the different wetland types and even the same wetland type at spatial dimension. The local adaptive modeling has been strengthen as:

Since we have simultaneously extracted the maximum coastal and inland wetland extents when deriving training samples from prior wetland datasets, the stratified classification strategy was adopted to fully use the maximum extent constraint. If a pixel was classified as a coastal wetland outside the maximum coastal wetland extents, it would be identified as a misclassification. Furthermore, there were two ideas for the large-area land-cover mapping including global classification modeling (using one universal model for the whole areas) and local adaptive modeling (using various models for different local zones) (Zhang et al., 2020). For example, Zhang and Roy (2017) demonstrated that local adaptive modeling outperformed the global classification modeling strategy. Therefore, the global land surface was first divided into 961 5° × 5° geographical tiles illustrated in Figure 5, which were inherited from the global 30 m land-cover mapping by (Zhang et al., 2021b). Then, **we trained the local adaptive classification models using derived training samples in Section 3 and multisource and multitemporal features (the highest, lowest water-level and phenological composites and topographical variables) at each 5° × 5° geographical tile.** It should be noted that we used the training samples from neighboring 3 × 3 geographical tiles to train the classification model and classify the central tile for guaranteeing the spatially continuous transition over adjacent regional wetland maps. Namely, we trained 961 local adaptive classification models and then produced 961 5° × 5° wetland maps. Finally, we spatially mosaiced these 961 regional wetland maps into the global 30 m wetland map in 2020.

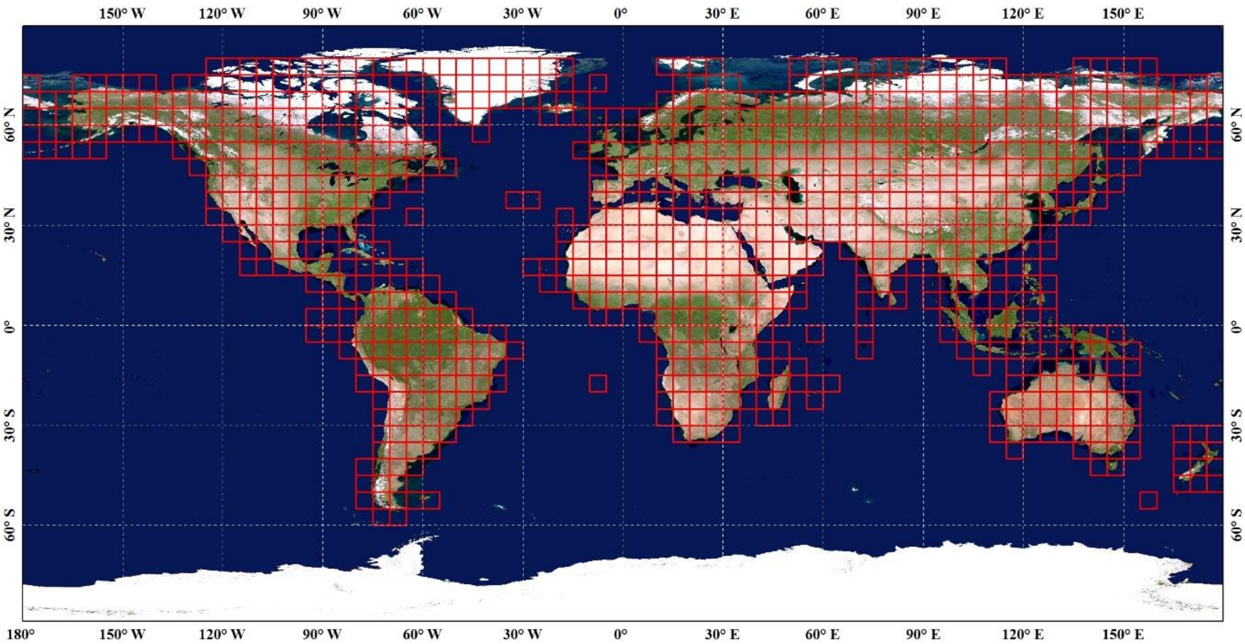

Figure 5. The spatial distribution of 961 5° × 5° geographical tiles used for local adaptive modeling, which was inherited from the global 30 m land-cover mapping by (Zhang et al., 2021b). The background imagery came from the National Aeronautics and Space Administration (https://visibleearth.nasa.gov, last access: 10 Nov 2022).

5. The authors used Sentinel SAR data, why do not produce the 10 m resolution product based on Sentinel 2?

Great thanks for the suggestion. Yes, we can combine the time-series Sentinel-1 and Sentinel-2 to develop the global 10m wetland maps, however, the reasons why we developed the global 30m wetland products are the following:

1) The spatial resolution of most prior global wetland products in Table 1 is 30 m, the derived training samples can be directly applied in the Landsat imagery for wetland mapping. If we used the derived training samples to Sentinel-1 and Sentinel-2, we must consider the spatial scale matching problem.
2) Compared to the Landsat imagery, the Sentinel-2 preprocessing method is not yet mature, namely, these bad quality (cloud, shadow, snow and ice) cannot be completely identified. It might be transferred to the wetland mapping especially in the tropics (cloudy regions) and high latitudes areas (frequent snow and ice covering).
3) The global 10-m wetland mapping also means 10 times the amount of computation when comparing to the global 30 m wetland mapping. Although the GEE provides free computation and storage ability, the time consumption is also a factor that cannot be ignored in global wetland mapping
4) Our further works would focus on the spatiotemporal dynamics of global wetlands over long time spans, which is also a hot spot in wetland monitoring today, however, the Sentinel-2 has shorter time span than the Landsat (since 1984).

Based on the above factors, we choose the Landsat imagery as our main data to develop the global 30 m fine wetland mapping.

Response to comments
Paper #: essd-2022-180
Title: GWL_FCS30: global 30 m wetland map with fine classification system using multi-sourced and time-series remote sensing imagery in 2020
Journal: Earth System Science Data

Reviewer #2

The submitted manuscript provides a global wetland map including inland and tidal sub-classes based on remote sensing data. Currently, we are still lacking a multi-class global wetland data including inland and tidal wetlands simultaneously, and the map produced by this work provides valuable information for related wetland studies. The manuscript is well-written and easy to follow. Above all, I recommend their publication provided that a moderate revision is carried out.

Great thanks for the positive comments. The manuscript has been further improved based on your and other two reviewers' comments and suggestions.

1. Wetlands are classified as inland or coastal wetlands in this study, and the latter includes mangroves, salt marshes, and tidal flats. For these three wetland types, the term "tidal wetlands" is more appropriate than "coastal wetlands", for example, in Murray et al., 2022. Coastal wetlands include other terrestrial and shoreline constituents like riparian wetlands and tidal freshwater marshes, but not just mangroves, salt marshes and tidal flats. As such, I suggest using "tidal wetlands" to make the classification system more accurate.

Great thanks for your useful suggestion. The 'coastal wetland' has been changed as the 'tidal wetland' in our fine wetland classification system as:

Table 2. The description of wetland classification system in this study

Category I	Category II	Description
Tidal wetland	Mangrove	The forest or shrubs which grow in the coastal blackish or saline water
	Salt marsh	Herbaceous vegetation (grasses, herbs and low shrubs) in the upper coastal intertidal zone
	Tidal flat	The tidal flooded zones between the coastal high and low tide levels including mudflats and sandflats.
Inland wetland	Swamp	The forest or shrubs which grow in the inland freshwater
	Marsh	Herbaceous vegetation (grasses, herbs and low shrubs) grows in the freshwater
	Flooded flat	The non-vegetated flooded areas along the rivers and lakes
	Saline	Characterized by saline soils and halophytic (salt tolerant) plant species along saline lakes
	Permanent water	Lakes, rivers and streams that are always flooded

2. Section 2.4: This section is about generating validation samples, thus should be moved to the "Accuracy assessment" section as a validation step. Another thing is how did the authors determine the size of total validation samples (i.e., 18,701)?

Great thanks for the comment. First, Based on the suggestion, the section 2.4 of how to generate the global validation samples has been moved to the Section 4.3 Accuracy Assessment.

Then, as for how to determine the size of total validation samples, we combined the stratified random sampling method and the proportions of various land-cover types to determine the sample size of each land-cover type based on the work of Foody et al. (2009) and Olofsson et al. (2014) as:

$$n = \frac{\left(\sum W_h \sqrt{p_h(1-p_h)}\right)^2}{V + \sum W_h P_h(1-P_h)/N}$$

where N is the number of pixel units in the study region; V is the standard error of the estimated overall accuracy that we would like to achieve, $V = (d/t)^2$ (t = 1.96 for a 95% confidence interval, t = 2.33 for a 97.5% confidence interval, and d is the desired half-width of the confidence interval); W_h is the weight distribution of class h; p_h is the producer's accuracy. These sample size calculations should be repeated for a variety of choices of V and p_h before reaching a final decision. We try to achieve producer's accuracies of 0.9 of non-wetland class and 0.8 of the seven wetland classes. Meanwhile, using the parameters of d = 0.0125, t = 2.33, the sample size can be determined as approximately 18500. In addition, there is a little uncertainty for interpreting the validation points, so we randomly generate 20000 validation points over the globe and then discard 1299 uncertain points (these disagreement points over five experts), so a total of 18701 validation points are used to assess the GWL_FCS30-2020 performance.

Pontus Olofsson, G. M. F. (2014). Good practices for estimating area and assessing accuracy of land change. Remote Sensing of Environment, 148(25), 42-57, https://doi.org/10.1016/j.rse.2014.02.015.
Foody, Giles M. "Sample size determination for image classification accuracy assessment and comparison." International Journal of Remote Sensing 30.20 (2009): 5273-5291.

This amount seems disproportionately less than the number of training samples (more than 20 million).

As for the unbalance of the training samples and validation samples, it is mainly because our training and validation samples are completely independent. Specifically, **we combined many pre-existing global wetland datasets to automatically derive the training samples over the globe** while **the validation points must be interpreted by visual interpretation**. As we all known, collecting validation points through visual interpretation is time-consuming and labor-intensive, therefore, we cannot to interpret a large amount of validation points.

(3) Lines 250-255: The tidal flat samples were collected from the global tidal flat map (Murray et al., 2019), and thus would suffer from the inherent error of the data. Several studies found that Murray's tidal flat map failed to distinguish between nearshore ponds and tidal flats, mainly because these ponds also have water-level variations (Jia et al., 2021; Zhang et al., 2022). The error of commission (i.e., classifying ponds into tidal flats) is also indicated in the tidal flat map generated by this study, as shown in the upper panels of Fig. 13. I suggest the authors mask out ponds and lakes from their tidal flat map because it would substantially improve the accuracy. There is a new dataset that provides global lakes and reservoirs may be helpful: Khandelwal et al. 2022.

Great thanks for the comment and useful suggestion. Yes, we agree that the Murray's tidal flat suffered the commission error especially over the nearshore ponds. Based on your suggestion, the new global lakes and reservoirs dataset is used to further optimize tidal flat layer in our GWL_FCS30.

In addition, as the tidal flats were demonstrated to overestimate some coastal pones as the tidal flats, the global lake and reservoir dataset, developed by Khandelwal et al. (2022), was applied to optimize the tidal flat.
The local comparisons in the Figure 16 shows that the updated GWL_FCS30 dataset has better performance than Murray's tidal flat products in excluding these ponds and lakes.

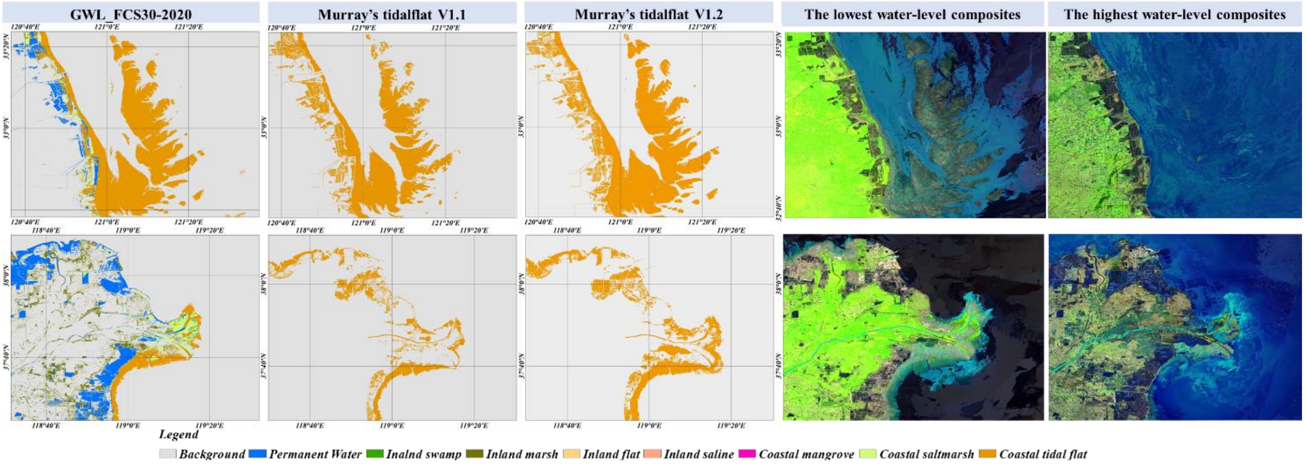

Figure 16. The comparisons between the tidal flat of GWL_FCS30 in 2020, Murray's tidal flat V1.1 in 2016 (Murray et al., 2019), and Murray's tidal flat V1.2 in 2019 (Murray et al., 2022) for two local regions. In each case, the highest and lowest tidal-level composites, composited by SWIR1, NIR, and red bands, are illustrated.

(4) Line 286: These thresholds proposed by Wang et al. 2020 were designed for tidal wetlands, but their application in this study was to inland wetlands. Therefore, the authors need to prove that these thresholds have robust performance in mapping inland wetlands.
Great thanks for the comment. Yes, the rule of 'EVI⩾0.1, NDVI⩾0.2, and LSWI>0' is referenced from the work of Wang et al. (2020) in tidal wetland mapping, actually, whether the rule is also suitable for inland wetlands has been demonstrated on the work of Xiao et al. (2009) and Hao et al. (2022) who used these thresholds to identify the vegetated land-cover types over the inland regions.
Wang, X., Xiao, X., Zou, Z., Hou, L., Qin, Y., Dong, J., Doughty, R. B., Chen, B., Zhang, X., Chen, Y., Ma, J., Zhao, B., and Li, B.: Mapping coastal wetlands of China using time series Landsat images in 2018 and Google Earth Engine, ISPRS J Photogramm Remote Sens, 163, 312-326, https://doi.org/10.1016/j.isprsjprs.2020.03.014, 2020.
Xiao, Xiangming, et al. "A simple algorithm for large-scale mapping of evergreen forests in tropical America, Africa and Asia." Remote Sensing 1.3 (2009): 355-374.
Hao, Ying-Ying, et al. "A cascading reaction by hydrological spatial dynamics alternation may be neglected." Environmental Research Letters 17.8 (2022): 084034.
Meanwhile, we also use these thresholds to split the vegetated and non-vegetated areas over several inland regions (including: Poyang Lake, Caspian Sea, Congo Rainforests and so on), Figure S1 illustrates that these thresholds are also robust in splitting vegetated and non-vegetated land-cover types in inland areas. For example, in the First panel over Poyang Lake, the non-vegetated areas (water body, impervious surfaces) are both clearly excluded and these cropland, forest and grassland are completely included. In the second panel over semi-arid region, the bare area and water body are masked while the sparse vegetation (upper left) and inland marsh are included. The third panel in the Congo rainforests, these small rivers and reservoirs are accurately captured.

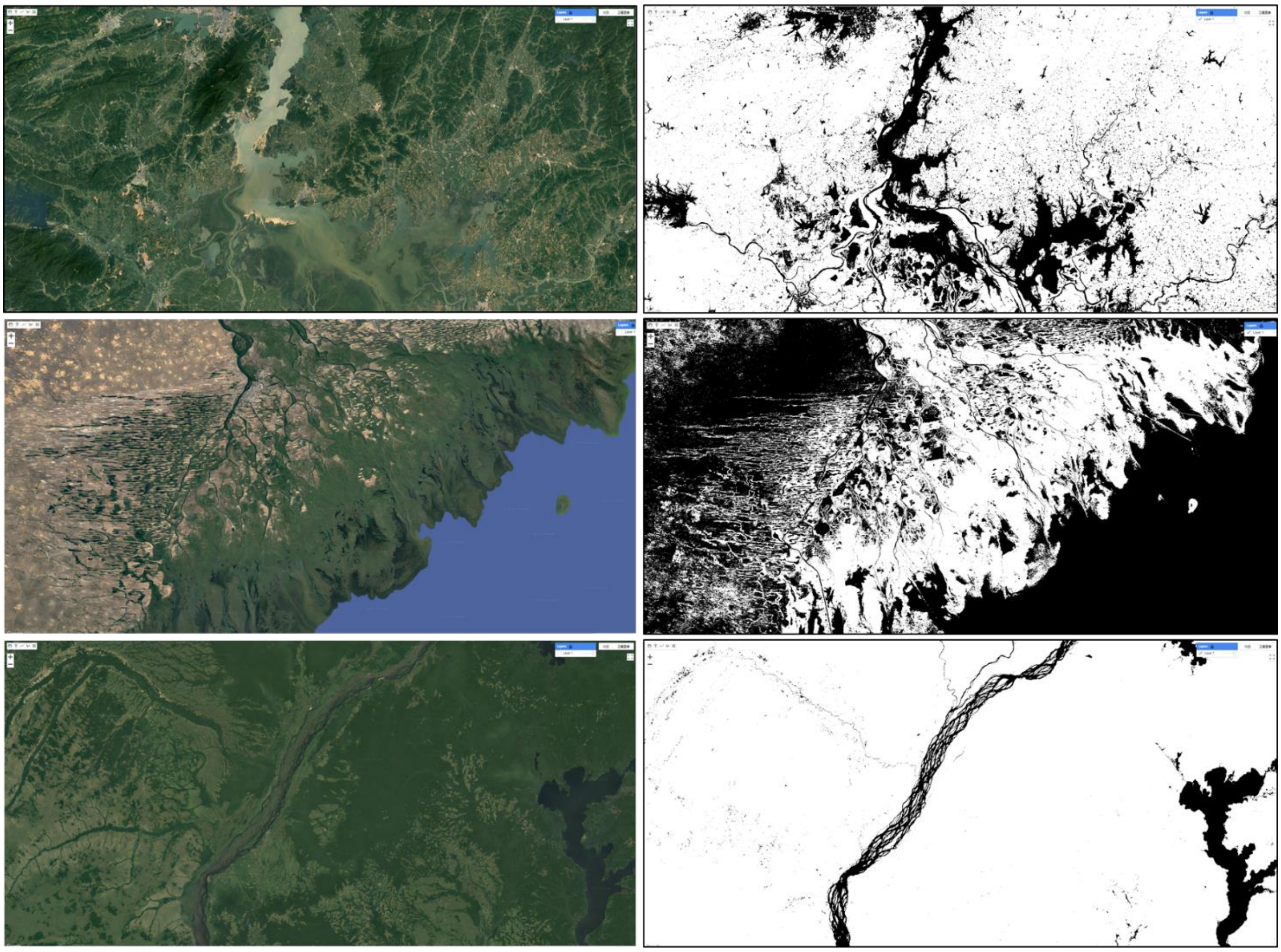

Figure S1. The vegetated and non-vegetated masks (white and black) over three typical inland areas using the rule of ‘EVI⩾0.1, NDVI⩾0.2, and LSWI>0’.

(5) Line 297, Equation 3: This maximum extent of inland wetlands also contains tidal wetlands (since the wetland layer in the global land cover data failed to distinguish them), so how did the authors ensure that the generated samples from inland wetland have corrected labels?

Great thanks for the comment. Yes, the maximum extent of inland wetlands also contains a small amount of tidal wetlands. However, we derive inland training samples from five inland wetland products using a series of refinement measures **instead of directly generating from the inland maximum wetland extents**. Specifically, the consistency analysis of five global wetland datasets (TROP-SUBTROP Wetland, GLWD, CCI_LC, GlobeLand30, and GLC_FCS30) and the temporal stability checking for CCI_LC (1992–2020), GlobeLand30 (2000-2020) and GLC_FCS30 (2015-2020) were applied to identify these temporally stable and high cross-consistency wetland points. It should be noted that the coarse wetland products (GLWD, TROP-SUBTROP and CCI_LC) were resampled to 30 m using the nearest neighbor method on the GEE platform and the coastal wetland layers in these products were excluded. Namely, only the pixel identified as inland wetland in all five products was retained. Then, the morphological erosion filter with a local window of 3 × 3 was also used to decrease the sampling uncertainty over these land-cover transition areas because the transition zones between two different land-cover types are likely to be misclassified. The details of how to derive inland training samples has been strengthen as:

The pre-existing inland wetland datasets usually suffered from lower accuracy compared to coastal wetland products; for example, the wetland layer in the GlobeLand30-2010 and GLC_FCS30-2015 was validated to achieve a user accuracy of 74.9% (Chen et al., 2015) and 43.4% (Zhang et al., 2021b), respectively. Therefore, **we first generated high-confidence inland wetland samples and then determined their sub-categories (swamp, marsh, inland flat, saline wetland and permanent water). Specifically, the consistency analysis of five global wetland datasets (TROP-SUBTROP Wetland, GLWD, CCI_LC, GlobeLand30, and GLC_FCS30) and the temporal stability checking for CCI_LC (1992–2020), GlobeLand30 (2000-2020) and GLC_FCS30 (2015-2020) were applied to identify these temporally stable and high cross-consistency wetland points ($P_{inlandWet}^{Tstable,Scons}$).** It should be noted that the coarse wetland products (GLWD, TROP-SUBTROP and CCI_LC) were resampled to 30 m using the nearest neighbor method on the GEE platform and the coastal wetland layers in these products were excluded. **Only the pixel identified as inland wetland in all five products was retained. Then, the morphological erosion filter with a local window of 3 × 3 was also used to decrease the sampling uncertainty over these land-cover transition areas because the transition zones between two different land-cover types are likely to be misclassified** (Lu and Wang, 2021; Radoux et al., 2014).

Afterward, to determine the wetland sub-category for each inland wetland sample, we first used the empirical vegetation rule (EVI ≥ 0.1, NDVI ≥ 0.2, and LSWI > 0) proposed by Wang et al. (2020) and time-series Landsat imagery to split candidate samples into two parts: vegetated wetland samples (swamp and marsh) and non-vegetated wetland samples (flooded flat, saline and permanent water). Then, as the swamp was defined as the forest or shrubs which grow in the inland freshwater, the global 30-m tree cover dataset (GFCC30TC) was adopted to distinguish the swamp and marsh from vegetated wetland samples. Specifically, if the tree cover of the sample was greater than 30% (Hansen et al., 2013), it was labeled as swamp, and the remaining vegetated wetland samples were labeled as marsh. Furthermore, to distinguish between the inland flat, saline samples and permanent water, the saline blocks in the prior GLWD products were first checked by visual interpretation and then imported as the reference dataset to identify all saline wetland samples. The remaining non-vegetated wetland samples were further refined using the time series of the JRC-GSW datasets, only water probability of these remaining samples less than the threshold of 0.95 (suggested by Wang et al. (2020)) were labeled as flooded flat. Lastly, regarding the permanent water samples, the JRC_GSW water dynamic dataset was validated and achieved producer's and user's accuracies of 99.7% and 99.1% for permanent water (Pekel et al., 2016). The permanent water training samples were directly derived from the JRC_GSW dataset without any refinement rules.

Lastly, although the maximum extent of inland wetlands (Eq. (3)) contains tidal wetlands, our post-processing method also minimize this issue in Section 4.2 as:

As the inland and coastal tidal wetlands were independently produced, some pixels in the overlapping area of maximum inland and coastal wetland extents were simultaneously labeled as inland wetlands and coastal wetlands. However, as the final global wetland map was a hard classification, **these pixels should be post-processed into one label. As the random forest classifier could provide the posterior probability for each pixel, we determined the labels of the confused pixels by comparing the posterior probabilities.**

(6) Section 4.2: The description for obtaining training samples is unclear. What are the strata here, wetland classes or 5°×5° tiles?

Great thanks for the comment. The description of how to obtain the training samples has been strengthen by your and other reviewer's suggestions. Specifically, we further adjust the Section 3 (Deriving training samples and determining maximum wetland extents) into four parts. In the first three parts, we separately introduce how to derive coastal tidal wetland samples in Section 3.1, inland wetland samples in Section 3.2, and non-wetland samples in Section 3.3, and determine the sample size and distributions. We think the updated manuscript in Section 3 is easier to follow.

As for 'What are the strata here' in Section 4.2, we actually simultaneously consider the wetland classes and 5°×5° tiles. To make the local adaptive and stratified modeling more intuitive, the Section 4.2 has been strengthen as:

Since we have simultaneously extracted the maximum coastal and inland wetland extents when deriving training samples from prior wetland datasets, the stratified classification strategy was adopted to fully use the maximum extent constraint. If a pixel was classified as a coastal tidal wetland outside the maximum coastal tidal wetland extents, it would be identified as a misclassification. Furthermore, there were two ideas for the large-area land-cover mapping including global classification modeling (using one universal model for the whole areas) and local adaptive modeling (using various models for different local zones) (Zhang et al., 2020). For example, Zhang and Roy (2017) demonstrated that local adaptive modeling outperformed the global classification modeling strategy. Therefore, the global land surface was first divided into 961 5° × 5° geographical tiles illustrated in Figure 5, which were inherited from the global 30 m land-cover mapping by (Zhang et al., 2021b). Then, we trained the local adaptive classification models using derived training samples in Section 3 and multisource and multitemporal features (the highest, lowest water-level and phenological composites and topographical variables) at each 5° × 5° geographical tile. It should be noted that we used the training samples from neighboring 3 × 3 geographical tiles to train the classification model and classify the central tile for guaranteeing the spatially continuous transition over adjacent regional wetland maps. Namely, we trained 961 local adaptive classification models and then produced 961 5° × 5° wetland maps. Finally, we spatially mosaiced these 961 regional wetland maps into the global 30 m wetland map in 2020.

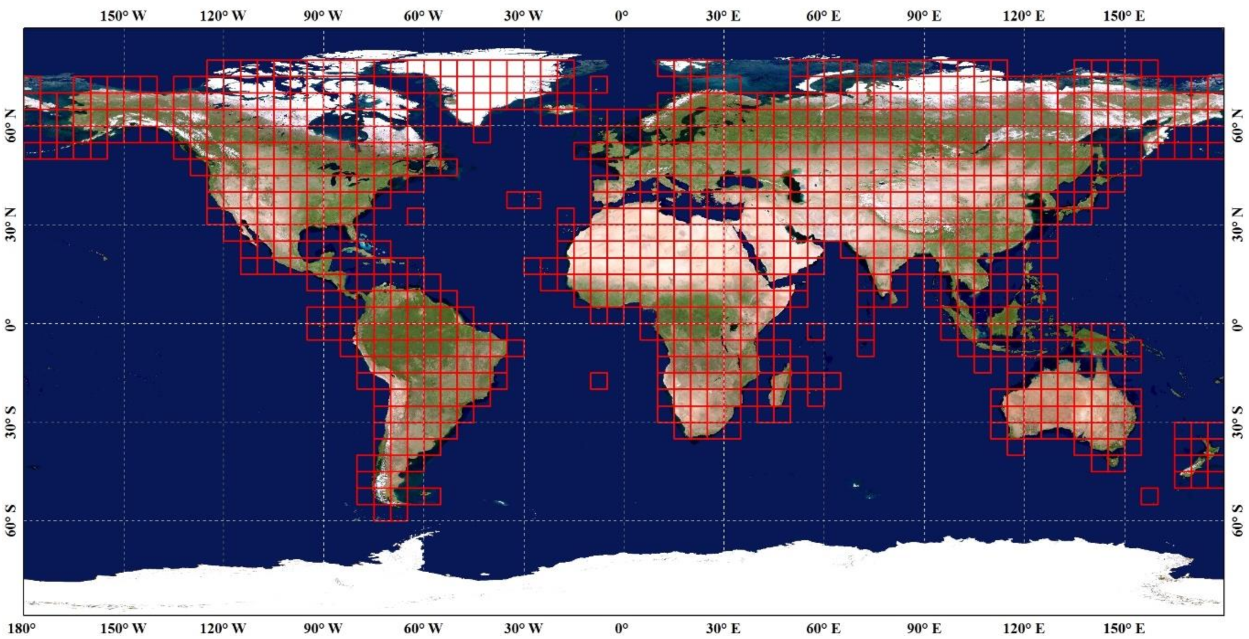

Figure 5. The spatial distribution of 961 5° × 5° geographical tiles used for local adaptive modeling, which was inherited from the global 30 m land-cover mapping by (Zhang et al., 2021b). The background imagery came from the National Aeronautics and Space Administration (https://visibleearth.nasa.gov, last access: 10 Nov 2022).

In addition, the training samples selected from the maximum wetland extent may be of low quality. The authors do explain that the map accuracy is insensitive to low-quality samples within a 20% threshold, but it's still missing a map representing the percentage of real erroneous samples. I think the training samples need to be filtered according to some criterion before classification to improve their accuracy. I recommend clarifying the process of sample generating and the quality-control procedures.

Great thanks for the comment. Yes, we agree that the quality of training samples is important for accurate wetland mapping. In this study, we have used a lot of rules to guarantee the confidence of training samples instead of directly deriving from maximum wetland extents.

Firstly, as for **the mangrove training samples**:

…we first measured the temporal consistency of the three time-series mangrove forest products (CGMFC, GMW, and GBTM mangroves), and only these temporally stable mangrove forest pixels were selected as the primary candidate points ($P_{mangrove}^{Tstable}$). Meanwhile, to minimize the influence of classification error in each mangrove forest product, the cross-consistency of five mangrove products was analyzed, and only the pixel, simultaneously identified as mangrove forest in all five products, was labeled as stable and consistent candidate points ($P_{mangrove}^{Tstable,Scons}$). Furthermore, considering that there was a temporal interval between prior mangrove products and our study, and that mangrove deforestation usually followed the pattern of edge-to-center contraction, a morphological erosion filter with a local window of 3×3 was applied to the $P_{mangrove}^{Tstable,Scons}$ points to further ensure the confidence of mangrove training samples.

Secondly, as for **the tidal flat samples**:

To ensure the accuracy of tidal flat samples, we first applied temporal consistency analysis to the time series of tidal flat datasets from 2000 to 2016 and identified the temporally stable tidal flat pixels ($P_{tidal}^{Tstable}$) during 16 consecutive years. The reason why we discarded the tidal flat datasets before 2000 was that the available Landsat imagery were sparse and could not accurately capture the high-tidal and low-tidal information, and suffered lower monitoring accuracy. Next, Radoux et al. (2014) found that transition zones between two different land-cover types are likely to be misclassified; therefore, the candidate tidal flat samples $P_{tidal}^{Tstable}$ were further refined by the morphological erosion filter with a local window of 3×3. Furthermore, as a tidal flat is a non-vegetated coastal wetland, we combined the empirical rule (EVI ≥ 0.1, NDVI ≥ 0.2, and LSWI > 0) proposed by Wang et al. (2020) and time-series Landsat imagery in 2020 (approximately 142 thousand Landsat scenes) to exclude all vegetated pixels from tidal flat training samples.

Thirdly, as for **the salt marsh samples**:

The global distribution of the salt marsh dataset contained 350,985 individual vector polygons and was the most complete dataset on salt marsh occurrence and extent at the global scale (McOwen et al., 2017). However, after careful review, we found some mislabeled salt marsh polygons, so this dataset cannot be used directly to derive training samples. This study first used the random sampling method to generate 35,099 salt marsh points (approximately 10% of the total polygons) based on prior datasets. We combined the visual interpretation method and high-resolution imagery to check each salt marsh point. After discarding the incorrect and uncertain samples, a total of 32,712 salt marsh points were retained.

Fourthly, as for **the inland wetland samples:**

…we first generated high-confidence inland wetland samples and then determined their sub-categories (swamp, marsh, inland flat, saline wetland and permanent water). Specifically, the consistency analysis of five global wetland datasets (TROP-SUBTROP Wetland, GLWD, CCI_LC, GlobeLand30, and GLC_FCS30) and the temporal stability checking for CCI_LC (1992–2020), GlobeLand30 (2000-2020) and GLC_FCS30 (2015-2020) were applied to identify these temporally stable and high cross-consistency wetland points ($P_{inlandWet}^{Tstable,Scons}$). It should be noted that the coarse wetland products (GLWD, TROP-SUBTROP and CCI_LC) were resampled to 30 m using the nearest neighbor method on the GEE platform. Namely, only the pixel identified as inland wetland in all five products was retained. Then, the morphological erosion filter with a local window of 3 × 3 was also used to decrease the sampling uncertainty over these land-cover transition areas because the transition zones between two different land-cover types are likely to be misclassified (Lu and Wang, 2021; Radoux et al., 2014).

Afterward, to determine the wetland sub-category for each inland wetland sample, we first used the empirical vegetation rule (EVI ≥ 0.1, NDVI ≥ 0.2, and LSWI > 0) proposed by Wang et al. (2020) and time-series Landsat imagery to split candidate samples into two parts: vegetated wetland samples (swamp and marsh) and non-vegetated wetland samples (flooded flat, saline and permanent water). Then, as the swamp was defined as the forest or shrubs which grow in the inland freshwater, the global 30-m tree cover dataset (GFCC30TC) was adopted to distinguish the swamp and marsh from vegetated wetland samples. Specifically, if the tree cover of the sample was greater than 30% (Hansen et al., 2013), it was labeled as swamp, and the remaining vegetated wetland samples were labeled as marsh. Furthermore, to distinguish between the inland flat, saline samples and permanent water, the saline blocks in the prior GLWD products were first checked by visual interpretation and then imported as the reference dataset to identify all saline wetland samples. The remaining non-vegetated wetland samples were further refined using the time series of the JRC-GSW datasets, only water probability of these remaining samples less than the threshold of 0.95 (suggested by Wang et al. (2020)) were labeled as flooded flat. Lastly, regarding the permanent water samples, the JRC_GSW water dynamic dataset was validated and achieved producer's and user's accuracies of 99.7% and 99.1% for permanent water (Pekel et al., 2016). The permanent water training samples were directly derived from the JRC_GSW dataset without any refinement rules.

Lastly, as for **the non-wetland samples:**

To automatically derive these non-wetland samples, the multi-epochs GlobeLand30, GLC_FCS30 and CCI_LC global land-cover products were integrated. Specifically, the temporal stability and cross-consistency analysis were applied to three land-cover products to identify temporally stable forest/shrubland, grassland, cropland, and other candidate samples. Furthermore, the morphological erosion filter with the local window of 3 × 3 was also adopted to decrease the sampling uncertainty over land-cover transition areas.

(7) Section 5.3: The comparison here uses the old-version GMW mangrove map. However, the GMW mangrove map was updated to version 3.0 recently (Bunting et al., 2022), which substantially improved the accuracy by filling gaps caused by the strips in the Landsat-7 images. A detailed comparison with this new version is encouraged.

Great thanks for the suggestion. The new GWM_V3 mangrove map has been used in the revised manuscript as:

Figure 14 illustrates the comparisons between our fine wetland maps with three widely used global mangrove forest products (Atlas mangrove, GMW_V3 (Global Mangrove Watch Version3), and USGS Mangrove) listed in Table 1 in two typical mangrove regions (coastal Indonesia and Sundarbans). Intuitively, there was great consistency over four mangrove datasets because the mangrove forest reflected obvious and strong vegetation reflectance characteristics and was easier to identify than other wetland sub-categories. However, the Atlas mangrove dataset suffers from the underestimation problem; namely, the mangrove area in the Atlas mangrove dataset was obviously lower than the other three products, especially in coastal Indonesia (local enlargements). The USGS mangrove product can comprehensively and accurately capture the spatial distribution of mangroves over two regions. Still, it missed small and isolated fragments of mangrove forests in two regions (green rectangle) based on high-resolution imagery. The GMW_V3 dataset was validated to achieve an overall accuracy of 95.25%, with user and producer accuracies of mangrove forests of 97.5% and 94.0%, respectively (Bunting et al., 2018; Thomas et al., 2017), which shows great agreement with our fine wetland maps and confirms that this dataset accurately identified the spatial patterns of mangrove forest in both regions.

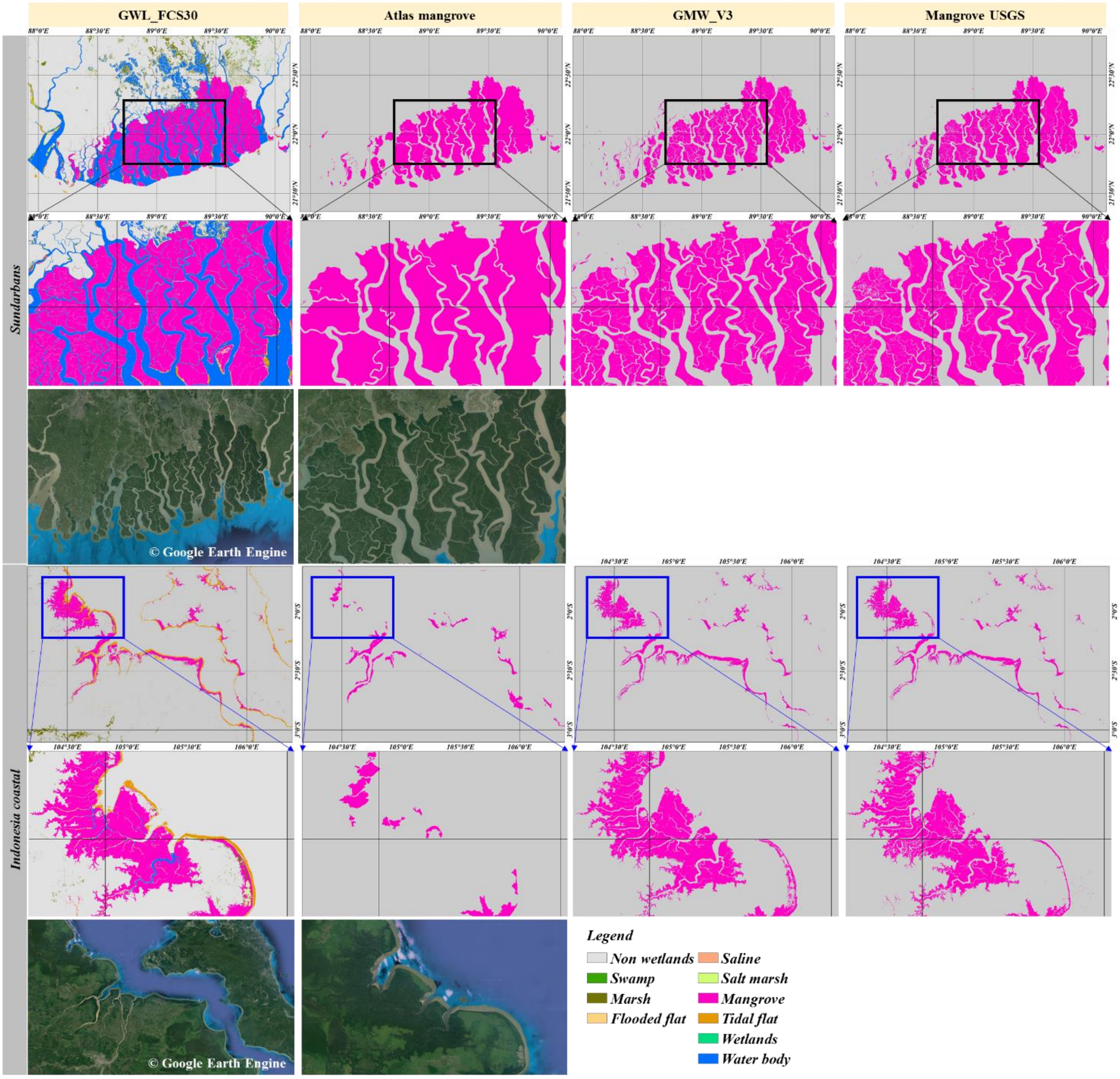

Figure 14. The cross-comparisons between our GWL_FCS30 wetland maps with three mangrove products (Atlas mangrove developed by Spalding (2010), GMW_V3 developed by Bunting et al. (2022) and Mangrove USGS developed by Giri et al. (2011)) in Sundarbans and coastal Indonesia. The high-resolution imagery came from the Google Earth Engine platform (https://earthengine.google.com; last access: 16 May 2022).

Also, a product of global tidal wetland dynamics provided by Murray et al. (2022) could be an important reference for comparison.

Great thanks for the comments. Based on your suggestion, the new global tidal flats in Murray et al. (2022) has been added into the comparisons.

Figure 16 illustrated the comparisons between GWL_FCS30 tidal flat layer with the Murray's tidal flat V 1.1 in 2016 and the updated Murray's tidal flat V1.2 in 2019 (Murray et al., 2022) in two local regions, and the corresponding highest and lowest tidal-level composites are also listed. Overall, three products can comprehensively capture the spatial patterns of tidal flats in these two regions, and the GWL_FCS30-2020 and Murray's tidal flat V1.2 performed higher spatial consistency while the Murray's tidal flat V1.1 suffered the obvious omission error in three typical areas (red rectangles). Detailedly, we can find that the Murray's tidal flat products misclassified some coastal ponds and lakes into the tidal flats especially in the first region while the GWL_FCS30-2020 accurately excluded these ponds and lakes.

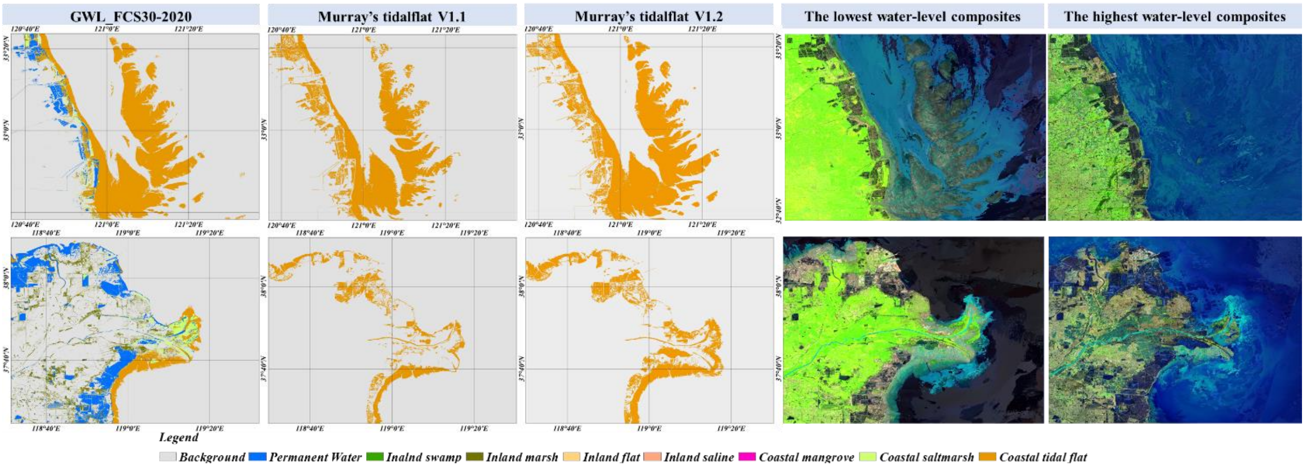

Figure 16. The comparisons between the tidal flat of GWL_FCS30 in 2020, Murray's tidal flat V1.1 in 2016 (Murray et al., 2019), and Murray's tidal flat V1.2 in 2019 (Murray et al., 2022) for two local regions. In each case, the highest and lowest tidal-level composites, composited by SWIR1, NIR, and red bands, are illustrated.

(8) Figure 8 lacks a legend.

Great thanks for pointing out the problem. The legend has been added in the Figure 8 as:

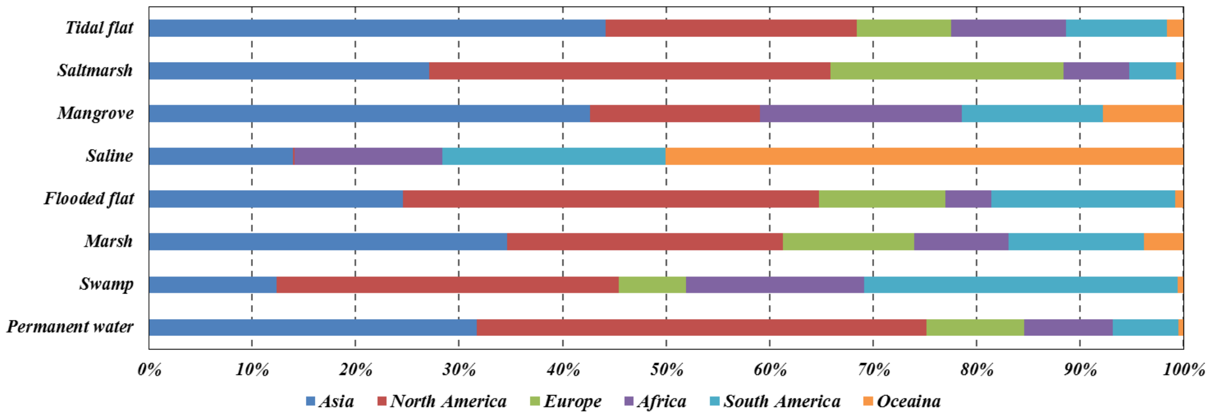

Figure 11. The area proportions of eight wetland sub-categories over each continent.

Response to comments

Paper #: essd-2022-180
Title: GWL_FCS30: global 30 m wetland map with fine classification system using multi-sourced and time-series remote sensing imagery in 2020
Journal: Earth System Science Data

Reviewer #3

The authors developed a global wetland mapping product based on multiple approaches in the GEE environment, called the GWL_FCS30. They reported some 3.6 million km2 of global wetlands, making the data freely available. The authors' efforts are laudable, yet I have many concerns about the presentation and the analyses themselves that preclude my acceptance of this paper for publication. For the presentation, I would argue that the paper itself is overly long and dense. The approaches could be more clearly articulated and sign-posted for the readers. Parts that are results are introduced in the Discussion section (e.g., some validation data, as I note below) and the length of the paper makes it a long slog. However, my main issues are with the analytical approaches and base assumption.

Great thanks for the comment. The manuscript has been greatly improved based on your and two other reviewers' comments.

First, the authors introduce wetlands in the very first sentence using the Ramsar Convention definition to include waters up to 6 m in depth. Then, they go on to conduct their analysis but exclude any and all inland open waters as they are assumed to be greater than 6 m in depth. They backstop their findings on global wetland abundance by stating at L535 "the estimated total wetland area in this study was more reasonable [than four previous analyses] because permanent water bodies with depths of more than six meters were not considered wetlands, according to the RAMSAR (sic) Convention…". The assumption that any and all open water on the global landmass is >6m in depth – and hence not possibly a wetland – does not resonate. Yes, larger and deeper lakes could be greater than 6m. But open waters, especially smaller ones are frequently considered wetlands and are typically <6m in water depth (see, e.g., China's State Forestry Administration [www.forestry.gov.cn] or a recent paper by Ye et al. (2022, https://doi.org/10.3390/w14071152); see also the Canadian Wetland Inventory [https://open.canada.ca/data/en/dataset/09f46d71-6feb-4f8f-8eb5-a58a58b06af5] or the United States National Wetlands Inventory [https://www.fws.gov/program/national-wetlands-inventory] identifying open waters as a wetland type). The point is that the Ramsar definition of wetlands is used, but then a major type of wetlands are excluded. The authors must acknowledge this in their study. For instance, it could be noted in the title and should definitely be noted in the abstract. I do wish that the authors would redo their analysis and incorporate open waters as a wetland type to include a major wetland type in their global analysis, alas.

Great thanks for pointing out this issue and giving useful suggestion. The **permanent water body** has been added into our fine wetland classification system in method Section as:

In this study, after considering the applicability of moderate resolution (10–30 m) imagery, their practical use for ecosystem management, and the available pre-existing global wetland dataset, the fine wetland classification system, containing eight sub-categories (three coastal tidal sub-categories and five inland sub-categories), was proposed to comprehensively depict the spatial patterns of global wetlands (Table 2). Specifically, the sub-categories of coastal tidal wetlands consist of mangroves, salt marshes, and tidal flats. By importing the vegetation and water cover information associated with this land cover, these categories were widely recognized in many previous studies (Wang et al., 2021; Zhang et al., 2022b). The inland wetland types shared similar characteristics and were grouped into swamp, marsh, and flooded flat. Meanwhile, in order to capture saline soils and halophytic plant species along saline lakes, the inland saline wetland, inherited from the Global Lakes and Wetlands Dataset (GLWD) (Lehner and Döll, 2004), was also imported. **Lastly, the permanent water, including lakes, rivers and streams that are always flooded, was widely identified as a wetland layer in previous studies (Davidson, 2014; Dixon et al., 2016; Hu et al., 2017b)**.

Table 2. The description of wetland classification system in this study

Category I	Category II	Description
Tidal wetland	Mangrove	The forest or shrubs which grow in the coastal blackish or saline water
	Salt marsh	Herbaceous vegetation (grasses, herbs and low shrubs) in the upper coastal intertidal zone
	Tidal flat	The tidal flooded zones between the coastal high and low tide levels including mudflats and sandflats.
Inland wetland	Swamp	The forest or shrubs which grow in the inland freshwater
	Marsh	Herbaceous vegetation (grasses, herbs and low shrubs) grows in the freshwater
	Flooded flat	The non-vegetated flooded areas along the rivers and lakes
	Saline	Characterized by saline soils and halophytic (salt tolerant) plant species along saline lakes
	Permanent water	**Lakes, rivers and streams that are always flooded**

Meanwhile, after adding the permanent water into our wetland system, the Result Section has been revised as:

Figure 9 illustrates the spatial distributions of our GWL_FCS30 wetland map and their area statistics in latitudinal and longitudinal directions in 2020. Overall, the GWL_FCS30 map accurately captured the spatial patterns of wetlands. It mainly concentrated on the high latitude areas in North Hemisphere and the rainforest areas (Congo Basin and Amazon rainforest in South America). Quantitatively, according to the latitudinal statistics, approximately 72.96% of wetlands were distributed poleward of 40°N (a large number of wetlands are located in Canada and Russia), and 10.6% of wetlands were located in equatorial areas, between 10°S~10°N, within which the Congo and Amazon rainforest wetlands are located. As for the longitudinal direction, there were mainly four statistical peak intervals: 120°W~50°W (Canada wetlands and Amazon wetlands), 15°E~25°E (Congo wetlands), 40°E~55°E (the Caspian Sea), and 60°E~90°E (Russia wetlands). Afterward, to more intuitively understand the performance of our GWL_FCS30 wetland map, four local enlargements in Florida, the Congo Basin, Sundarbans, and Poyang Lake were also illustrated. All of them comprehensively captured the wetland patterns in these local areas. For example, there was significant consistency between our results and Hansen’s regional wetland maps in the Congo Basin (Bwangoy et al., 2010); both results indicated that the wetlands occurred closer to major rivers and floodplains. Next, according to the lowest and highest water-level features derived from Sentinel-1 SAR and Landsat optical imagery in Figure 4, the inland wetlands, varied with the water-levels, were also comprehensively identified in the Poyang wetland map (Figure 9d). Figure 9c illustrates the spatial distributions of the world’s largest mangrove forest in the Sundarbans (Figure 9c), and the cross-comparison in Figure 14 also demonstrates the great performance of the GWL_FCS30 dataset. Lastly, the Florida wetlands simultaneously contained six sub-categories (mangrove, tidal flat, salt marsh, marsh, permanent water and swamp). These were distributed along the coastlines and rivers and are accurately captured in Figure 9a.

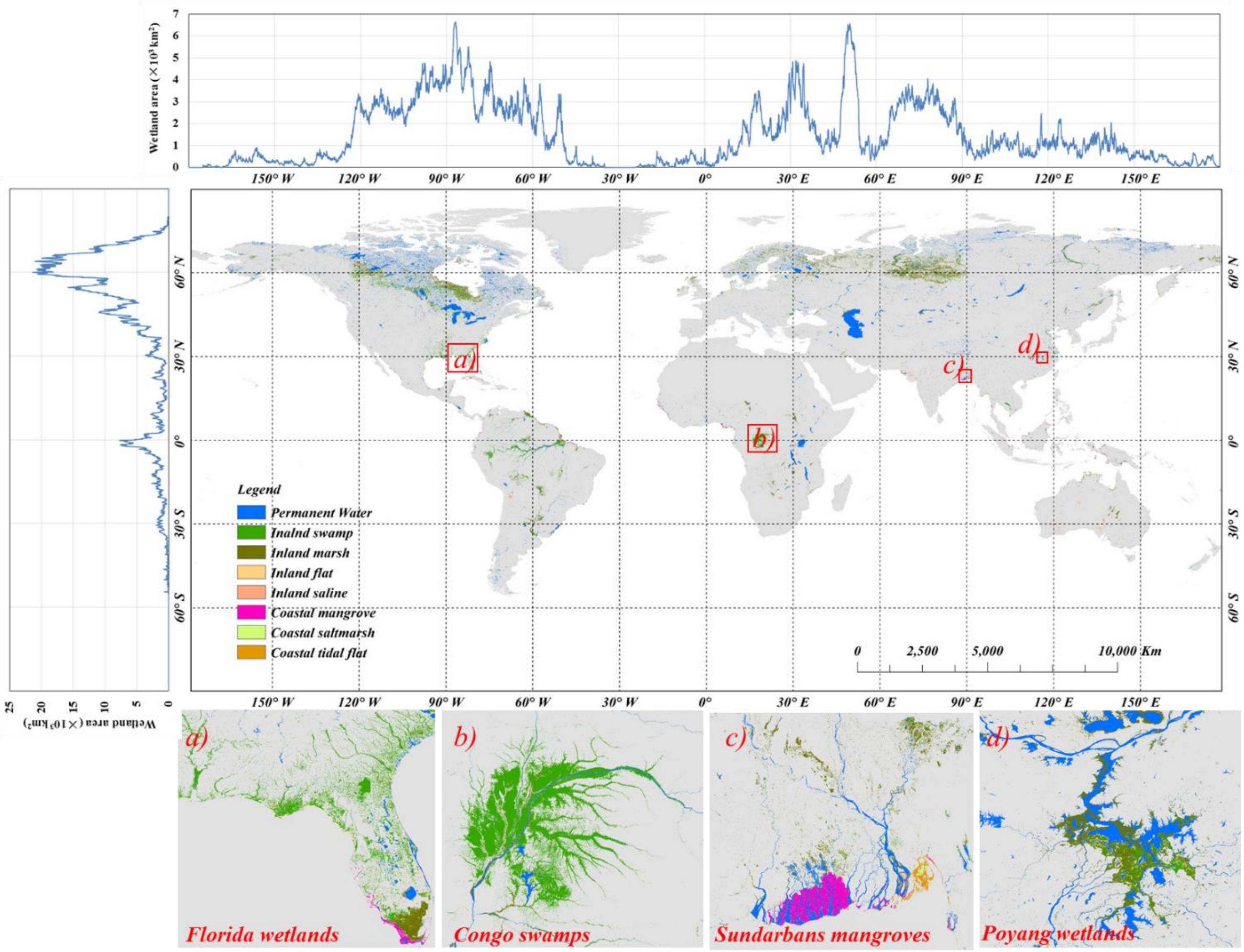

Figure 9. The overview of global 30-m fine wetland maps and their area statistics in latitudinal and longitudinal directions in 2020. Four local enlargements in (a) Florida, (b) Congo Basin, (c) Sundarbans, and (d) Poyang Lake were also illustrated.

Figure 10 illustrates the spatial distribution of eight sub-category wetlands after aggregating to the 0.5° × 0.5° grid cell. Intuitively, permanent water body, swamp and marsh accounted for most inland wetlands, and all of them showed significant spatial coexistence, in which they mainly concentrated on the . In contrast, flooded tidal wetlands had obviously lower proportions, and the inland saline type was only distributed along the surroundings of several saline lakes. In terms of the spatial distribution, it can be found that: 1) the swamp wetlands mainly were concentrated in the Congo and Amazon rainforests, Southern United States, and Northern Canada; 2) most marsh wetlands were located in high latitude areas in the Northern Hemisphere including Northern Canada, Russia, and Sweden; 3) there were significant coexistent relationships between flooded flat, swamp, and marsh wetlands. Similar to coastal wetlands, the mangrove forests were only found in coastal areas below 30°N and were mainly concentrated in regions between 30°N ~ 30°S, including Southeast Asia, West Africa, and the east coast of South America. The salt marshes and tidal flats shared similar spatial distributions.

They were widely distributed globally and can be observed along most coastlines. In addition, the tidal flat distributions were closely related to the slope of coastlines, tidal ranges, and sediment inflows. For example, the tidal flats in Asia and Europe usually were located in the tide-dominated estuaries and deltas. Similarly, Murray et al. (2019) also demonstrated that there were often more tidal flats where the river flowed into the sea.

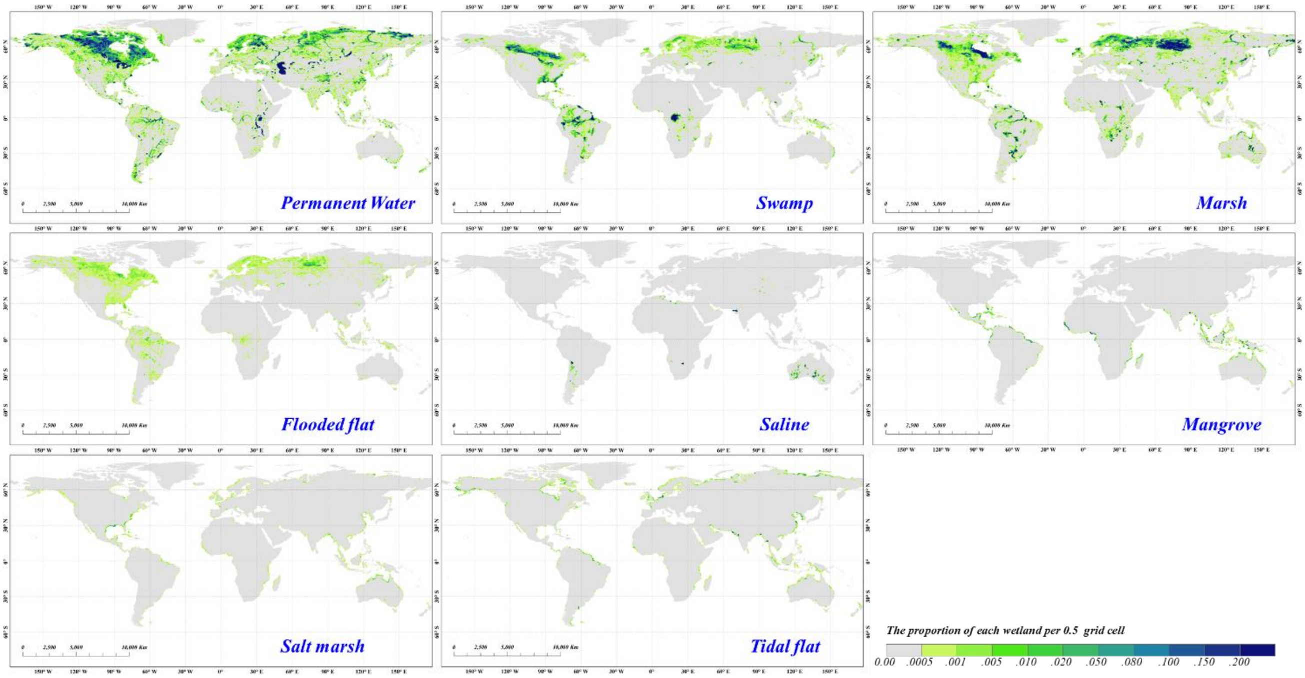

Figure 10. The spatial distributions of the eight wetland sub-categories after aggregating them to a resolution of 0.5° × 0.5°.

A further issue I have with this paper is that the data are considered mis-classified if they occur as wetlands in an area outside the [wetland type] maximum extent. However, this max extent assumes that all the previous analyses had zero omission error.

Great thanks for the comment. In this study, as the maximum extents of inland/coastal wetlands derived by combining several global prior products, the omission error in each prior product might be complemented by other products. For example, the inland maximum extent is derived from five products (TROP-SUBTROP Wetland, GLWD, CCI_LC, GlobeLand30, and GLC_FCS30). The CCI_LC, GlobeLand30 and GLC_FCS30 had serious omission errors, but the GLWD and TROP-SUBTROP products, produced by the compilation and model simulation method (Gumbricht, 2015; Lehner and Döll, 2004), can capture most wetland areas at the expense of a higher commission error. On the other hand, the union of five global wetland datasets in Eq. (3) also minimized the omission error of each dataset for inland wetland sub-categories. Therefore, the derived inland maximum extents actually fulfilled the assumption of zero omission error. The rationality of the maximum extents has been added and discussed in the Discussion Section as:

In addition, we used the derived maximum extents as the boundary for identifying inland and coastal tidal wetlands, in other words, we assumed that the derived maximum extents contained all inland and coastal tidal wetlands with zero omission error. Actually, the inland maximum extents in Eq. (3) fulfilled the assumption of zero omission error, because the GLWD and TROP-SUBTROP products, produced by the compilation and model simulation method (Gumbricht, 2015; Lehner and Döll, 2004), can capture almost all wetland areas at the expense of a higher commission error. For example, the Figure 13 illustrated the cross-comparisons between our GWL_FCS30 wetland maps with four existing wetland products, and the GLWD obviously overestimated the inland wetlands. On the other hand, the union of five global wetland datasets in Eq. (3) also minimized the omission error of each dataset for inland wetland sub-categories. Next, as for the maximum mangrove forest extents (Eq. (1)), as the high producer's and user's accuracies were achieved by five prior mangrove products (explained in Section 2.2) and the time-series mangrove products were integrated that these missed mangroves may be complemented by other products or time-series products, the derived maximum extents also can be considered as zero omission error and covered almost all mangrove forests. Recently, Bunting et al. (2022) developed the newest mangrove products covering 1996-2020, it can be used as another important prior dataset in our further works for deriving the maximum mangrove extents. Lastly, the maximum tidal flat extents, derived from time-series Murray's products from 1985~2016 by using the union operation (Eq. (2)), can also contain almost all tidal flats because previous studies demonstrated that they suffered higher commission error than the omission error (Jia et al., 2021; Zhang et al., 2022b).The missed tidal flats would concentrate on these newly increased tidal flats during 2016-2020, fortunately, the new time-series global tidal flat products during 1999-2019 was developed (Murray et al., 2022) and can be used as an important supplement in our further work for deriving the maximum tidal flat extent with zero omission error.

Another concern of mine is that their error assessment was done using a relatively paltry number of wetlands for the global extent of their analysis. For instance, they have ~8,000 wetland validation points to cover seven different wetland types. From Figure 2, it appears that ~7,000 of these points are inland "wetlands" versus coastal systems. Even with 7000 points for validation, that seems small considering the global extent of inland systems (swamps, marshes, flooded flats). And ~1000 points are used to validate the global population of saline, salt marsh, mangrove, and tidal flats. Their validation points were visually validated – though the authors explain five experts had to agree on the typology, the disagreements or data supporting those validations are also not presented.

Great thanks for the comment. First, we agree that a large amount of validation points play great role in comprehensively assess the performance of the developed products, however, it should be noted that the collection of validation points, especially for water-level sensitive wetlands with fine classification system, is time-consuming and labor-intensive. In addition, Foody et al. (2009) and Olofsson et al. (2014) have detailedly described how to determine the size of total validation points by using stratified random sampling theory as:

$$n = \frac{\left(\sum W_h \sqrt{p_h(1-p_h)}\right)^2}{V + \sum W_h P_h(1-P_h)/N}$$

where N is the number of pixel units in the study region; V is the standard error of the estimated overall accuracy that we would like to achieve, $V = (d/t)^2$ (t = 1.96 for a 95% confidence interval, t = 2.33 for a 97.5% confidence interval, and d is the desired half-width of the confidence interval); W_h is the weight distribution of class h; p_h is the producer's accuracy. These sample size calculations should be repeated for a variety of choices of V and p_h before reaching a final decision. We try to achieve producer's accuracies of 0.9 of non-wetland class and 0.8 of the seven wetland classes. Meanwhile, using the parameters of d = 0.0125, t = 2.33, the sample size can be determined as approximately 18700.

Pontus Olofsson, G. M. F. (2014). Good practices for estimating area and assessing accuracy of land change. Remote Sensing of Environment, 148(25), 42-57, https://doi.org/10.1016/j.rse.2014.02.015.

Foody, Giles M. "Sample size determination for image classification accuracy assessment and comparison." International Journal of Remote Sensing 30.20 (2009): 5273-5291.

In order to make the validation assessment more comprehensive, we also replenish 7008 wetland validation points, including 212 non-wetland points and 6796 wetland points (4538 inland wetland points and 2258 tidal wetland points), and the description of these updated global validation points (25709 points) has been revised as:

To quantitatively analyze the performance of our GWL_FCS30 wetland map, a total of 25,709 validation samples (illustrated in Figure 6), including 10,558 non-wetland points and 15,151 wetland points, were collected. Firstly, as the wetland was sparse land-cover type compared to the non-wetlands (forest, cropland, grassland and bare land), the stratified random strategy was applied to randomly derive validation points at each strata. Then, as the wetlands had significant correlation with the water levels (Zhang et al., 2022b), the time-series optical observations archived on the GEE cloud platform were used as the auxiliary dataset to interpret these water-level sensitive wetlands such as: tidal flat and flooded flat. It should be noted that the visual interpretation was implemented on the GEE cloud platform because it archives a large amount of satellites imagery with various time spans and spatiotemporal resolution (Zhang et al., 2022a). Meanwhile, each validation point is independently interpreted by five experts for minimizing the effect of expert's subjective knowledge, and only these complete agreement points were retained otherwise they were discarded. Then, we employed four metrics typically used to evaluate accuracy, which include the kappa coefficient, overall accuracy, user's accuracy (measuring the commission error), and producer's accuracy (measuring the omission error) (Gómez et al., 2016; Olofsson et al., 2014), were calculated using 25709 global wetland validation samples.

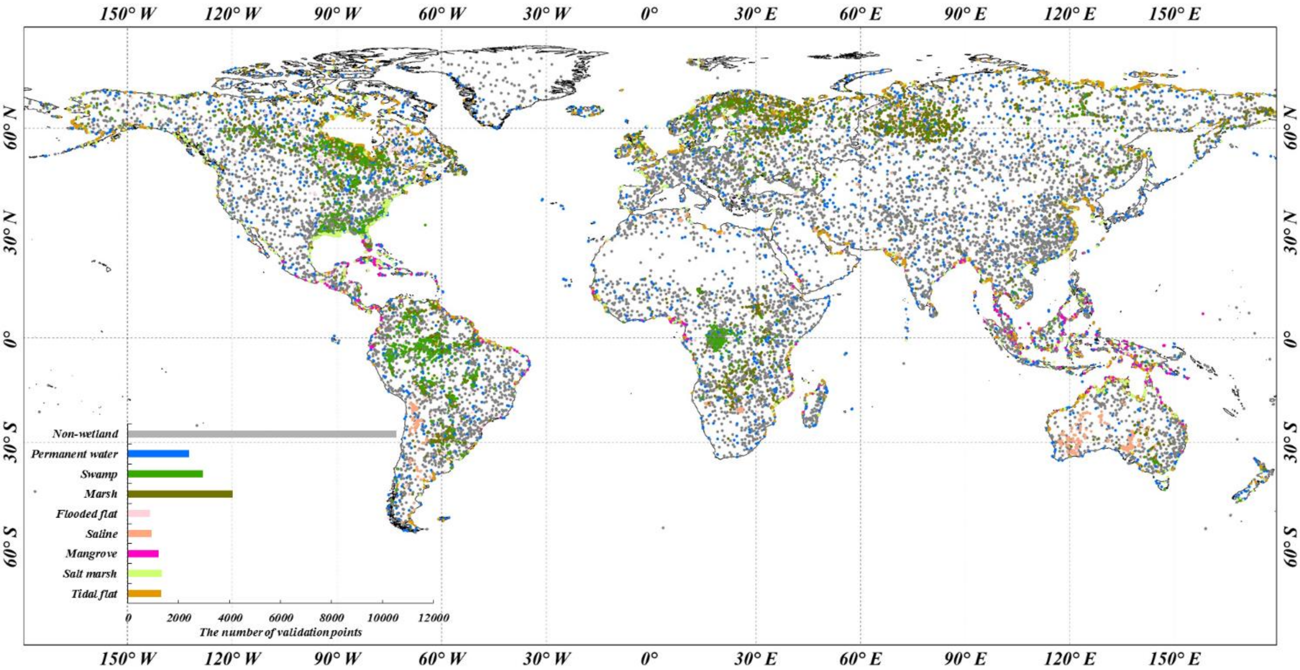

Figure 6. The spatial distribution of 25,709 global wetland validation samples using stratified sampling strategy.

Afterwards, the updated confusion matrix has been revised after replenishing 8007 validation points as:

Table 5. The confusion matrix of the global 30 m fine wetland map using 25,709 validation points.

	NWT	PW	SWP	MSH	FFT	SAL	MGV	SMH	TFT	Total	P.A.

NWT	9950	17	254	224	39	3	12	33	26	10588	94.24
PW	69	2251	4	15	63	0	0	8	9	2419	93.06
SWP	272	5	2127	452	74	11	3	9	0	2953	72.03
MSH	546	18	135	3218	149	18	2	34	1	4121	78.09
FFT	145	21	26	95	574	3	1	5	2	872	65.83
SAL	26	1	0	43	5	846	0	0	0	921	91.86
MGV	65	4	11	2	2	1	1109	15	3	1213	91.43
SMH	157	15	6	85	9	30	26	998	22	1347	74.09
TFT	78	13	0	11	7	11	6	29	1150	1305	88.12
Total	11308	2345	2563	4145	922	923	1159	1131	1213	25709	
U.A.	87.99	95.99	82.99	79.56	62.26	91.66	95.69	88.24	94.81		
O.A.						86.44					
Kappa						0.822					

Note: **NWT**: non-wetlands, **PW:** permanent water, **SWP**: swamp, **MSH**: marsh, **FFT**: flooded flat, **SAL**: saline, **SMH**: salt marsh, **MGV**: mangrove forest, **TFT**: tidal flat, **O.A.**: overall accuracy, **P.A.**: producer's accuracy, **U.A.**: user's accuracy.

I would argue that there exist multiple independent data layers that could be used to provide a much greater assessment of their relative accuracy (perhaps in addition their visual validation). For instance, the Chinese SFA, Canadian CWI, US NWI are all available datasets for validation. Within the US, there's also the National Land Cover Data (e.g., Wickham et al. 2018 that has the contiguous US land cover at 30 m pixel resolution, including both wetlands AND permanent water; https://doi.org/10.1080/01431161.2017.1410298).

Great thanks for the comment. Based on your suggestion, the comparisons at national scale between GWL_FCS30, NWI and NLCD, and CLC databases have been added in the Section 6.2, and the descriptions of NLCD, NWI and CLC have also been added in the Section 2.4 . As for the Canadian CWI and Chinese SFA, we are temporarily unable to obtain sufficient data for comparative analysis and then use the ESA CORINE Land Cover database for another comparative data.

2.4 National wetland products

Three national wetland products including: NLCD (National Land Cover Database) (Homer et al., 2020), NWI (National Wetlands Inventory) (Wilen and Bates, 1995) and CLC (CORINE Land Cover) (Büttner, 2014), were used as the comparative datasets to analyze the performance of developed global wetland maps in Section 6.2. Specifically, the NLCD contained open water, woody wetlands and emergent herbaceous wetlands, the NWI contained eight sub-categories (estuarine and marine deep-water, estuarine and marine wetland, freshwater emergent wetland, freshwater forest/shrub wetland, freshwater pond, lake, other, and Riverine), and the CLC identified the wetlands into nine sub-categories as: inland marshes, peat bogs, salt marshes, saline, intertidal flats, water courses, water bodies, coastal lagoons, estuaries, as well as sea and oceans.

6.2 Comparisons with the national wetland products

Using 1835 validation points (from the global validation points in Section 4.3) over the continuous United States, we quantitatively assessed the accuracy metrics of NLCD (National Land Cover Database) with GWL_FCS30 after merging the wetland subcategories into 4 classes in Table 6. Overall, the GWL_FCS30 achieved a higher performance than that of the NLCD mainly because a lot of herbaceous wetlands were misclassified into the open water in the NLCD, so the user's accuracy of herbaceous wetland and producer's accuracy of open water in NLCD was lower than that of GWL_FCS30. Then, as the NWI (National Wetlands Inventory) had different wetland system with the NLCD and GWL_FCS30, we also analyzed the metrics of NWI with GWL_FCS30 after merging into 5 classes. It can be found that the NWI shared similar performances with GWL_FCS30 on the non-wetlands and marine wetlands, but the user's accuracies of forest wetland and herbaceous wetland of NWI were lower than that of GWL_FCS30 mainly because some non-wetlands and open water were overestimated as the wetland in NWI. Similarly, Gage et al. (2020) also demonstrated that the NWI was easier to overestimate the wetland areas.

Table 6. The accuracy metrics of NLCD, NWI and GWL_FCS30 using 1835 validation points over the continuous United States

(a) NLCD vs GWLFCS30							
NLCD		NWT	Open water	Woody wetland	Emergent herbaceous wetland	O.A.	Kappa
	U.A.	96.46	93.98	77.92	61.97	83.58	0.756
	P.A.	88.80	53.65	85.96	87.61		
GWL_FCS30		NWT	PW FFT TFT	SWP MGV	MSH SMH	O.A.	Kappa
	U.A.	90.55	94.81	69.87	87.61	85.76	0.786
	P.A.	85.99	95.52	77.97	88.36		
(b) NWI vs GWLFCS30							
NWI		NWT	FPD EMD RVR LKE	FSSW	FEW	EMW	O.A.	Kappa
	U.A.	94.45	94.74	67.58	60.25	85.71	83.49	0.762
	P.A.	84.93	63.32	86.62	82.76	91.53		
GWL_FCS30		NWT	PW	SWP	MSH TFT	MGV SMH TFT	O.A.	Kappa
	U.A.	90.55	94.74	68.96	80.75	90.08	85.23	0.789
	P.A.	85.99	95.45	76.76	78.78	94.98		

Note: NWT: non-wetlands, PW: permanent water, SWP: swamp, MSH: marsh, FFT: flooded flat, SMH: salt marsh, MGV: mangrove forest, TFT: tidal flat, FPD: Freshwater Pond, EMD: Estuarine and Marine Deepwater, RVR: Riverine, LKE: Lake, FSSW: Freshwater Forested/Shrub Wetland, FEW: Freshwater Emergent Wetland, EMW: Estuarine and Marine Wetland, O.A.: overall accuracy, P.A.: producer's accuracy, U.A.: user's accuracy.

Figure 16 illustrated the comparisons between our GWL_FCS30-2020, National Land Cover Database (NLCD) wetland layer and National Wetlands Inventory (NWI) in San Francisco and Florida. It should be noted that the ocean was excluded in the GWL_FCS30-2020 while NLCD and NWI still contained these coastal oceans. Overall, three wetland products performed great spatial consistency and accurately captured the spatial patterns of wetlands over two regions. From the perspective of diversity of wetland sub-category, the GWL_FCS30 and NWI had obvious advantages over the NLCD which simply divided the wetlands into open water, woody wetlands and emergent herbaceous wetlands. Specifically, the NWI had the largest wetland areas in the San Francisco because it included the irrigated cropland (red color) while the other two datasets excluded irrigated cropland. Then, the local enlargement showed that the GWL_FCS30 and NWI also had better performance than NLCD, because they comprehensively captured the coastal tidal wetlands, and our GWL_FCS30 further distinguished the tidal flats and salt marshes which also demonstrated that GWL_FCS30 performed better than NWI over the coastal wetlands. In the Florida, the NWI and GWL_FCS30 accurately divided the inland and coastal wetlands and the GWL_FCS30 further identified the coastal wetlands into the mangrove forest. Meanwhile, the local enlargement also demonstrated the great consistency of three wetland products. However, it can be found that there was obvious difference between GWL_FCS30 and NWI over the wetland categories, in which GWL_FCS30 classified most inland wetlands into marshes while NWI classified them as emergent wetlands and forest/shrub wetlands, mainly because of the differences in the definition of the classification system (GWL_FCS30 defined those low shrubs that grown in the freshwater as marsh, in Table 1).

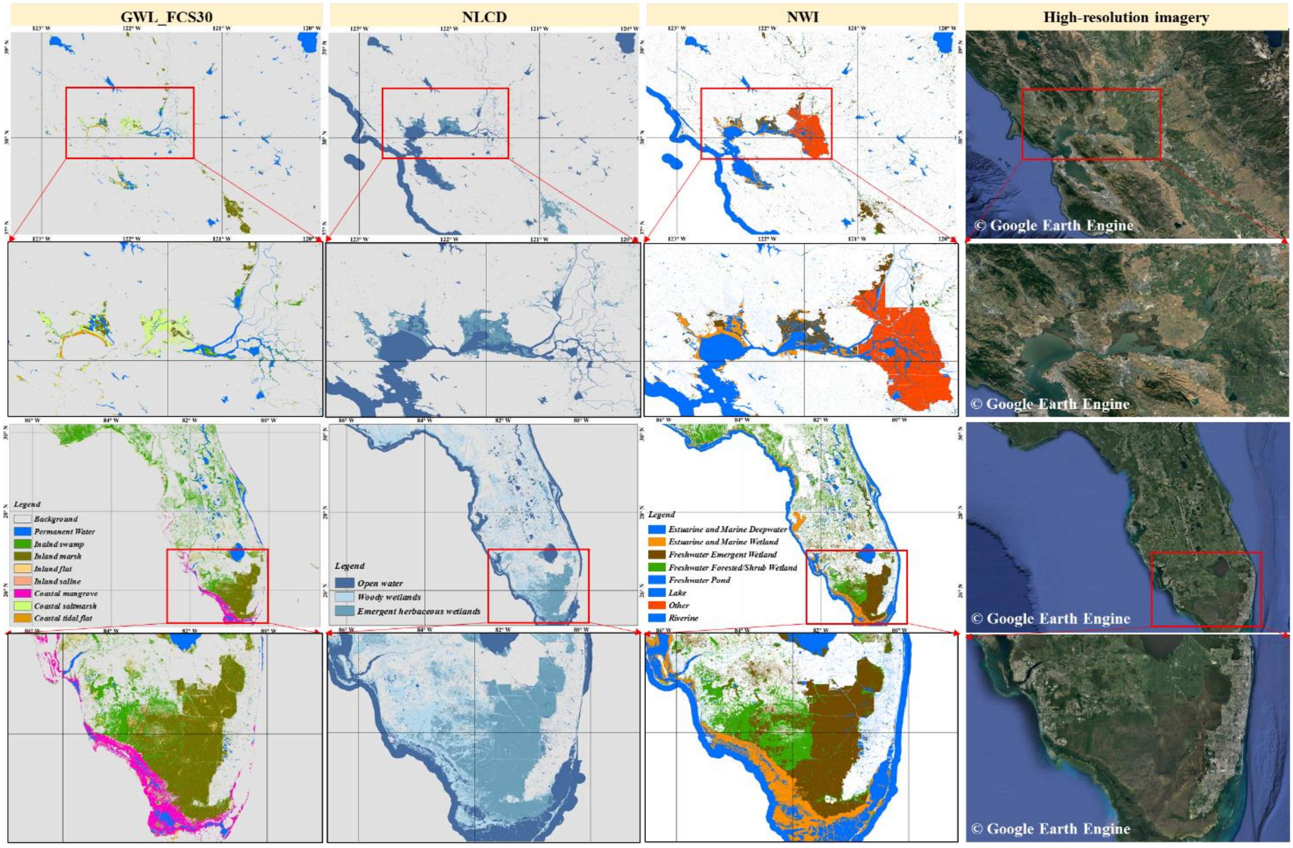

Figure 16. The comparisons between GWL_FCS30 in 2020, National Land Cover Database (NLCD) wetland Layer (Homer et al., 2020) and National Wetlands Inventory (NWI, https://www.fws.gov/program/national-wetlands-inventory, last access: Nov 12, 2022) in San Francisco and Florida. The high-resolution imagery came from the Google Earth Engine platform (https://earthengine.google.com; last access: 12 Nov 2022).

Table 7 illustrated the accuracy metrics of CLC (CORINE Land Cover) and GWL_FCS30 after merging the wetland categories over the European Union area using 1996 validation points from the global validation points in Section 4.3. Overall, the GWL_FCS30 performed better than the CLC and the former mainly had lower commission errors than that of the CLC for salt marsh and tidal flat. To intuitively understand the overestimation of tidal flat, Figure 17 illustrated the comparison between our GWL_FCS30-2020 and CLC wetland layer in 2018 over the Nordic, in which mainly distributed in tidal flats and open water, and these tidal flats gathered around the coastline. In term of specific wetland subcategory, it can be found that the CLC database had larger tidal flat area than that of the GWL_FCS30, however, the lowest tidal-level composite from time-series Landsat imagery indicated that the CLC overestimated the tidal flats in the region. For example, the local enlargement showed that a lot of permanent ocean pixels were wrongly labelled as the tidal flats in CLC and accurately identified as ocean in the GWL_FCS30. The comparison also demonstrated why the CLC had low user's accuracy of 62.90% for tidal flat and producer's accuracy of 57.76% for water bodies. Then, the local enlargement also indicated that the total area of salt marsh in CLC was lower than that of GWL_FCS30 (green rectangles), namely, some salt marshes were wrongly labelled as tidal flat and water body, so the accuracy metrics in Table 7 showed the user’s accuracy of salt marsh in CLC was 35.86%.

Table 7. The accuracy metrics between CLC and GWL_FCS30 after merging the wetland categories

		NWT	WC WB CL ET SO	Peat bogs & Inland marshes	SMH	TFT	O.A.	Kappa
CLC	U.A.	92.94	94.81	68.63	35.86	62.90	80.75	0.706
	P.A.	82.80	57.76	83.93	91.23	75.00		
		NWT	PW	SWP MSH FFT	SMH	TFT	O.A.	Kappa
GWL_FCS30	U.A.	91.22	88.02	80.98	86.21	94.35	88.10	0.816
	P.A.	88.54	97.69	80.82	91.91	97.50		

Note: NWT: non-wetlands, WC: water courses, WB: water bodies, CL: coastal lagoons, ET: estuaries, SO: sea and ocean, PW: permanent water, SWP: swamp, MSH: marsh, FFT: flooded flat, SAL: saline, SMH: salt marsh, MGV: mangrove forest, TFT: tidal flat, O.A.: overall accuracy, P.A.: producer’s accuracy, U.A.: user’s accuracy.

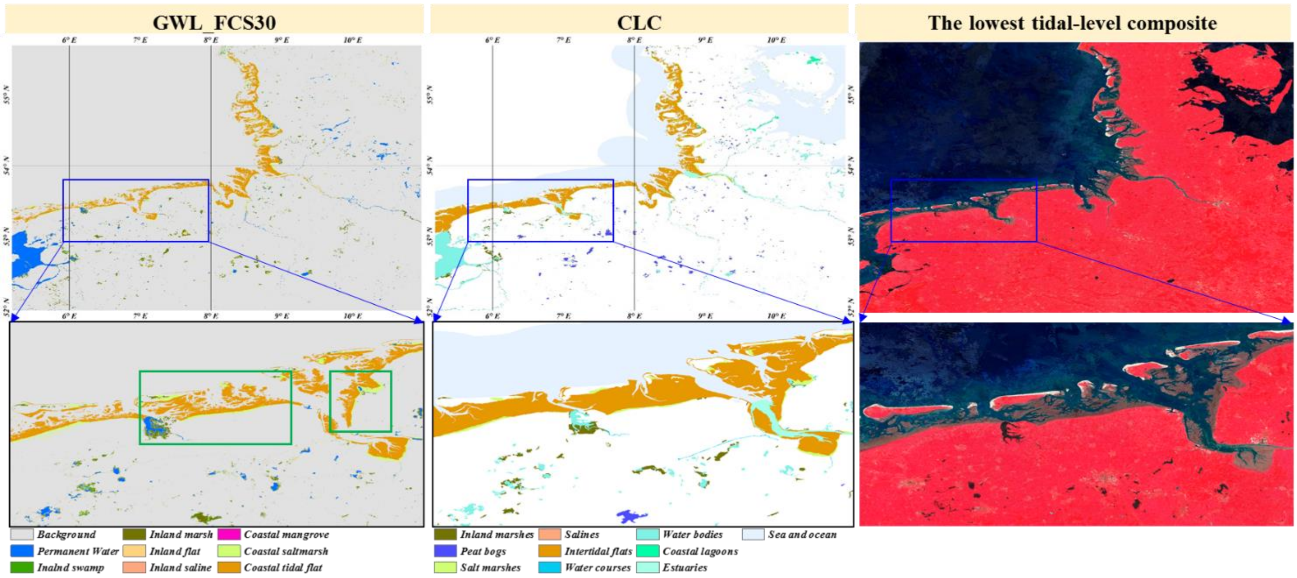

Figure 17. The comparisons between GWL_FCS30 and CORINE Land Cover (CLC) wetland layer in 2018 (https://land.copernicus.eu/pan-european/corine-land-cover/clc2018?tab=metadata, last access: Nov 12, 2022). The lowest tidal-level Landsat composite, composited by NIR, red, and green bands, was illustrated.

Lastly, the Discussion section should focus on their position in the data libraries of the world and not have more results within (e.g., why do they have relatively few wetlands versus other global data?).

Great thanks for the comment. Based on this comment and later suggestions, the two results sections about training samples and feature importance have been moved to the Results Section. The update Discussion section focus on analyzing the performance of GWL_FCS30 with other wetland products (including: inland wetland products, coastal wetland products and national wetland databases).

Ultimately, there’s excitement and possibility with these data – the inclusion of multiple data layers and stacks in a random forest analysis within the GEE is exciting, especially considering the abundance of spatial data available for analyses. Yet while the authors have presented a welcome analysis, I find they leave enough to be desired to suggest a major revision to a) shorten, b) clarify approaches so that they can be repeated, c) appropriately and abundantly defend their approach to not include any open waters as a wetland type (which I do not agree with), d) place their findings against other datasets through accuracy analyses (e.g., CWI, NLCD, NWI, etc.) such that readers can determine that this data layer is better to use than those that have come before. We're lacking that confidence at this juncture, at least from my point of view.

Great thanks for the comments and suggestions.

(a) Since we need to fully consider that the method can be repeated at details and some cross-comparisons also are strengthen by other reviewers' comments, we try our best to shorten some redundant statements in the Method (in Section 4.3 Accuracy Assessment), Results (Section 5.2 Importance of multisourced features) and Discussion (Section 6.1 Cross-comparisons with other global products).

(b) Based on your later comments and suggestions, the method has been greatly strengthen, the details have also been added. The specific revisions have been explained in the following comments.

(c) Based on your comment and later suggestions, the permanent water has been added into our fine wetland system, and the detailed replay has been answered in the Comment 1.

(d) As for the comparisons with other dataset (including: CWI, NLCD and NWI), comparisons at national scale between GWL_FCS30, NWI and NLCD, and CLC databases have been added in the Section 6.2 and the accuracy analyses are also added, and the detailed replay has also been answered in the Comment 3.

Specific comments

L43 Ramsar is a city in Iran and not an abbreviation to be capitalized.

Thanks for the comment. It has been corrected.

L108: Is there indeed "…no 30-m dataset covering both inland and coastal wetlands" until now? One could argue that the authors introduce ~8 different data layers doing that. For instance, the ESA products, the CCI, etc. Tootchi et al. (2019), referenced in this paper, have Table 1, "Summary of water body, wetland, and related proxy maps and datasets from the literature" that summarize the state of the literature in 2019, too. ESA recently released a worldcover database at 10-m – how does this contrast to the authors' analyses (and ESA includes herbaceous wetlands and mangroves as specific land covers; https://esa-worldcover.org/en).

Great thanks for pointing out the inaccurate statement. Yes, the statement in the Line 108 is inaccurate, the sentence has been revised as:

"Due to the complicated temporal dynamics and spatial and spectral heterogeneity of wetlands, there is very few global **thematic** wetland dataset covering both inland and coastal regions **with fine classification system and high spatial resolution**, which cause that global 30 m wetland mapping with a fine classification system remains a challenging task."

In addition, as your mentioned, although the ESA WorldCover dataset contains herbaceous wetlands and mangroves, we find that the herbaceous wetlands suffered serious omission errors and the mangrove layer also had lower performance than the global mangrove thematic datasets. Therefore, we give up to use the ESA WorldCover10 dataset to derive our training samples in this study. And the reasons why the WorldCover10 had poor performance in wetland mapping because **their classification algorithms were not specifically designed for the wetland environment**.

Recently, with the improvement of computing power and storage abilities, three global 30-m land-cover products (including GlobeLand30 (Chen et al., 2015), FROM_GLC (Gong et al., 2013) and GLC_FCS30 (Zhang et al., 2021b)) **and several 10-m land-cover products (WorldCover (Zanaga et al., 2021), Dynamic**

World (Brown et al., 2022) and FROM_GLC10 (Gong et al., 2019)), containing an independent wetland layers, were produced, **but their classification algorithms were not specifically designed for the wetland environment, so the wetland usually suffered from low accuracy in these products**.

L119 Why 2019-2021? I recognize that the authors ended up with nearly 800,000 LS images, yet since the GEE can handle so much, why stop there? It's not a fault, but the authors should explain why this time period was selected versus any other available time period.

Thanks for the comment. We used the time-series Landsat imagery during 2019-2021 for the nominal year of 2020 for **minimizing the influence of frequent cloud contamination in the tropics and snow and ice in the high latitudes.** The reason why we only used the Landsat imagery during 2019~2021 because they can guarantee the sufficient observation even in the tropics illustrated in Figure 1. The reasons have been added as:

"First, all available Landsat imagery during 2019–2021 was obtained for the nominal year of 2020 via the Google Earth Engine platform for minimizing the influence of frequent cloud contamination in the tropics and snow and ice in the high latitudes."

L123 what are saturated pixels? How does CFMask assist that (vs cloud, cloud shadow, and snow)?

Thanks for the comment. The 'saturated pixels' represents these pixels whose surface reflectance exceeds the theoretical value of 1 especially for ETM+ imagery. And the CFmask algorithm has been explained as:

"And these 'bad quality' observations (shadow, cloud, snow, and saturated pixels) in Landsat imagery were masked using CFmask cloud detection method, **which built a series of decision rules, using temperature, spectral variability, brightness and geometric relationship between cloud and shadow, to identify these 'poor quality' pixels and achieved the overall accuracy of 96.4%** (Zhu et al., 2015; Zhu and Woodcock, 2012)"

L124 Which Landsat platforms were used? Which LS satellite data were used? What sort of processing was done on the LS images? Which bands were used? Etc. etc.

Thanks for the comment. The Landsat 7 ETM+ and Landsat 8 OLI imagery are used, and the pro-processing order in the Landsat imagery has been introduced in the manuscript as: 1) atmospheric correction using LaSRC method; 2) masking 'poor quality' observations using Fmask method.

all available Landsat imagery, including Landsat 7 ETM+ and Landsat 8 OLI missions, during 2019–2021 was obtained for the nominal year of 2020 via the Google Earth Engine platform for minimizing the influence of frequent cloud contamination in the tropics and snow and ice in the high latitudes. To minimize the effect of atmosphere, each Landsat image was **atmospherically corrected** to the surface reflectance by the United States Geological Survey using Land Surface Reflectance Code (LaSRC) method (Vermote et al., 2016) and then archived on the GEE platform. And these **'bad quality' observations** (shadow, cloud, snow, and saturated pixels) in Landsat imagery were masked using CFmask cloud detection method, which built a series of decision rules, using temperature, spectral variability, brightness and geometric relationship between cloud and shadow, to identify these 'poor quality' pixels and achieved the overall accuracy of 96.4% (Zhu et al., 2015; Zhu and Woodcock, 2012).

Then, in this study, six optical bands, including: blue, green, red, NIR (near infrared), SWIR1 (Shortwave Infrared 1) and SWIR2 (Shortwave Infrared 2), are used. The supplement information has been added as:

In this study, six optical bands, including: blue, green, red, NIR (near infrared), SWIR1 (shortwave infrared 1) and SWIR2 (shortwave infrared 2) bands, were used for wetland mapping. Totally, 764,239 Landsat scenes, including Landsat 7 ETM+ and Landsat 8 OLI missions, were collected to capture various water-level and phenological features presented in Section 4.

L125 LS images were used to select the "water level" or the presence of inundation as inferred from reflectance values?

Great thanks for the comment. Yes, we used multitemporal compositing method from time-series Landsat imagery to capture the highest water-level and lowest water-level composites according to the spectral characteristics of water body and other land-cover types. It has been detailedly descripted in the Section 4.1, for example, the figure 4 illustrated the presence of inundation status in the Poyang Lake using time-series Landsat imagery.

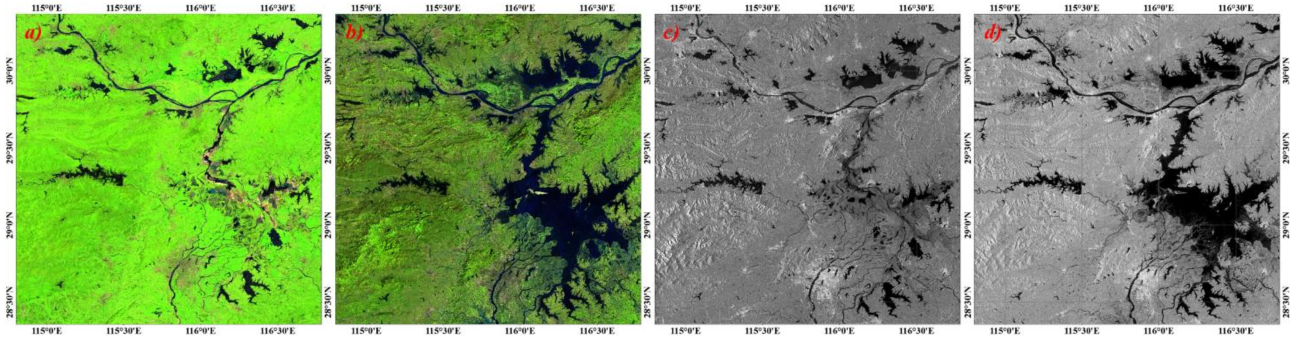

Figure 4. The lowest and highest water-level features derived from (a-b) time-series Landsat optical reflectance data and (c-d) the Sentinel-1 SAR imagery using the time-series compositing method in Poyang Lake, China.

L126 These are not necessarily clear sky, but they are images that passed through the CFMask filter. Please clarify in text.

Great thanks for pointing out the mistake. Yes, **all Landsat imagery** during 2019-2021 were used and then these 'poor quality' pixels would be masked using CFmask method.

The Figure 1 illustrated the availability of clear-sky observations after masking 'poor quality' pixels, namely, we actually count the frequency of these clear observations at each pixel instead of the frequency of Landsat scenes. So, the statement has been revised as:

Figure 1a illustrates the spatial distribution of all clear-sky observations for all Landsat scenes, and it can be seen that there were more than 10 clear observations after masking these 'poor quality' observations at each region even if in the tropics.

L135 How did the authors discern what were sufficient Sentinel-1 images to "capture the temporal dynamics of wetlands"? What are those temporal dynamics? Seasonal? Intermittent inundation from rainstorms? Please clarify in text.

Great thanks for the comment. As Sentinel-1 SAR platform is **immune to the cloud and shadow and has a revisit cycle of 6 days**, the time-series Sentinel-1 imagery in 2020 are sufficient to capture water-level dynamics. The "temporal dynamics" refers to the water-level dynamics. The statement has been revised as:

Figure 1b also illustrates the spatial distribution of all available Sentinel-1 SAR imagery, there were enough Sentinel-1 SAR observations in each area to capture the water-level dynamics of wetlands **because it was immune to the cloud and shadow and had a revisit time of 6 days after launching the Sentinel-1B mission**.

L138 How were the ASTER data used as ancillary information? Please specify how these data on slope, aspect, etc. were used here for the purposes of the paper.

Great thanks for the comment. The elevation, slope and aspect, derived from the ASTER dataset, are the input features to train the random forest models, because many studies have demonstrated that the topography would directly affect the spatial distribution of wetlands, which are mainly distributed in low-lying areas. It has been explained as:

Figure 3 illustrates the flowchart of the proposed method for generating the global 30-m fine wetland maps. First, we combined the time-series Landsat-8, Sentinel-1 SAR observations and ASTER DEM topographical image to derive multisource and multitemporal features including: various water-level, phenological and **three topographical features**. Then, the training samples (coastal tidal, inland wetlands and no-wetlands) and **derived multisource and multitemporal features** were combined to train the stratified random forest classifiers (a classic and widely used machine learning classification model (Breiman, 2001)) at each local region. Next, using the trained random forest models and derived multisource and multitemporal features, we could develop corresponding coastal tidal wetland and inland wetland maps.

As I see later that it was used in the random forest, the authors need to introduce to the readers that a random forest approach is used and conduct a literature review noting the utility of random forest and limitations.

Thanks for the comment. The random forest approach is a classic and widely used machine learning method, it has been reviewed in many studies (Gislason et al., 2006; Belgiu et al., 2016; Boulesteix et al., 2012), so it was not the focus of this article. The disadvantages and disadvantages of random forest are listed below:

The advantages of the random forest has been introduced in the manuscript as: 1) dealing with high-dimensional data, 2) robustness for training noise and feature selection, 3) achieving higher classification when compared to other widely used machine learning classifiers.

Afterward, the random forest (RF) classifier was demonstrated to have obvious advantages including: **dealing with high-dimensional data, robustness for training noise and feature selection, as well as achieving higher classification when compared to other widely used machine learning classifiers (e.g., support vector machines, neural networks, decision trees, etc.)** (Belgiu and Drăguţ, 2016; Gislason et al., 2006).

As for the disadvantages of the RF are: 1) it surely does a good job at classification but not as for regression problem as it does not gives precise continuous nature prediction; 2) it can feel like a black box approach for a statistical modelers we have very little control on what the model does. **However, these two drawbacks can be ignored for land-cover classifications, so it is currently the most popular machine learning algorithm and is widely used in land cover classifications at various scale (region, nation, continent and globe).**

Gislason, P. O., Benediktsson, J. A., and Sveinsson, J. R.: Random Forests for land cover classification, Pattern Recognition Letters, 27, 294-300, https://doi.org/10.1016/j.patrec.2005.08.011, 2006.

Belgiu, M. and Drăguţ, L.: Random forest in remote sensing: A review of applications and future directions, ISPRS Journal of Photogrammetry and Remote Sensing, 114, 24-31, 2016.

Boulesteix, Anne‐Laure, et al. "Overview of random forest methodology and practical guidance with emphasis on computational biology and bioinformatics." Wiley Interdisciplinary Reviews: Data Mining and Knowledge Discovery 2.6 (2012): 493-507.

L142 Figure 1 would be much clearer if it were a vertical panel of a) over b) versus a) next to b). Please modify. Also please change the caption to clarify that that images were not necessarily ‘clear sky’ but did otherwise pass the CFMask filter. See, e.g., L395.

Great thanks for the suggestion. The layout of the figure has been revised as:

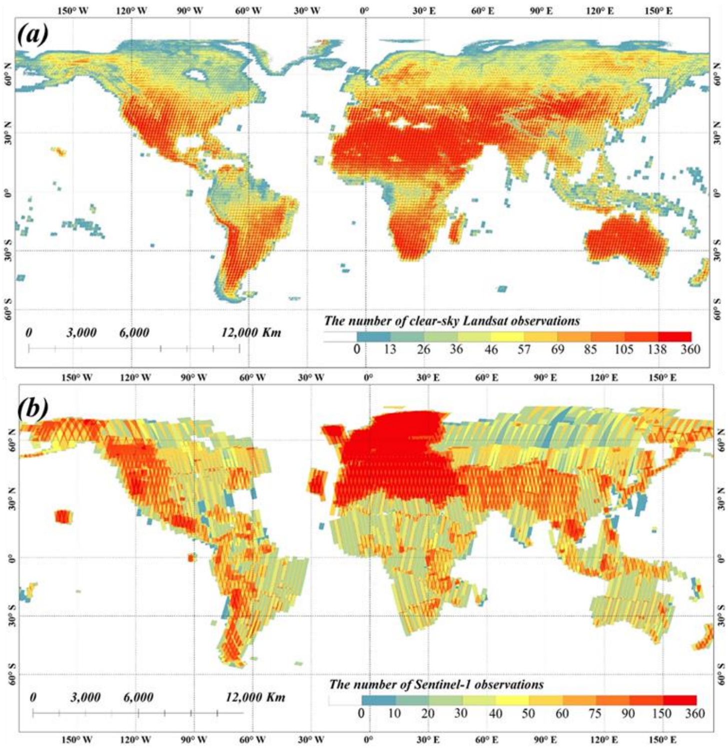

Figure1. The spatial distribution of clear observations after masking these ‘poor quality’ observations during 2019-2021 (a), and availability of time-series Sentinel-1 SAR observations in 2020 (b).

L165 The JRC_GSW data layer does not identify wetlands per se but identifies inundated pixels. Therefore it is inaccurate to say that the JRC captured “wetlands around rivers, ponds, etc.” because the data layer would include rivers and ponds – or any pixel that was deemed to be inundated by the Pekel et al. (2016) algorithm. Please revise to acknowledge these data from Pekel identify inundated pixels.

Great thanks for the comment and suggestion. Yes, the statement in manuscript is inaccurate, and JRC_GSW dataset is used to identify these inundated pixels, so it has been revised as:

The JRC_GSW dynamic water dataset achieved a producer accuracy of 98.5% for these seasonal waters (Pekel et al., 2016) and was used to **identify inundated pixels.**

Note this also comes up with L281 wherein the authors state they are “excluding permanent water bodies”. Why? Permanent water bodies are a massive abundance of the global wetland data layers (e.g., in addition to the Ramsar Convention definition used earlier, see also

Davidson, N. C. 2014. How much wetland has the world lost? Long-term and recent trends in global wetland area. Marine and Freshwater Research65: 934-941

Dixon, M. J. R. et al.2016. Tracking global change in ecosystem area: the Wetland Extent Trends index. Biological Conservation 193: 27-35

Hu, S. et al.2017. Global wetlands: Potential distribution, wetland loss, and status. Science of the Total Environment586: 319-327

Thanks for the comment. Based on your useful suggestion, the permanent water has been added in our wetland classification system as:

The inland wetland types shared similar characteristics and were grouped into swamp, marsh, and flooded flat. Meanwhile, in order to capture saline soils and halophytic plant species along saline lakes, the inland saline wetland, inherited from the Global Lakes and Wetlands Dataset (GLWD) (Lehner and Döll, 2004), was also imported. Lastly, the permanent water, including lakes, rivers and streams that are always flooded, was widely identified as a wetland layer in previous studies (Davidson, 2014; Dixon et al., 2016; Hu et al., 2017b).

Table 2. The description of wetland classification system in this study

Category I	**Category II**	**Description**
Tidal wetland	Mangrove	The forest or shrubs which grow in the coastal blackish or saline water
	Salt marsh	Herbaceous vegetation (grasses, herbs and low shrubs) in the upper coastal intertidal zone
	Tidal flat	The tidal flooded zones between the coastal high and low tide levels including mudflats and sandflats.
Inland wetland	Swamp	The forest or shrubs which grow in the inland freshwater
	Marsh	Herbaceous vegetation (grasses, herbs and low shrubs) grows in the freshwater
	Flooded flat	The non-vegetated flooded areas along the rivers and lakes
	Saline	Characterized by saline soils and halophytic (salt tolerant) plant species along saline lakes
	Permanent water	**Lakes, rivers and streams that are always flooded**

L169 Table 1 – considering this product is a global data layer, it would be useful to the readers to see the relative abundance of wetlands that each of these named datasets have identified. Furthermore, it's important to note if indeed these are global products (versus near-global products, such as those within the latitudinal bands of 60N and 60S, for instance). Also convert the arc-seconds to meters (at the equator) for consistency between the data products.

Great thanks for the comment. The total area and spatial coverage of these prior wetland datasets has been added and the arc-second unit has been converted to length unit as:

Table 1. The characteristics of 13 global wetland products with various spatiotemporal resolutions (unit of area: million km^2)

Dataset name and reference	**Wetland categories**	**Year**	**Resolution**	**Total area**	**Coverage**
World atlas of mangroves (WAM) Spalding (2010)	Mangrove	2010	1:1000000	0.152	Global
Global mangrove watch (GWM) Thomas et al. (2017)		1996-2016	~25m	~0.136	Global
A global biophysical typology of mangroves (GBTM) Worthington et al. (2020)		1996-2016	~25m	~0.136	Global
Continuous global mangrove forest cover (CGMFC)		2000-2010	30 m	0.083	Global

Hamilton and Casey (2016)					
Global distribution of mangroves USGS (GDM_USGS) Giri et al. (2011)		2011	30 m	~0.138	Global
Global distribution of tidal flat ecosystems Murray et al. (2019)	Tidal flat	1984-2016	30 m	0.124~0.132	60°S~60°N
Global distribution of saltmarsh McOwen et al. (2017)	Salt marsh	1973-2015	1:10,000	~0.05	Global
Tropical and subtropical wetland distribution Gumbricht (2015)	Open water, mangrove, swamps, fens, riverine, floodplains, marshes	2011	~231 m	4.7	60°S~40°N
Global lakes and wetlands database (GLWD) Lehner and Döll (2004)	Lake, reservoir, river, marsh, swamps, coastal wetland, saline wetland, and peatland	2004	~1 km	10.7–12.7	Global
JRC-GSW Pekel et al. (2016)	Water	1984-2021	30 m	~4.46	Global
ESA CCI_LC Defourny et al. (2018)	Swamps, mangrove, and Shrub or herbaceous cover wetlands	1992-2020	300 m	6.1	Global
GlobeLand30 Chen et al. (2015)	Wetland	2000-2020	30 m	7.01~7.17	Global
GLC_FCS30 Zhang et al. (2021b)	Wetland	2015, 2020	30 m	6.36	Global

L189 How many of the 18,701 data validation points did NOT have complete agreement between the five validation experts? Noting here that 8,355 points were used to discern amongst the seven classes of wetlands. Relative to the other possible ways to assess their study – and convince people to use it – this number of validation points is very small. Too small, by my assessment.

Great thanks for the comment. Approximately 1/10 validation points (1291points) have been discarded because of the disagreement between five interpreters. Yes, we agree that a large amount of validation points play great role in comprehensively assess the performance of the developed products, however, it should be noted that the collection of validation points, especially for water-level sensitive wetlands with fine classification system, is time-consuming and labor-intensive. In addition, Foody et al. (2009) and Olofsson et al. (2014) had detailedly described how to determine the size of total validation points by using stratified random sampling theory as:

$$n = \frac{\left(\sum W_h \sqrt{p_h(1-p_h)}\right)^2}{V + \sum W_h P_h(1-P_h)/N}$$

where N is the number of pixel units in the study region; V is the standard error of the estimated overall accuracy that we would like to achieve, $V = (d/t)^2$ (t = 1.96 for a 95% confidence interval, t = 2.33 for a 97.5% confidence interval, and d is the desired half-width of the confidence interval); W_h is the weight distribution of class h; p_h is the producer's accuracy. These sample size calculations should be repeated for a variety of choices of V and p_h before reaching a final decision. We try to achieve producer's accuracies of 0.9 of non-wetland class and 0.8 of the seven wetland classes. Meanwhile, using the parameters of d = 0.0125, t = 2.33, the sample size can be determined as approximately 18500. In addition, there is a little uncertainty for interpreting the validation points, so we randomly generate 20000 validation points over the globe and then discard 1299 uncertain points (these disagreement points over five experts), so a total of 18701 validation points are used to assess the GWL_FCS30-2020 performance.

In order to make the validation assessment more comprehensive, we also replenish 7008 wetland validation points, including 212 non-wetland points and 6796 wetland points, and the description of these updated global validation points (25709 points) has been revised as:

To quantitatively analyze the performance of our GWL_FCS30 wetland map, a total of 25,709 validation samples, including 10,558 non-wetland points and 15,151 wetland points, were collected by combining high-resolution imagery, time-series Landsat and Sentinel observations and visual interpretation method. Firstly, as the wetland was sparse land-cover type compared to the non-wetlands (forest, cropland, grassland and bare land), the stratified random strategy was applied to randomly derive validation points at each strata. Then, as the wetlands had significant correlation with the water levels (Zhang et al., 2022b), the time-series optical observations archived on the GEE cloud platform were used as the auxiliary dataset to interpret these water-level sensitive wetlands such as: tidal flat and flooded flat. It should be noted that the visual interpretation was implemented on the GEE cloud platform because it archives a large amount of satellites imagery with various time spans and spatiotemporal resolution (Zhang et al., 2022a). Meanwhile, each validation point is independently interpreted by five experts for minimizing the effect of expert's subjective knowledge, and only these complete agreement points were retained otherwise they were discarded. Figure 6 intuitively illustrated the spatial distribution of global wetland validation points, it can be found that the distribution of wetland points accurately revealed the spatial patterns of global wetlands.

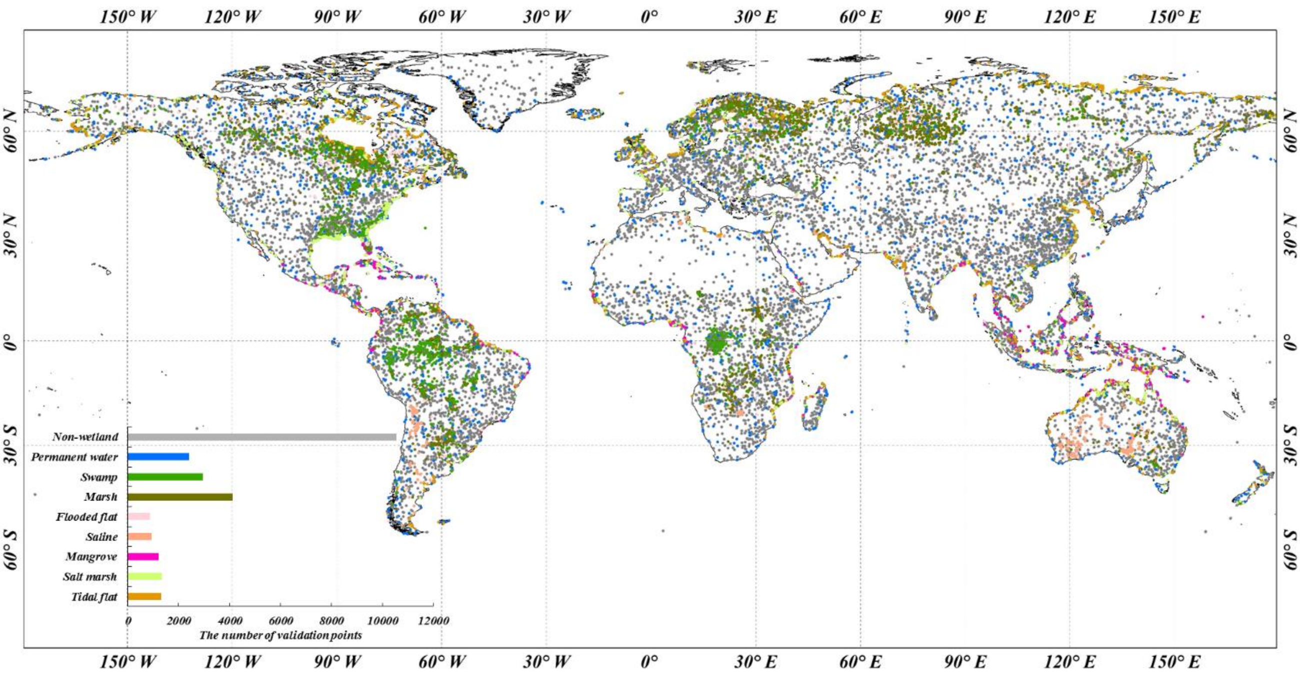

Figure 6. The spatial distribution of 25,709 global wetland validation samples using stratified sampling strategy.

L207 There are many wetland definitions. That the Ramsar definition is quoted, noting that it includes waters to the depth of 6 m, suggests that open waters should be a wetland type in this analysis. I recognize that flooded flats – located along rivers and lakes – are included. But what of lakes themselves? Ponds? Smaller waters that are important to the global wetland data layer? Are these considered lakes? This is an important factor to consider when assessing global wetland coverage.

Great thanks for the comment. Based on your suggestion, the open waters have been included in our updated wetland classification system as the "permanent water", which mainly includes lakes, rivers and streams that are always flooded. The revised wetland classification system as:

The inland wetland types shared similar characteristics and were grouped into swamp, marsh, and flooded flat. Meanwhile, in order to capture saline soils and halophytic plant species along saline lakes, the inland saline wetland, inherited from the Global Lakes and Wetlands Dataset (GLWD) (Lehner and Döll, 2004), was also imported. **Lastly, the permanent water, including lakes, rivers and streams that are always flooded, was widely identified as a wetland layer in previous studies (Davidson, 2014; Dixon et al., 2016; Hu et al., 2017b).**

Table 2. The description of wetland classification system in this study

Category I	Category II	Description
Tidal wetland	Mangrove	The forest or shrubs which grow in the coastal blackish or saline water
	Salt marsh	Herbaceous vegetation (grasses, herbs and low shrubs) in the upper coastal intertidal zone
	Tidal flat	The tidal flooded zones between the coastal high and low tide levels including mudflats and sandflats.
Inland wetland	Swamp	The forest or shrubs which grow in the inland freshwater
	Marsh	Herbaceous vegetation (grasses, herbs and low shrubs) grows in the freshwater
	Flooded flat	The non-vegetated flooded areas along the rivers and lakes
	Saline	Characterized by saline soils and halophytic (salt tolerant) plant species along saline lakes
	Permanent water	**Lakes, rivers and streams that are always flooded**

Another consideration would be submergent vegetation. The marsh class is noted as including grasses, herbs, and low shrubs. What about, say, ponds covered with Nymphaea spp (lily pads)? What about Potamogeton spp. growing submersed in the water? Are these not wetland species? Wetland scientists would say they are. Here's a good reference in re: this discussion:

Richardson, D. C., et al. 2022. A functional definition to distinguish ponds from lakes and wetlands. Scientific Reports 12(1): 10472.

Great thanks for the comment. Yes, we agree the submergent vegetation can be considered as a special wetland sub-category, however, the remote sensing observations have poor ability to penetrate water body and then capture these underground vegetation characteristics. Namely, we cannot identify these submergent vegetation at global scale using remote sensing observations, therefore, our future work would pay attention on these special wetland categories, it has been added in the Discussion as:

Then, in this study, we combined the multisourced wetland products and their practical use for ecosystem management to define a fine wetland classification system containing eight sub-categories, however, there are still many wetland sub-categories, such as: submergent vegetation (nymphaea), groundwater-dependent wetlands (karst and cave systems) and seagrass beds (Richardson et al., 2022), cannot be captured because remote sensing observations usually had poor performance on penetrating water body and then capturing underwater characteristics, and there was currently no prior dataset for global underwater wetlands. So, our further work would pay attention to combine multisourced auxiliary datasets, such as hydrological data, bathymetry depth and climate data, for targeted monitoring these special wetland sub-categories.

L252 Provide a number of LS images used for this analysis.

Thanks for the comment. The total number of Landsat imagery for distinguish salt marsh and tidal flat is 140902, it also added in the manuscript as:

as a tidal flat is a non-vegetated coastal wetland, we combined the empirical rule (EVI $\geqslant$ 0.1, NDVI $\geqslant$ 0.2, and LSWI > 0) proposed by Wang et al. (2020) and time-series Landsat imagery in 2020 **(approximately 142 thousand Landsat scenes)** to exclude all vegetated pixels from tidal flat training samples.

L257 Clarify – 50 km buffer along the coastal zone between 60N – 90N are salt marsh? That seems to be quite excessive, a 50 km buffer. Please clarify.

Great thanks for the comment. The 50 km buffer is only the maximum boundary for tidal flat and salt marsh between 60N – 90N, namely, the both of them are impossible to be outside this buffer area. Actually, we then used the classification method to identify these salt marsh and tidal flat pixels within the region.

In addition, as for the buffer radius of 50 km, it is used in the works of Wang et al. (2020) and (Murray et al., 2019)) for tidal flat mapping.

Wang, X., Xiao, X., Zou, Z., Hou, L., Qin, Y., Dong, J., Doughty, R. B., Chen, B., Zhang, X., Chen, Y., Ma, J., Zhao, B., and Li, B.: Mapping coastal wetlands of China using time series Landsat images in 2018 and Google Earth Engine, ISPRS J Photogramm Remote Sens, 163, 312-326, https://doi.org/10.1016/j.isprsjprs.2020.03.014, 2020.

Murray, N. J., Phinn, S. R., DeWitt, M., Ferrari, R., Johnston, R., Lyons, M. B., Clinton, N., Thau, D., and Fuller, R. A.: The global distribution and trajectory of tidal flats, Nature, 565, 222-225, https://doi.org/10.1038/s41586-018-0805-8, 2019.

The description about the 50 km buffer has been strengthened in the manuscript as:

therefore, we used the coastal shorelines ($Line_{coastal}$) to create a 50 km buffer (applied by the Wang et al. (2020) and (Murray et al., 2019)) as the potential tidal flat zones in the high latitude regions (>60°N) as in Eq. (2). It should be noted that we only identified and retained these tidal flat pixels within the maximum extents by using the classification models in the Section 4.2.

L258 What's the proportion of overlap between the different data layers? A spatial correlation table/matrix should be presented to the readers (see, e.g., Tootchi et al. 2019, supplemental information Table S1).

Thanks for the comment. The overlap proportions of 6 coastal wetland products have been calculated in the Table S1 as:

Table S1. The overlap proportions of six coastal wetland products

	GDM_USGS	GWM	GBTM	WAM	McOwen's saltmarsh	Murry's tidalflat
GDM_USGS	1.000	0.775	0.776	0.700	0.027	0.147
GWM	0.828	1.000	0.997	0.788	0.031	0.155
GBTM	0.825	0.992	1.000	0.787	0.032	0.154

WAM	0.661	0.697	0.699	1.000	0.024	0.134
McOwen's saltmarsh	0.073	0.081	0.082	0.071	1.000	0.151
Murry's tidalflat	0.153	0.152	0.152	0.148	0.057	1.000

L270 These data were imported…and what was done with them?

Thanks for the comment. How to import the CCI_LC, GLC_FCS30 and GlobeLand30 has been added as:

as the wetland layer in the global land-cover products (GLC_FCS30, GlobeLand30, and CCI_LC) also covered some coastal wetlands, the saline-water wetland layer in the CCI_LC and the wetland data closed to the coastal shorelines in other two products were also imported as supplement when determining the maximum coastal wetland extents.

L296 The GLWD data are at 1 km pixel. How did the authors include 1 km data plus all the 30-m data products? What's the final resolution of these data? Also, what's the proportion of the overlap between them (a spatial correlation table/matrix would be interesting here).

Thanks for the comment. The GLWD, TROP-SUBTROP Wetland, CCI_LC, with spatial resolutions of 231m~1 km, are resampled to 30 m using the nearest neighbor sampling method on the GEE platform, thus, the derived maximum inland wetland extends is the spatial resolution of 30 m.

Specifically, the consistency analysis of five global wetland datasets (TROP-SUBTROP Wetland, GLWD, CCI_LC, GlobeLand30, and GLC_FCS30) and the temporal stability checking for CCI_LC (1992–2020), GlobeLand30 (2000-2020) and GLC_FCS30 (2015-2020) were applied to identify these temporally stable and high cross-consistency wetland points ($P_{inlandWet}^{Tstable,Scons}$). **It should be noted that the coarse wetland products (GLWD, TROP-SUBTROP and CCI_LC) were resampled to 30 m using the nearest neighbor method on the GEE platform.**

Then, overlap proportions of 6 inland wetland products have been calculated in the Table S2 as:

Table S2. The overlap proportions of six inland wetland products

	CIFOR	GLWD	JRC-GSW	CCI_LC	GlobeLand30	GLC_FCS30
CIFOR	1.000	0.406	0.172	0.341	0.213	0.194
GLWD	0.105	1.000	0.186	0.343	0.234	0.215
JRC-GSW	0.093	0.386	1.000	0.434	0.135	0.108
CCI_LC	0.132	0.513	0.308	1.000	0.187	0.160
GlobeLand30	0.223	0.957	0.223	0.487	1.000	0.817
GLC_FCS30	0.231	0.992	0.235	0.496	0.897	1.000

L338 This is the first time that the use of random forest was noted.

Thanks for the comment. The random forest classification model is a classic and widely used machine learning classifier for land-cover mapping. To make readers to understand the random forest, it has been explained as:

Figure 3 illustrates the flowchart of the proposed method for generating the water-level, phenological and three topographical features and producing the global 30-m fine wetland maps using the stratified random forest (**a classic and widely used machine learning classification model (Breiman, 2001)**) modeling strategy.

Breiman, L.: Random Forests, Machine Learning, 45, 5-32, https://doi.org/10.1023/a:1010933404324, 2001.

In L138, I questioned how the ASTER data were used – I suggest revising the methods to introduce the reader early on to the overall approach (i.e., letting them know that the RF algorithm was used).

Great thanks for the comment. The ASTER GDEM elevation and derived slope and aspect were used as auxiliary information for training the random forest classification models, and further used as the auxiliary features for wetland mapping. Based on your suggestion, we briefly introduced the overall approach in Section 4 as:

Figure 3 illustrates the flowchart of the proposed method for generating the global 30-m fine wetland maps. **First, we combined the time-series Landsat-8, Sentinel-1 SAR observations and ASTER DEM topographical image to derive multisource and multitemporal features including: various water-level, phenological and three topographical features. Then, the training samples (coastal tidal, inland wetlands and no-wetlands) and derived multisource and multitemporal features were combined to train the stratified random forest (a classic and widely used machine learning classification model (Breiman, 2001)) models at each local region. Next, using the trained random forest models and derived multisource and multitemporal features, we could develop corresponding coastal tidal wetland and inland wetland maps. Finally, the post-processing step was used to generate the global 30 m fine wetland map in 2020.**

L341 Figure 4 the use of the ASTER DEM includes slope and aspect? Or was slope and DEM used? If the DEM was used, what information within the DEM was used? See, e.g., L400.

Great thanks for pointing out the mistake in the Figure 4. We used three topographical variables (elevation, slope and aspect) derived from the ASTER DEM dataset. The revised figure 4 as:

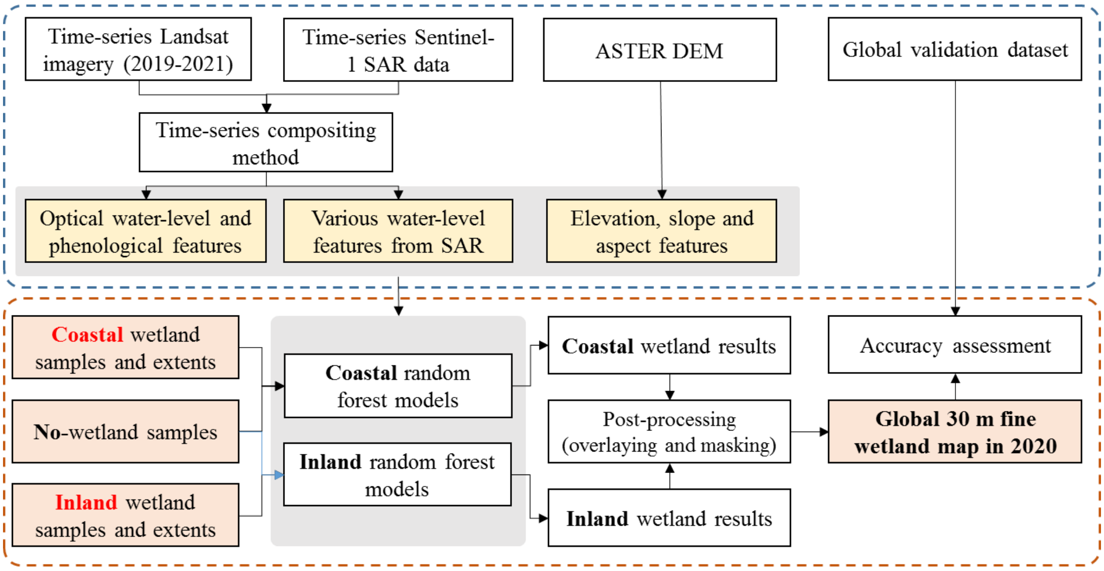

Figure 3. The flowchart of wetland mapping using water-level, phenological and topographical features and a stratified classification strategy.

Furthermore, the Landsat and Sentinel data were used for identifying inundated pixels. NOT for identifying water levels. I recommend changing the heading title in 4.1 as well.

Great thanks for the comment. We used the time-series Landsat imagery to simultaneously capture the water-level composites (the highest and lowest water-level composites) and **multitemporal phenological information** (five temporal percentiles), and used the time-series Sentinel-1 SAR imagery to capture the water-level composites (the highest and lowest water-level composites). Then, the inundated pixels could be identified by combining the highest and lowest water-level composites in the optical and SAR composites. So, we still think use the "**Generating various water-levels and phenological composites**" might be more suitable.

L393 Ultimately, why were five LS clusters chosen versus three or just the one? Was parsimony considered in the analyses?

Great thanks for the comment. The reasons why we used five percentiles are: 1) the five percentiles had greater performance on capture phenological variability than three and one percentiles, which also suggested by our previous study in Xie et al. (2021); 2) if we used the seasonal compositing method can generate four seasonal composites, we used five percentiles to better capture the phenological variability; 3) these five LS percentiles are used in many phenological-based studies (Hansen et al., 2014; Zhang and Roy, 2017).

This study composited time-series Landsat reflectance bands and four spectral indexes into five percentiles (15th, 30th, 50th, 70th and 85th) **because we wanted to capture as much of the phenological changes in wetlands as possible when comparing to the four seasonal composites (Zhang and Roy, 2017).**

Yes, we consider the parsimony using percentile-based compositing method for capturing phenological variability when comparing with seasonal-based method. It has been explained in the manuscript as:

Azzari and Lobell (2017) quantitatively analyzed the performance of two compositing methods and found that both of them had similar mapping accuracy for land-cover mapping. Meanwhile, the seasonal-based compositing method needed the prior phenological calendar, while the percentile compositing method did not require any prior knowledge or explicit assumptions regarding the timing of the season.

Xie, S.; Liu, L.; Yang, J. Time-Series Model-Adjusted Percentile Features: Improved Percentile Features for Land-Cover Classification Based on Landsat Data. Remote Sens. 2020, 12, 3091. https://doi.org/10.3390/rs12183091

Hansen, M. C., Egorov, A., Potapov, P. V., Stehman, S. V., Tyukavina, A., Turubanova, S. A., Roy, D. P., Goetz, S. J., Loveland, T. R., Ju, J., Kommareddy, A., Kovalskyy, V., Forsyth, C., and Bents, T.: Monitoring conterminous United States (CONUS) land cover change with Web-Enabled Landsat Data (WELD), Remote Sensing of Environment, 140, 466-484, https://doi.org/10.1016/j.rse.2013.08.014, 2014.

Zhang, H. K. and Roy, D. P.: Using the 500 m MODIS land cover product to derive a consistent continental scale 30 m Landsat land cover classification, Remote Sensing of Environment, 197, 15-34, https://doi.org/10.1016/j.rse.2017.05.024, 2017.

L404 This assumes that the maximum extent of the coastal wetlands (equation 1 for mangroves) has zero omission error. I understand why this was done, yet it requires explanation and accounting for the reader here and possibly in the Discussion section as well.

Thanks for the suggestion. The assumption has been added as:

Since we have simultaneously extracted the maximum coastal and inland wetland extents when deriving training samples from prior wetland datasets, the stratified classification strategy was adopted to fully use the maximum extent constraint. Namely, if a pixel was classified as a coastal wetland outside the maximum coastal wetland extents, it would be identified as a misclassification. I**n other words, we assumed there was zero omission error for these derived maximum wetland extents in Eq. (1-3) by merging several prior wetland products**.

In the Discussion Section, the maximum extents of the inland and coastal wetlands have also been added and discussed as:

In addition, we used the derived maximum extents as the boundary for identifying inland and coastal tidal wetlands, in other words, we assumed that the derived maximum extents contained all inland and coastal wetlands with zero omission error. Actually, the inland maximum extents in Eq. (3) fulfilled the assumption (zero omission error), because the GLWD and TROP-SUBTROP products, produced by the compilation and model simulation method (Gumbricht, 2015; Lehner and Döll, 2004), can capture almost all wetland areas at the expense of a higher commission error. For example, the Figure 13 illustrated the cross-comparisons between our GWL_FCS30 wetland maps with four existing wetland products, and the GLWD obviously overestimated the inland wetlands. On the other hand, the union of five global wetland datasets in Eq. (3) also minimized the omission error of each dataset for inland wetland sub-categories. As for the mangrove forest, due to the high producer and user accuracies of five prior mangrove products (explained in Section 2.2), the derived maximum mangrove extents (Eq. (1)) can covered almost all mangrove forests because the missed mangroves maybe complemented by other products. Recently, Bunting et al. (2022) developed the newest mangrove products covering 1996-2020, it can be used as the important prior dataset in our further works for deriving the maximum mangrove extents. However, the zero omission error assumption maybe run into problem when targeting tidal flat and saltmarsh. Specifically, the global tidal flat dataset only covered the period of 1984~2016 and the producer's accuracy of tidal flat was 83.0%. Although we used the union operations for time-series Murray's tidal flats during 1984~2016 (Eq. (2)) to include these potential tidal flats, the newly increased tidal flats during 2016-2020 and missed tidal flats in time-series products would be missed in our maximum tidal flat extents in Eq. (2). Fortunately, the new time-series global tidal flat products during 1999-2019 (Murray et al., 2022), which greatly improved the mapping accuracy based on previous time-series tidal flat products, can be used as prior datasets. Lastly, as the global saltmarsh products were sparse, the maximum extents of tidal flat salt marsh were combined for saltmarsh mapping in Section 3.1. However, there was still missed a lot of saltmarshes, so our further work would pay more attention on accurately saltmarsh mapping.

L410 The local adaptive modeling section is too quickly glossed over. Explain more on how this was done. How were the data trained? What were the specifications of the training here? It would be hard for others to replicate the process based on the data provided thus far.

Great thanks for pointing out the problem. The description of the local adaptive modeling has been greatly strengthen as:

Since we have simultaneously extracted the maximum coastal and inland wetland extents when deriving training samples from prior wetland datasets, the stratified classification strategy was adopted to fully use the maximum extent constraint. Namely, if a pixel was classified as a coastal wetland outside the maximum coastal wetland extents, it would be identified as a misclassification. In other words, we assumed there was zero omission error for these derived maximum wetland extents in Eq. (1-3) by merging several prior wetland products. Furthermore, there were two ideas for the large-area land-cover mapping including global classification modeling (using one universal model for the whole areas) and local adaptive modeling (using various models for different local zones) (Zhang et al., 2020). For example, Zhang and Roy (2017) demonstrated that local adaptive modeling outperformed the global classification modeling strategy. Therefore, the global land surface was first divided into 961 5° × 5° geographical tiles illustrated in Figure 5, which were inherited from the global 30 m land-cover mapping by (Zhang et al., 2021b). Then, we trained the local adaptive classification models using derived training samples in Section 3 and multisource and multitemporal features (the highest, lowest water-level and phenological composites and topographical variables) at each 5° × 5° geographical tile. It should be noted that we used the training samples from neighboring 3 × 3 geographical tiles to train the classification model and classify the central tile for guaranteeing the spatially continuous transition over adjacent regional wetland maps. Namely, we trained 961 local adaptive classification models and then produced 961 5° × 5° wetland maps. Finally, we spatially mosaiced these 961 regional wetland maps into the global 30 m fine wetland map in 2020.

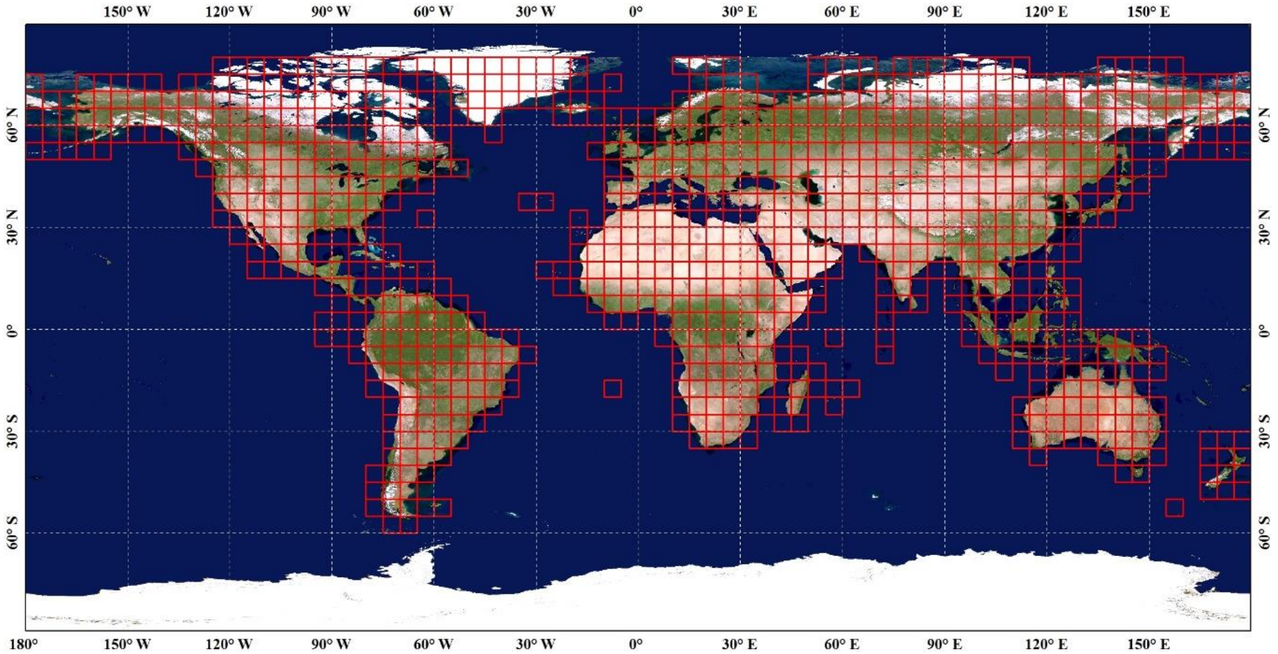

Figure 5. The spatial distribution of 961 5° × 5° geographical tiles used for local adaptive modeling, which was inherited from the global 30 m land-cover mapping by (Zhang et al., 2021b). The background imagery came from the National Aeronautics and Space Administration (https://visibleearth.nasa.gov, last access: 10 Nov 2022).

How many of the 961 5x5 tiles had zero coverage of wetlands (e.g., mid-ocean tiles)?

Thanks for the comment and interesting question. According to our statistics, there was 41 5x5 tiles had zero coverage of wetlands.

L413 What statistical program was used to conduct the RF analyses? Furthermore, while RF may have advantageous, it also has detractions. Please introduce the "obvious advantageous" for those who are not aware as well as mention some of the drawbacks.

Thanks for the comment. The RF analysis has been conducted on the GEE platform.

Therefore, the RF classifier was selected for mapping inland and coastal tidal wetlands using multi-sourced features **on the GEE platform**.

The advantages of the RF have been listed in the manuscript as: 1) dealing with high-dimensional data, 2) robustness for training noise and feature selection, 3) achieving higher classification when compared to other widely used machine learning classifiers.

Afterward, the random forest (RF) classifier was demonstrated to have obvious advantages including: **dealing with high-dimensional data, robustness for training noise and feature selection, as well as achieving higher classification when compared to other widely used machine learning classifiers** (e.g., support vector machines, neural networks, decision trees, etc.) (Belgiu and Drăguţ, 2016; Gislason et al., 2006).

As for the disadvantages of the RF are: 1) it surely does a good job at classification but not as for regression problem as it does not gives precise continuous nature prediction; 2) it can feel like a black box approach for a statistical modelers we have very little control on what the model does. **However, these two drawbacks can be ignored for land-cover classifications, so it is currently the most popular machine learning algorithm and is widely used in land cover classifications at various scale (region, nation, continent and globe).**

L435 Note that 18k samples were analyzed across the globe. Consider the relative dearth noted in Figure 2 (see summary above).
Great thanks for the comment. Yes, a large amount of validation points can more comprehensively evaluate the performance of developed GWL_FCS30 dataset. However, as mentioned before, the size of validation points in this study is determined by using the stratified random sampling theory proposed by the Foody et al. (2009) and Olofsson et al. (2014) as:

$$n = \frac{\left(\sum W_h \sqrt{p_h(1-p_h)}\right)^2}{V + \sum W_h P_h(1-P_h)/N}$$

where N is the number of pixel units in the study region; V is the standard error of the estimated overall accuracy that we would like to achieve, $V = (d/t)^2$ (t = 1.96 for a 95% confidence interval, t = 2.33 for a 97.5% confidence interval, and d is the desired half-width of the confidence interval); W_h is the weight distribution of class h; p_h is the producer's accuracy. These sample size calculations should be repeated for a variety of choices of V and p_h before reaching a final decision. We try to achieve producer's accuracies of 0.9 of non-wetland class and 0.8 of the seven wetland classes. Meanwhile, using the parameters of d = 0.0125, t = 2.33, the sample size can be determined as approximately 18500.

Based on your suggestion, we also replenish 7008 wetland validation points, including 212 non-wetland points and 6796 wetland points, so the updated global validation dataset contains 25709 validation points.

L461 The authors need to introduce Figures 7-10 before introducing Figure 11.
Thanks for the comment. Yes, we first introduce Figure 7-10 and then introduce Figure 11.

L538 The point behind the Ramsar Convention's of 6 m was to address depths that diving birds were expected/known to use aquatic systems. It is disingenuous to state that all permanent water bodies have depths >=6 m. This is a possibly fatal flaw in this analysis.
Great thanks for pointing out the issue. The statement has been removed in the revised manuscript, and there was no water depth database derived from remote sensing imagery until now, so the permanent water bodies are also included in the updated GWL_FCS30 products. The statement has been revised as:
To comprehensively understand the performance of the GWL_FCS30 wetland maps, four existing global wetland datasets (GLC_FCS30, GlobeLand30, CCI_LC, and GLWD), listed in Table 1, were selected. Figure 12 quantitatively illustrates the total wetland area of five products over each continent. Specifically, the total wetland area of different wetland products varied. The GLWD obviously overestimated the wetland area on each continent mainly because it was derived from the compilation model instead of actual remote sensing observations (Lehner and Döll, 2004). Namely, the GLWD classified a large amount of non-wetlands as potential wetlands. The remaining four wetland products, derived from the Landsat and PROBE-V remote sensing imagery, shared a total wetland area of 4.128~7.364 million km^2, and our GWL_FCS30 wetland dataset

had the total area of 6.347 million km^2 among these datasets. The CCI LC wetland layer contained the smallest wetland area of 4.128 million km2, and the estimated area in North America was profoundly lower than the other datasets, mainly because the CCI LC heavily underestimated the wetland distribution in Canada after a comparison with the Canadian Wetland Inventory (Amani et al., 2019). Next, the total wetland area in GlobeLand30 and GLC_FCS30 wetland layer was higher than the developed GWL_FCS30 wetland dataset because some water-level sensitive non-wetlands (such as: irrigated cropland) were also captured in these two datasets.

L555 It would be good to see the analyses done in Table 4 for these two areas shown in Figure 10. For instance, the authors have chosen to not include permanent water as a wetland type but yet show 'water body' in their panel map, which implies it was correctly mapped yet it is not a land use type they map.
Great thanks for the comment. Based on your suggestion in previous comments, the 'permanent water body' has been added into our fine classification system.

L576 Figure 10 the panel caption for GWL_FCS30 doesn't match the panel (GWM_FCS30).
Great thanks for pointing out the mistake. The mistake has been corrected.

L630 These selected training sample results should be in the Results section, not here.
Great thanks for the suggestion. This section has moved to the Results Section 5.1.

L634 Was this inclusion of steps noted in the methods? I don't recall it.
Great thanks for the comment. The reliability analysis of the training samples was not included in the method, because the specific processing flow has been explained in this section as:
To demonstrate the reliability of the derived training samples for wetland mapping, we randomly selected approximately 10,000 points from the sample pool and checked their confidence using visual interpretation. It should be noted that we cannot check all the training samples because the number of derived samples was massive (exceeding 20 million training samples in Section 3). After a point-to-point inspection, these selected training samples achieved an overall accuracy of 91.53% in 2020. Meanwhile, we also used 10,000 selected wetland training samples and many non-wetland samples to analyze overall and producer's accuracies of coastal and inland wetlands versus number of erroneous training samples. Specifically, we gradually increased the "contaminated" samples by randomly altering the label of a certain percentage of training samples in steps of 0.01, and then used these "contaminated" samples to build the RF classification model.

L675 These are results and need to be in that section explaining the outcomes of the RF analysis.
Great thanks for the suggestion. This section has moved to the Results Section 5.2.

GWL_FCS30: global 30 m wetland map with fine classification system using multi-sourced and time-series remote sensing imagery in 2020

Xiao Zhang[1, 2], Liangyun Liu[1, 2, 3, *], Tingting Zhao[1, 4], Xidong Chen[5], Shangrong Lin[6], Jinqing Wang[1, 2, 3], Jun Mi[1, 2, 3] and Wendi Liu[1, 2, 3]

1 International Research Center of Big Data for Sustainable Development Goals, Beijing 100094, China

2 Key Laboratory of Digital Earth Science, Aerospace Information Research Institute, Chinese Academy of Sciences, Beijing 100094, China

3 School of Electronic, Electrical and Communication Engineering, University of Chinese Academy of Sciences, Beijing 100049, China

4 College of Geomatics, Xi'an University of Science and Technology, Xi'an 710054, China

5 North China University of Water Resources and Electric Power, Zhengzhou 450046, China

6 School of Atmospheric Sciences, Southern Marine Science and Engineering Guangdong Laboratory (Zhuhai), Sun Yat-sen University, Zhuhai 519082, Guangdong, China

* Corresponding author Email: liuly@radi.ac.cn

Abstract

Wetlands, often called the "kidneys of the earth", play an important role in maintaining ecological balance, conserving water resources, replenishing groundwater, and controlling soil erosion. Wetland mapping is very challenging because of its complicated temporal dynamics and large spatial and spectral heterogeneity. An accurate global 30-m wetland dataset that can simultaneously cover inland and coastal zones is lacking. This study proposes a novel method for wetland mapping by combining an automatic sample extraction method, multisource existing products, time-series satellite images, and a stratified classification strategy. This approach allowed for the generation of the first global 30-m wetland map with a fine classification system (GWL_FCS30), including ~~four~~ five inland wetland sub-categories (permanent water, swamp, marsh, flooded flat, and saline) and three ~~coastal wetland~~coastal tidal wetland sub-categories (mangrove, salt marsh, and tidal flats), which was developed using Google Earth Engine platform. We first combined existing multi-sourced global wetland products, expert knowledge, training sample refinement rules, and visual interpretation to generate a large and geographically distributed wetland training samples. Second, we integrated the time-series Landsat reflectance products and Sentinel-1 SAR imagery to generate various water-level and phenological information to capture the complicated temporal dynamics and spectral heterogeneity of wetlands. Third, we applied a stratified classification strategy and the local adaptive random forest classification models to produce the wetland dataset with a fine classification system at each 5°×5° geographical tile in 2020. Lastly, the GWL_FCS30, mosaicked by 961 5°×5° regional wetland maps, was validated using ~~18,701~~25,708 validation samples, which achieved an overall accuracy of ~~87~~86.~~7~~44% and a kappa coefficient of 0.~~810~~822. The cross-comparisons with other global wetland products demonstrated that the GWL_FCS30 dataset performed better in capturing the spatial patterns of wetlands and had significant advantages over the diversity of wetland subcategories. The statistical analysis showed that the global wetland area reached ~~3.57~~6.38 million km^2, including ~~3.10~~6.03 million km^2 of inland wetlands and 0.~~47~~ 35 million km^2 of ~~coastal wetland~~coastal tidal wetlands, approximately ~~62.3~~72.96% of which were distributed poleward of 40°N. Therefore, we can conclude that the proposed method is suitable for large-area wetland mapping and that the GWL_FCS30 dataset is an accurate wetland mapping product that has the potential to provide vital support for wetland management. The GWL_FCS30 dataset in 2020 is freely available at https://doi.org/10.5281~~/~~/zenodo.7340516~~zenodo.6575731~~ (Liu et al. 2022).

1. Introduction

The ~~RAMSAR~~ Ramsar Convention defines a wetland as an "areas of marsh, fen, peatland or water, whether natural or artificial, permanent or temporary, with water that is static or flowing, fresh, brackish or salt, including areas of marine water the depth of which at low tide does not exceed six meters" (Gardner and Davidson, 2011). Wetlands not only provide humans with a large amount of food, raw materials and water resources (Ludwig et al., 2019; Zhang et al., 2022b) but also play an important role in maintaining ecological balance, conserving water resources, replenishing groundwater, and controlling soil erosion (Hu et al., 2017a; Mao et al., 2021; Wang et al., 2020; Zhu and Gong, 2014). Therefore, they are also called the "kidneys of the earth" (Guo et al., 2017). However, due to increasing human activities, including agriculturalization, industrialization and urbanization (McCarthy et al., 2018; Xi et al., 2020), and climatic changes such as sea-level rise and coastal erosion (Cao et al., 2020; Wang et al., 2021), wetlands have been seriously degraded and threatened over the past few decades (Mao et al., 2020). Thus, having access to timely and accurate wetland mapping information is pivotal for protecting biodiversity and supporting the sustainable development goals.

Along with the rapid development of remote sensing techniques and computing abilities, a variety of regional or global wetland datasets have been produced with spatial resolutions ranging from 30 m to 1° (~112 km) (Chen et al., 2022; Gumbricht et al., 2017; Lehner and Döll, 2004; Mao et al., 2020; Matthews and Fung, 1987; Tootchi et al., 2019). Recently, Tootchi et al. (2019) and Hu et al. (2017a) have systematically reviewed the generation process of global wetland datasets with various spatial and temporal resolutions and wetland categories and found significant uncertainties and inconsistencies among these datasets. For example, the global total wetland area reviewed by Hu et al. (2017a) ranged from 2.12 to 7.17 million km^2 based on remote sensing products. Therefore, great uncertainties among global wetland datasets directly hindered wetland applications and analysis. Furthermore, from the perspective of spatial resolution, although many wetland products have been produced, at regional or global scales, using various remote sensing imagery and different methods (Guo et al., 2017; Tootchi et al., 2019), most of them were coarse spatial resolution datasets, ranging from 100 m to 25 km. Recently, with the improvement of computing power and storage abilities, three global 30-m land-cover products (including GlobeLand30 (Chen et al., 2015), FROM_GLC (Gong et al., 2013) and GLC_FCS30 (Zhang et al., 2021c)) and several 10-m land-cover products (WorldCover (Zanaga et al., 2021), Dynamic World (Brown et al., 2022) and FROM_GLC10 (Gong et al., 2019)), containing an independent wetland layers, were produced, but their classification algorithms were not specifically designed for the wetland environment, so the wetland usually suffered from low accuracy in these products. In addition, several global ~~coastal wetland~~coastal tidal wetland products have been developed, including the global mangrove extent (Bunting et al., 2018; Hamilton and Casey, 2016) and global 30 m tidal flat datasets from 1984 to 2016 (Murray et al., 2019), but these only covered the intertidal zones. Thus, an accurate global 30 m thematic wetland dataset, with fine wetland categories and covering both inland and coastal zones, is still lacking.

One of the largest challenges of current state-of-the-art methods for large-area wetland mapping is to collect massive amount of training samples (Liu et al., 2021; Ludwig et al., 2019). Zhang et al. (2021b) mentioned two options for collecting training samples, including the visual interpretation method and deriving training samples from pre-existing products. First, since the visual interpretation method had significant advantage over the confidence of training samples, it was widely used for local or regional wetland mapping (Amani et al., 2019; Wang et al., 2020). However, collecting accurate and sufficient training samples is usually a time-consuming process and involves a large amount of manual work, so it was impractical and nearly impossible to use the visual interpretation for collecting global wetland samples. Comparatively, deriving training samples from existing products and applying some rules or refinement methods to identify these high confidence samples from existing products shows promise (Zhang et al., 2021c). So this approach is practical in that it could quickly large and geographically diverse distribution of training samples without much manual effort. Thus, the second option attached increasing attention and has been successfully used for large-area land-cover mapping (Zhang and Roy, 2017; Zhang et al., 2021c; Zhang et al., 2020). For example, Zhang et al. (2021b) used derived global training samples from the combination of the CCI_LC and MCD43A4 NBAR datasets to produce a global 30-m land-cover product with a fine classification system in 2015 and 2020 (GLC_FCS30) with an overall accuracy of 82.5%. Therefore, if we take effective measures to fuse these existing products and then derive high confidence training samples using some refinement rules, the deriving approach would exude great potential for global wetland mapping.

Another major challenge inherent to wetland mapping is the complicated temporal dynamics and spatial and spectral heterogeneity. The spectral characteristics of the wetlands would quickly change with the seasonal or daily water levels of the underlying surface (Ludwig et al., 2019; Mahdianpari et al., 2020). Therefore, many studies proposed to combine multi-sourced, time-series remote sensing imagery for capturing the spatial extent and temporal dynamics of wetlands (LaRocque et al., 2020; Ludwig et al., 2019; Murray et al., 2019; Wang et al., 2021; Zhang et al., 2022b). For example, Zhang et al. (2022b) and Murray et al. (2019) used the time-series Landsat imagery to generate tidal-level and phenological features for identifying ~~coastal wetland~~coastal tidal wetlands and successfully produced the ~~coastal wetland~~coastal tidal wetlands in China with an overall accuracy of 97.2% (Zhang et al., 2022b) and global trajectory tidal flats with the overall map accuracy of 82.3% (Murray et al., 2019). Except for optical imagery, synthetic aperture radar (SAR) data, which was sensitive to soil moisture, vegetation structure, and inundation, enabled data acquisition regardless of solar illumination, clouds, or haze and was also widely used for wetland mapping, especially after the open-access of Sentinel-1 data became available (Li et al., 2020; Slagter et al., 2020; Zhang et al., 2018). For example, Li et al. (2020) used the time-series Sentinel-1 imagery to discriminate wetlands with and without trees and achieved an overall accuracy of 86.0±0.2%. Therefore, the fusion of multi-sourced and time-series remote sensing imagery is vital for accurate wetland mapping.

Due to the complicated temporal dynamics and spatial and spectral heterogeneity of wetlands, there is very few global thematic wetland dataset covering both inland and coastal regions with fine classification system and high spatial resolution, which also cause that global 30 m wetland mapping with a fine classification system remains a challenging task. ~~Consequently, there is no global 30-m dataset covering both inland and coastal wetlands until now.~~ In this study, we combined several existing wetland products and multi-sourced time-series remote sensing imagery to (1) derive a large and geographically distributed wetland training samples from multi-sourced pre-existing global wetland products to minimize the manual participation; (2) develop a robust method to capture the temporal dynamics of wetlands and then produce the first global 30-m wetland dataset with a fine classification system (GWL_FCS30); (3) quantitatively analyze the spatial distribution of different wetland categories and assess the accuracy of the GWL_FCS30 in 2020.

2. Datasets

2.1 Multi-sourced remote sensing imagery

Three types of remote sensing imagery were collected to capture the temporal dynamics and spatial and spectral heterogeneity of wetlands. These include Landsat optical data, Sentinel-1 SAR, and ASTER GDEM topographical data. First, all available Landsat imagery, including Landsat 7 ETM+ and Landsat 8 OLI missions, during 2019–2021 was obtained for the nominal year of 2020 via the Google Earth Engine platform for minimizing the influence of frequent cloud contamination in the tropics and snow and ice in the high latitudes. To minimize the effect of atmosphere, each Landsat image was atmospherically corrected to the surface reflectance by the United States Geological Survey using Land Surface Reflectance Code (LaSRC) method (Vermote et al., 2016) and then archived on the GEE platform. And these 'bad quality' observations (shadow, cloud, snow, and saturated pixels) in Landsat imagery were masked using CFmask cloud detection method, which built a series of decision rules, using temperature, spectral variability, brightness and geometric relationship between cloud and shadow, to identify these 'poor quality' pixels and achieved the overall accuracy of 96.4% (Zhu et al., 2015; Zhu and Woodcock, 2012). In this study, six optical bands, including: blue, green, red, NIR (near infrared), SWIR1 (shortwave infrared 1) and SWIR2 (shortwave infrared 2) bands, were used for wetland mapping. Totally, 764,239 Landsat scenes were collected to ~~extract~~ capture ~~the~~ various water-level and phenological features according to the spectral characteristics of various land-cover types, presented in Section 4. Figure 1a illustrates the spatial distribution of all clear-sky ~~Landsat imagery~~observations for all Landsat scenes,~~.~~ and ~~–~~i~~I~~t can be seen that there were more than 10 ~~Landsat~~ clear observations after masking these 'poor quality' observations at each ~~scene~~region even if in ~~, including~~ the tropics.

Then, the Sentinel-1 SAR data, which was demonstrated to be sensitive to the soil moisture, vegetation structure, and inundation information (Li et al., 2020), used dual-polarization C-band backscatter coefficients to measure the incident microwave radiation scattered by the land surface (Torres et al., 2012). This study obtained the time-series Sentinel-1 imagery archived on the GEE platform in 2020 in Interferometric Wide Swath mode with a dual-polarization of VV and VH. Notably, all Sentinel-1 SAR imagery on the GEE platform has been pre-processed by the Sentinel-1 Toolbox with thermal noise removal, radiometric calibration, and terrain correction using 30-m elevation data (Veci et al., 2014). Figure 1b also illustrates the spatial distribution of all available Sentinel-1 SAR imagery,~~. We found that~~ there were enough Sentinel-1 SAR observations in each area to capture the ~~temporal~~ water-level dynamics of wetlands because it was immune to the cloud and shadow and had a revisit time of 6 days after launching the Sentinel-1B mission. Lastly, as many studies have demonstrated that the topography would directly affect the spatial distribution of wetlands, which are mainly distributed in low-lying areas (Hu et al., 2017b; Ludwig et al., 2019; Tootchi et al., 2019), the ASTER GDEM elevation and derived slope and aspect were used as auxiliary information for wetland mapping. It had a spatial resolution of 30 m and covered the entire global land area (Tachikawa et al., 2011a). Quantitative assessment indicated that the GDEM achieved an absolute vertical accuracy of 0.7 m over bare areas and 7.4 m over forested areas (Tachikawa et al., 2011b).

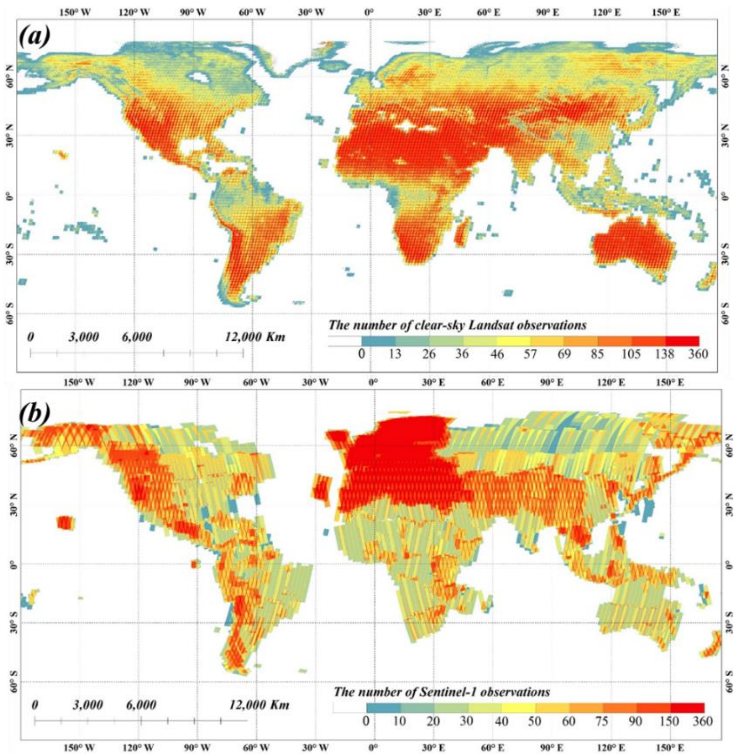

Figure1. The ~~availability~~ spatial distribution of clear~~-sky Landsat~~ observations after masking these ‘poor quality’ observations during 2019-2021 ~~–~~(a), and availability of time-series Sentinel-1 SAR observations ~~imagery~~in 2020 (b).

2.2 Global prior wetland datasets

To achieve the goal of deriving a large and geographically diverse distribution of training samples with minimum manual labor, we propose combining various prior global wetland datasets for generating high-confidence training samples. Table 1 lists the characteristics of several global wetland datasets. Specifically, we collected five global mangrove forest products with different spatial resolutions and time spans, and all of them achieved desirable accuracy. For example, the Global Mangrove Watch (GMW) was validated to reach an overall accuracy of 95.25%, and the user and producer accuracies of mangrove forest were 97.5% and 94.0%, respectively (Thomas et al., 2017). Furthermore, to derive the samples of salt marsh and tidal flats, we collected the time-series global 30-m tidal flats products from 1984 to 2016 with an interval of three years, achieving an overall map accuracy of 82.3% (Murray et al., 2019). The global salt marsh dataset, containing 350,985 individual occurrence polygon shapefiles, helped generate the global salt marsh estimation (McOwen et al., 2017).

Except for the ~~coastal wetland~~coastal tidal wetland products, two thematic wetland products (TROP-SUBTROP Wetland and GLWD contained various wetland sub-categories), three global land-cover products (GlobeLand30, GLC_FCS30, and CCI_LC contained an independent layer), and the time-series 30-m water dynamic dataset (JRC_GSW) were combined to determine the inland maximum wetland extents and generate the wetland training samples after using a series of refinement rules given in Section 3. Specifically, the TROP-SUBTROP was produced by combining the hydrological model and annual time series of soil moisture, mainly covering the tropics and sub-tropics (40°N ~ 60°S) with a resolution of 231 m (Gumbricht, 2015). The GLWD, combining the GIS functionality and a variety of existing maps and information, was developed with 12 wetland sub-categories at a resolution of 1 km (Lehner and Döll, 2004). The JRC_GSW dynamic water dataset achieved a producer accuracy of 98.5% for these seasonal waters (Pekel et al., 2016) and was used to identify inundated pixels~~capture those wetlands around rivers, ponds, etc~~. Furthermore, three global land-cover products, simultaneously containing wetland layer and non-wetland land-cover types, were used to determine the non-wetland samples and then served as the auxiliary datasets to improve the confidence of inland wetland samples.

Table 1. The characteristics of 13 global wetland products with various spatiotemporal resolutions (unit of area: million km^2)~~.~~

Dataset name and reference	**Wetland categories**	**Year**	**Resolution**	**Total area**	**Coverage**
World atlas of mangroves (WAM) Spalding (2010)	Mangrove	2010	~~1:1,000,000~~ 1:1000000	0.152	Global
Global mangrove watch (GWM) Thomas et al. (2017)	Mangrove	1996-2016	~25m~~0.8 seconds~~	~0.136	Global
A global biophysical typology of mangroves (GBTM) Worthington et al. (2020)	Mangrove	1996-2016	~~0.8 seconds~~~25 m	~0.136	Global
Continuous global mangrove forest cover (CGMFC) Hamilton and Casey (2016)	Mangrove	2000-2010	30 m	0.083	Global
Global distribution of mangroves USGS (GDM_USGS) Giri et al. (2011)	Mangrove	2011	30 m	~0.138	Global
Global distribution of tidal flat ecosystems Murray et al. (2019)	Tidal flat	1984-2016	30 m	0.124~0.132	60°S~60° N
Global distribution of saltmarsh McOwen et al. (2017)	Salt marsh	1973-2015	1:10,000	~0.05	Global
Tropical and subtropical wetland distribution (CIFOR) Gumbricht (2015)	Open water, mangrove, swamps, fens, riverine, floodplains, ~~and~~ marshes	2011	~231 m	4.7	60°S~40° N
Global lakes and wetlands database (GLWD) Lehner and Döll (2004)	Lake, reservoir, river, marsh, swamps, ~~coastal wetland~~coastal tidal wetland, saline wetland, and peatland	2004	~~30 second(~~~1 km~~)~~	10.7~12.7	Global
JRC-GSW Pekel et al. (2016)	Water	1984-2021	30 m	~4.46	Global
ESA CCI_LC Defourny et al. (2018)	Swamps, mangrove, and Shrub or herbaceous cover wetlands	1992-2020	300 m	6.1	Global
GlobeLand30 Chen et al. (2015)	Wetland	2000-2020	30 m	7.01~7.17	Global
GLC_FCS30 Zhang et al. (2021b)	Wetland	2015, 2020	30 m	6.36	Global

2.3 Global 30 m tree cover product

The global 30-m forest cover change in tree cover (GFCC30TC) data in 2015 was produced by downscaling the 250-m MODIS VCF (Vegetation Continuous Fields) tree cover product using Landsat imagery and then incorporating the MODIS cropland layer to guarantee the tree cover accuracy in agricultural areas (Sexton et al., 2016; Sexton et al., 2013). This product was used to accurately distinguish between inland swamp and marsh wetlands because both of them reflected obvious vegetation spectra characteristics. It was validated to achieve an overall accuracy of 91%; the average producer and user accuracy for stable forests were 92.5% and 95.4%, respectively (Sexton et al., 2016; Townshend et al., 2012).

2.4 National wetland products

Three national wetland products including: NLCD (National Land Cover Database) (Homer et al., 2020), NWI (National Wetlands Inventory) (Wilen and Bates, 1995) and CLC (CORINE Land Cover) (Büttner, 2014), were used as the comparative datasets to analyze the performance of developed global wetland maps in Section 6.2. Specifically, the NLCD contained open water, woody wetlands and emergent herbaceous wetlands, the NWI contained eight sub-categories (estuarine and marine deep-water, estuarine and marine wetland, freshwater emergent wetland, freshwater forest/shrub wetland, freshwater pond, lake, other, and Riverine), and the CLC identified the wetlands into nine sub-categories as: inland marshes, peat bogs, salt marshes, saline, intertidal flats, water courses, water bodies, coastal lagoons, estuaries, as well as sea and oceans.

~~Global wetland validation dataset~~

3. Collecting training samples and determining maximum wetland extents

In this study, after considering the applicability of moderate resolution (10–30 m) imagery, their practical use for ecosystem management, and the available pre-existing global wetland dataset, the fine wetland classification system, containing ~~seven~~ eight sub-categories (three coastal tidal sub-categories and ~~four~~ five inland sub-categories), was proposed to comprehensively depict the spatial patterns of global wetlands (Table 2). Specifically, the sub-categories of coastal tidal wetlands consist of mangroves, salt marshes, and tidal flats. By importing the vegetation and water cover information associated with this land cover, these categories were widely recognized in many previous studies (Wang et al., 2021; Zhang et al., 2022b). The inland wetland types shared similar characteristics and were grouped into swamp, marsh, and flooded flat. Meanwhile, ~~Except for the freshwater-related wetlands~~in order to capture saline soils and halophytic plant species along saline lakes, the inland saline wetland, inherited from the Global Lakes and Wetlands Dataset (GLWD) (Lehner and Döll, 2004), was also imported~~ to capture saline soils and halophytic plant species along saline lakes~~. Lastly, the permanent water, including lakes, rivers and streams that are always flooded, was widely identified as a wetland layer in previous studies (Davidson, 2014; Dixon et al., 2016; Hu et al., 2017b) and was also added into our fine wetland classification system.

Table 2. The description of wetland classification system in this study

Category I	Category II	Description
	Mangrove	The forest or shrubs which grow in the coastal blackish or saline water
~~Coastal~~ Tidal wetland	Salt marsh	Herbaceous vegetation (grasses, herbs and low shrubs) in the upper coastal intertidal zone
	Tidal flat	The tidal flooded zones between the coastal high and low tide levels including mudflats and sandflats.
	Swamp	The forest or shrubs which grow in the inland freshwater
Inland wetland	Marsh	Herbaceous vegetation (grasses, herbs and low shrubs) grows in the freshwater

	Flooded flat	The non-vegetated flooded areas along the rivers and lakes
	Saline	Characterized by saline soils and halophytic (salt tolerant) plant species along saline lakes
	Permanent water	Lakes, rivers and streams that are always flooded

Many studies have explained that the quality and confidence of training samples directly affected the classification performance (Zhang et al., 2021b; Zhu et al., 2016). The previously mentioned process of collecting sufficient training samples via visual interpretation was time-consuming and involved a lot of manual labor. Fortunately, a variety of regional and global wetland products have been developed and released over the past few decades (Table 1), and many studies have demonstrated that deriving training samples from existing products could be used for large-area classification and mapping (Huang et al., 2021; Zhang et al., 2021b). Therefore, we propose to combine existing global wetland datasets to independently derive coastal/inland wetland training samples and their maximum distribution extents (Figure ~~3~~2).

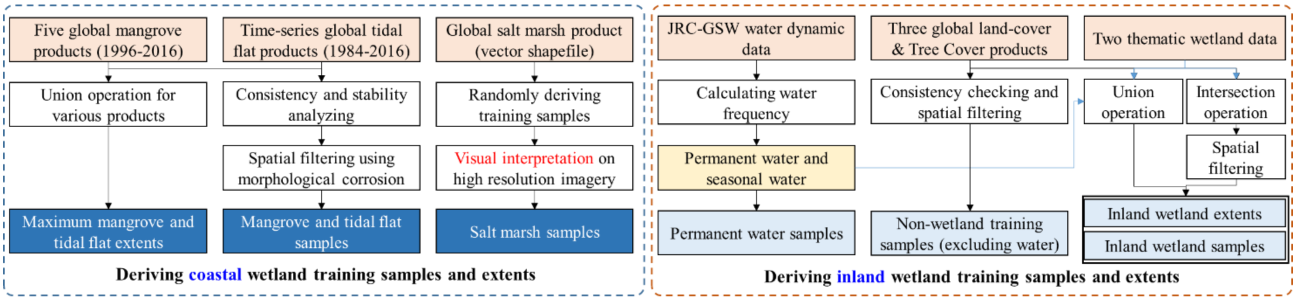

Figure ~~3~~2. The flowchart of deriving coastal and inland wetland samples from multiple pre-existing datasets

3.1 Deriving coastal tidal wetland training samples and maximum extents

This study divided the coastal tidal wetlands into three sub-categories: mangrove forest, salt marsh, and tidal flat. The previously existing products have been collected in Table 1. For the mangrove training samples, we collected five global mangrove products with different spatiotemporal resolutions, all of which achieved fulfilling performances. For example, Hamilton and Casey (2016) stated that their continuous mangrove forest cover (CGMFC) dataset could cover 99% of all mangrove forests from 2000 to 2012, and Thomas et al. (2017) validated their Global Mangrove Watch (GMW) products from 1996 to 2016 and reached an overall accuracy of 95.25%. Therefore, we first measure the temporal consistency of the three time-series mangrove forest products (CGMFC, GMW, and GBTM mangroves), and only these temporally stable mangrove forest pixels were selected as the primary candidate points ($P_{mangrove}^{Tstable}$). Meanwhile, to minimize the influence of classification error in each mangrove forest product, the cross-consistency of five mangrove products was analyzed, and only the pixel, simultaneously identified as mangrove forest in all five products, was labeled as stable and consistent candidate points ($P_{mangrove}^{Tstable,Scons}$). Furthermore, considering that there was a temporal interval between prior mangrove products and our study, and that mangrove deforestation usually followed the pattern of edge-to-center contraction, a morphological erosion filter with a local window of 3×3 was applied to the $P_{mangrove}^{Tstable,Scons}$ points to further ensure the confidence of mangrove training samples. Lastly, as for the maximum mangrove forest extents ($MaxExtent_{mangrove}$), the union operation was applied to five global mangrove products as shown in Eq. (1).

$$MaxExtent_{mangrove} = M_{WAM} \cup M_{GMW} \cup M_{GBTM} \cup M_{CGMFC} \cup M_{GDM\_USGS} \qquad (1)$$

where $[M_{WAM}, M_{GMW}, M_{GBTM\,,}\, M_{CGMFC}, M_{GDM\_USGS}]$ are the spatial distributions of five global mangrove forest products listed in Table 1. It should be noted that these prior mangrove products were demonstrated to cover almost all mangroves over the world, so the $MaxExtent_{mangrove}$ can be used as the boundary for mangrove mapping; namely, only the pixel within the maximum mangrove extent was labeled as mangrove forest.

Regarding the collection of tidal flat samples, the prior time-series global 30 m tidal flat products ($Gtidalflat$) from 1984 to 2016 were validated to achieve an overall map accuracy of 82.3%, and user accuracies for the non-tidal and tidal flat of 83.3% and 81.1%, respectively (Murray et al., 2019). To ensure the accuracy of tidal flat samples, we first applied temporal consistency analysis to the time series of tidal flat datasets from 2000 to 2016 and identified the temporally stable tidal flat pixels ($P_{tidal}^{Tstable}$) during 16 consecutive years. The reason why we discarded the tidal flat datasets before 2000 was that the available Landsat imagery were~~as~~ sparse and could not accurately capture the high-tidal and low-tidal information, and suffered lower monitoring accuracy. Next, Radoux et al. (2014) found that transition zones between two different land-cover types are likely to be misclassified; therefore, the candidate tidal flat samples $P_{tidal}^{Tstable}$ were further refined by the morphological erosion filter with a local window of 3×3. Furthermore, as a tidal flat is a non-vegetated ~~coastal wetland~~coastal tidal wetland, we combined the empirical rule (EVI ≥ 0.1, NDVI ≥ 0.2, and LSWI > 0) proposed by Wang et al. (2020) and time-series Landsat imagery in 2020 (approximately 142 thousand Landsat scenes) to exclude all vegetated pixels from tidal flat training samples. Lastly, to derive the maximum tidal flat extents ($MaxExtent_{tidalflat}$), the union operation was applied to the time-series tidal flat products from 1984 to 2016. It should be noted that the Murray's global 30 m tidal flat datasets only covered the regions of 60°N~60°S (Murray et al., 2019), therefore, we used the coastal shorelines ($Line_{coastal}$) to create a 50 km buffer (applied by the Wang et al. (2020) and (Murray et al., 2019)) as the potential tidal flat zones in the high latitude regions (>60°N) as in Eq. (2). It should be noted that we only identified and then retained these tidal flat pixels within the maximum extents by using the classification models in the Section 4.2.

$$MaxExtent_{tidalflat} = \begin{cases} \bigcup_{t=1984}^{2016} Gtidalflat_{t,s}\,, & s \in [60°S,\ 60°N] \\ Line_{coastal} \pm 50km, & s \in [60°N,\ 90°N] \end{cases} \quad (2)$$

Compared with the mangrove forest and tidal flat, the pre-existing global or regional salt marsh products were relatively sparse. The global distribution of the salt marsh dataset contained 350,985 individual vector polygons and was the most complete dataset on salt marsh occurrence and extent at the global scale (McOwen et al., 2017). However, after careful review, we found some mislabeled salt marsh polygons, so this dataset cannot be used directly to derive training samples. This study first used the random sampling method to generate 35,099 salt marsh points (approximately 10% of the total polygons) based on prior datasets. We combined the visual interpretation method and high-resolution imagery to check each salt marsh point. After discarding the incorrect and uncertain samples, a total of 32,712 salt marsh points were retained. However, the prior dataset only captured the extent of salt marshes in 99 countries worldwide (McOwen et al., 2017), further noting that the distribution of salt marshes was spatially correlated with tidal flat and mangrove forest (Wang et al., 2021). Consequently, the maximum extents of tidal flat and mangrove forest, in addition to the prior salt marsh extent were used for salt marsh mapping. Meanwhile, as the wetland layer in the global land-cover products (GLC_FCS30, GlobeLand30, and CCI_LC) also covered some ~~coastal wetland~~coastal tidal wetlands, the saline-water wetland layer in the CCI_LC and~~s~~ the wetland data in other two products closed to the coastal shorelines

~~in these land-cover products over coastal regions~~ were also imported as supplement when determining the maximum coastal tidal wetland extents.

3.2 Deriving inland wetland training samples and maximum extents

The pre-existing inland wetland datasets usually suffered from lower accuracy compared to ~~coastal wetland~~coastal tidal wetland products; for example, the wetland layer in the GlobeLand30-2010 and GLC_FCS30-2015 was validated to achieve a user accuracy of 74.9% (Chen et al., 2015) and 43.4% (Zhang et al., 2021b), respectively. Therefore, we first generated high-confidence inland wetland samples and then determined their sub-categories (swamp, marsh, inland flat~~, and~~, saline wetland and permanent water). Specifically, the consistency analysis of five global wetland datasets (TROP-SUBTROP Wetland, GLWD, CCI_LC, GlobeLand30, and GLC_FCS30) and the temporal stability checking for CCI_LC (1992–2020), GlobeLand30 (2000-2020) and GLC_FCS30 (2015-2020) were applied to identify these temporally stable and high cross-consistency wetland points ($P_{inlandWet}^{Tstable,Scons}$). It should be noted that the coarse wetland products (GLWD, TROP-SUBTROP and CCI_LC) were resampled to 30 m using the nearest neighbor method on the GEE platform and the ~~coastal wetland~~coastal tidal wetland layers in these products were excluded. Namely, only the pixel identified as inland wetland ~~(excluding permanent water bodies)~~ in all five products was retained. Then, the morphological erosion filter with a local window of 3 × 3 was also used to decrease the sampling uncertainty over these land-cover transition areas because the transition zones between two different land-cover types are likely to be misclassified (Lu and Wang, 2021; Radoux et al., 2014).

Afterward, to determine the wetland sub-category for each inland wetland sample, we first used the empirical vegetation rule (EVI ≥ 0.1, NDVI ≥ 0.2, and LSWI > 0) proposed by Wang et al. (2020) and time-series Landsat imagery to split candidate samples into two parts: vegetated wetland samples (swamp and marsh) and non-vegetated wetland samples (flooded flat, ~~and~~ saline and permanent water). Then, as the swamp was defined as the forest or shrubs which grow in the inland freshwater, the global 30-m tree cover dataset (GFCC30TC) was adopted to distinguish the swamp and marsh from vegetated wetland samples. Specifically, if the tree cover of the sample was greater than 30% (Hansen et al., 2013), it was labeled as swamp, and the remaining vegetated wetland samples were labeled as marsh. Furthermore, to distinguish between the inland flat, ~~and~~ saline samples and permanent water ~~from these non-vegetated wetland samples~~, the saline blocks in the prior GLWD products were first checked by visual interpretation and then imported as the reference dataset to identify all saline wetland samples. The remaining non-vegetated wetland samples were further refined using the time series of the JRC-GSW datasets, only water probability of these remaining samples less than the threshold of 0.95 (suggested by Wang et al. (2020)) were labeled as flooded flat. Lastly, ~~R~~regarding the permanent water samples, the JRC_GSW water dynamic dataset was validated and achieved producer's and user's accuracies of 99.7% and 99.1% for permanent water (Pekel et al., 2016). The permanent water training samples were directly derived from the JRC_GSW dataset without any refinement rules.

Lastly, as for determining the maximum inland wetland extents ($Mextent_{inWet}$), the union operation was conducted to six pre-existing global wetland datasets as in Eq. (3).

$$Mextent_{inWet} = W_{\mathrm{TROP-SUBTROP}} \cup W_{GLWD} \cup W_{CCI\_LC} \cup W_{GLC\_FCS30} \cup W_{Globeland30} \cup W_{JRC\_GSW} \quad (3)$$

Here, $[W_{\mathrm{TROP-SUBTROP}}, W_{GLWD}, W_{CCI\_LC}, W_{GLC\_FCS30}, W_{Globeland30}]$ were wetland distributions of five pre-existing global wetland products, and W_{JRC_GSW}~~.~~ was JRC-GSW time-series water dynamic datasets, which identified the inundated probability at a monthly history during 1984-2021(Pekel et al., 2016). It should be noted that the omission error can be ignored for derived maximum inland wetland extents ($Mextent_{inWet}$), because the GLWD and TROP-SUBTROP wetland datasets captured almost all potential wetlands using compilation and model simulation methods (Gumbricht, 2015; Lehner and Döll, 2004).~~To comprehensively capture these fragmented and small river and lake wetlands, the seasonal water extents derived from the JRC-GSW time-series water dynamic datasets (W_{JRC_GSW}) were also added to $Mextent_{inWet}$. Specifically, as the time series of the JRC-GSW datasets provided the water probability at a monthly history for 1984–2021, the seasonal water body could be separated by the water probability using the threshold of 0.95 suggested by.~~

3.3 Deriving non-wetland training samples from prior land-cover products

Except for ~~coastal and~~ inland and coastal tidal wetland samples, the non-wetland samples were also necessary because some non-wetland land-cover types were shown to have a similar spectrum to wetlands. For example, swamp and forest or shrubs exhibited the same vegetation reflectance characteristics in optical imagery, and marsh and grassland shared similar spectra curves during the growing season (Zhang et al., 2022b). ~~This study~~Except for eight fine wetland sub-categories training samples, we also divided the non-wetlands into forest/shrubland, grassland, cropland~~, permanent water~~, and others (bare land, impervious surfaces, and snow). To automatically derive these non-wetland samples, the multi-epochs GlobeLand30, GLC_FCS30 and~~,~~ CCI_LC global land-cover products~~, and the JRC-GSW water dynamic dataset~~ were integrated. Specifically, the temporal stability and cross-consistency analysis were applied to three land-cover products to identify temporally stable forest/shrubland, grassland, cropland, and other candidate samples. Furthermore, the morphological erosion filter with the local window of 3 × 3 was also adopted to decrease the sampling uncertainty over land-cover transition areas. ~~**Regarding the permanent water samples, the JRC_GSW water dynamic dataset was validated and achieved producer's and user's accuracies of 99.7% and 99.1% for permanent water . The permanent water training samples were directly derived from the JRC_GSW dataset without any refinement rules.**~~

3.4 Determining the sample size and distributions using stratified random sampling strategy

Except for the confidence of training samples, many studies also found that the size and distribution of training samples also affected classification performances (Jin et al., 2014; Zhu et al., 2016). As this study aimed to identify wetlands instead of all land-cover types, the equal allocation sample distribution would perform better than the proportional distribution (the sample size determined by the area) (Jin et al., 2014; Zhang et al., 2020). Namely, the approximate proportion of inland wetland, coastal tidal wetland, and non-wetland samples was ~~4~~5:3:4~~5~~ in the coexisting areas because the classification system was composed of ~~four~~ five inland and three coastal tidal wetland sub-categories and ~~five~~ four non-wetland land-cover types. Regarding the sample size, Zhu et al. (2016) had analyzed the quantitative relationships of sample size and the mapping accuracy and found that the mapping accuracies slowly increased and then remained stable with any further increase in the number of samples and suggested using a total of 20,000 samples in the Landsat scene. In this study, we used the stratified random sampling strategy to collect the training samples (excluding salt marsh because it was collected globally using visual interpretation in Section 3.1) at each 5° × 5° geographical grid (corresponding to the local adaptive modeling in the Section 4.2) using an approximate sample size of 2000 for each category. According to our statistics, this study derived exceeding 20 million training samples for mapping global fine wetlands.

4. Mapping wetland using the stratified classification strategy and the water-level, ~~and~~phenological features

~~Considering that the spectral characteristics of the wetlands would quickly change with the seasonal or daily water levels of the underlying surface, the time-series Landsat-8 and Sentinel-1 SAR observations, and ASTER DEM topographical image were combined to capture the complicated temporal dynamicsand spectral heterogeneity.~~ Figure ~~4~~ 3 illustrates the flowchart of the proposed method for generating the global 30-m fine wetland maps. First, we combined the time-series Landsat-8, Sentinel-1 SAR observations and ASTER DEM topographical image to derive multisource and multitemporal features including: various water-level, phenological and three topographical features. Then, the training samples (coastal tidal, inland wetlands and no-wetlands) and derived multisource and multitemporal features were combined to train ~~generating the water-level and phenological features and developing~~ the~~a~~ ~~global 30-m fine wetland map using a~~ stratified random forest classifiers (a classic and widely used machine learning classification model (Breiman, 2001)) ~~modeling strategy~~at each local region. Next, using the trained random forest models and derived multisource and multitemporal features, we could develop corresponding coastal tidal wetland and inland wetland maps. Finally, the post-processing step was used to generate the global 30 m fine wetland map in 2020.

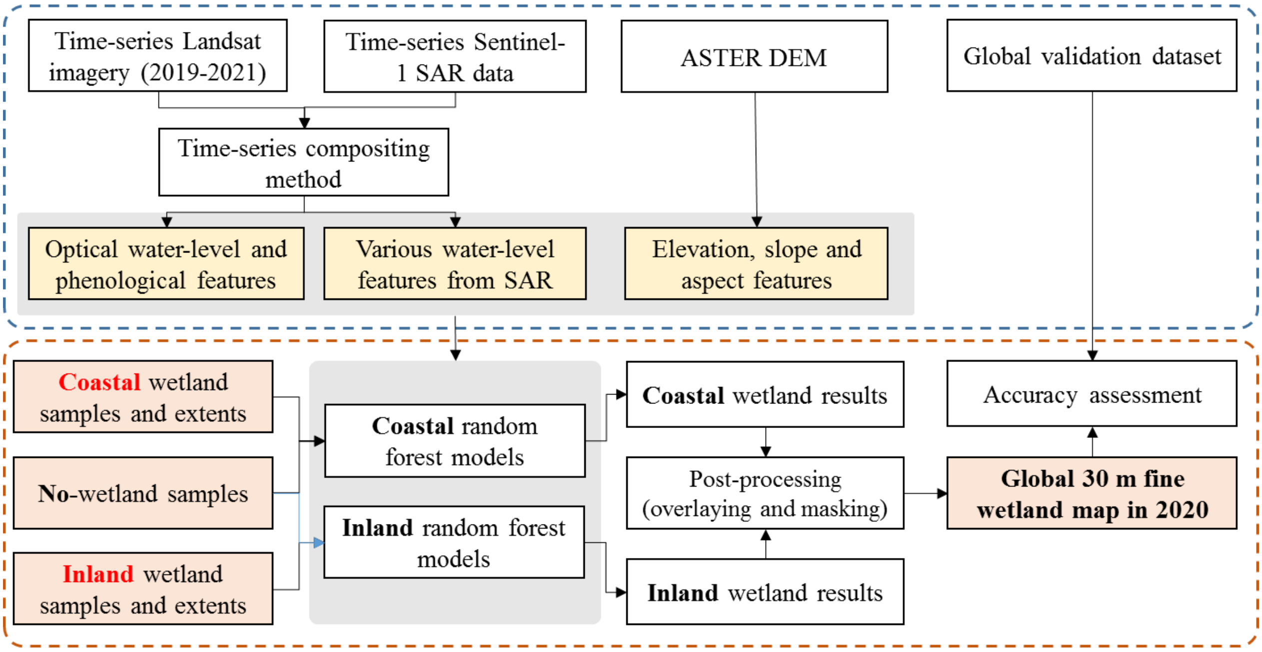

Figure ~~4~~3. The flowchart of wetland mapping using water-level, phenological and topographical features and a stratified classification strategy.

4.1 Generating ~~the~~ various water-levels and phenological ~~features~~ composites

Before generating various water-level and phenological features, four spectral indexes including normalized difference water index (NDWI), land surface water index (LSWI), normalized difference vegetation index (NDVI) and enhanced vegetation index (EVI) were imported because many studies have demonstrated that they were of great help in wetland mapping (Mao et al., 2020; Wang et al., 2020),

$$LSWI = \frac{\rho_{nir}-\rho_{swir1}}{\rho_{nir}+\rho_{swir1}}, NDWI = \frac{\rho_{green}-\rho_{swir1}}{\rho_{green}+\rho_{swir1}}, NDVI = \frac{\rho_{nir}-\rho_{red}}{\rho_{nir}+\rho_{red}},\ EVI = 2.5 \times \frac{\rho_{nir}-\rho_{red}}{\rho_{nir}+6\times\rho_{red}-7.5\times\rho_{blue}+1} \quad (4)$$

where ρ_{blue}, ρ_{green}, ρ_{red}, ρ_{nir}, ρ_{swir1} were the blue, green, red, near-infrared and shortwave infrared bands of Landsat imagery, respectively.

Then, the spectral characteristics of the wetlands would quickly change along with the seasonal or daily water levels of the underlying surface. For example, the tidal flat was the status of seawater at the high tidal stage and mud or sand flats at low tidal stages (Wang et al., 2021); therefore, it was necessary to extract the high~~-~~est and low~~-~~est water-level ~~features~~ composites to completely capture these ~~water-level sensitive~~inundated wetlands. Over the past several years, the time-series compositing strategy has been widely used to capture phenological and cloud-free composites (Jia et al., 2020; Ludwig et al., 2019; Murray et al., 2019; Zhang et al., 2021a). ~~For example, used the quantile compositing method to extract different tidal stage information, and successfully produced the global distribution of tidal flats. However, explained that the percentile composting method fails to capture the highest- and lowest-water stages and further proposed to use the maximum normalized index for compositing the highest- and lowest-water features. Meanwhile, a multi-temporal phenology was also essential for classifying the vegetated wetlands and excluding these non-wetland land-cover type~~

~~Regarding the highest and lowest water-level features~~In this study, considering that NDWI was sensitive to open surface water and that Zhang et al. (2022b) found a positive relationship between tidal height and NDWI using field survey data, the maximum NDWI compositing was applied to the time-series clear-sky Landsat imagery to capture the optical highest water-level composites illustrated in Figure ~~5b~~4b. As for the lowest water-level features, considering that the tidal/flooded flat or marsh usually reflected higher NDVI and EVI values than water bodies and that Zhang et al. (2022b) also used the field data to demonstrate that there was a negative relationship between tidal-level height and NDVI, the maximum NDVI composite was applied to capture the optical lowest water-level information illustrated in Figure ~~5a~~4a. Considering that optical observations were usually contaminated by clouds, especially during the rainy seasons, and that the SAR back coefficients had a great advantage in the presence of cloud coverage and were found to be sensitive to the soil moisture, vegetation structure, and inundation information, the time-series Sentinel-1 SAR imagery could be used as a complementary dataset for capturing the highest and lowest water-level ~~features~~ composites (DeVries et al., 2020; Li et al., 2020; Mahdianpari et al., 2018). Specifically, as the SAR active transmitting signals were heavily absorbed when they reached the water body, the corresponding SAR back coefficients in the water body had lower values compared to other land-cover types. To capture the high water-level features from the time-series Sentinel-1 imagery, the percentile compositing method using the 5th percentile was applied, as illustrated in Figure ~~5d~~4d. Conversely, the 95th percentile of Sentinel-1 VV and VH were generated to capture the lowest water-level information (Figure ~~5c~~4c). It should be noted that the minimum and maximum percentiles were not used because the time-series Sentinel-1 imagery still contained the residual errors caused by the quantitative processing.

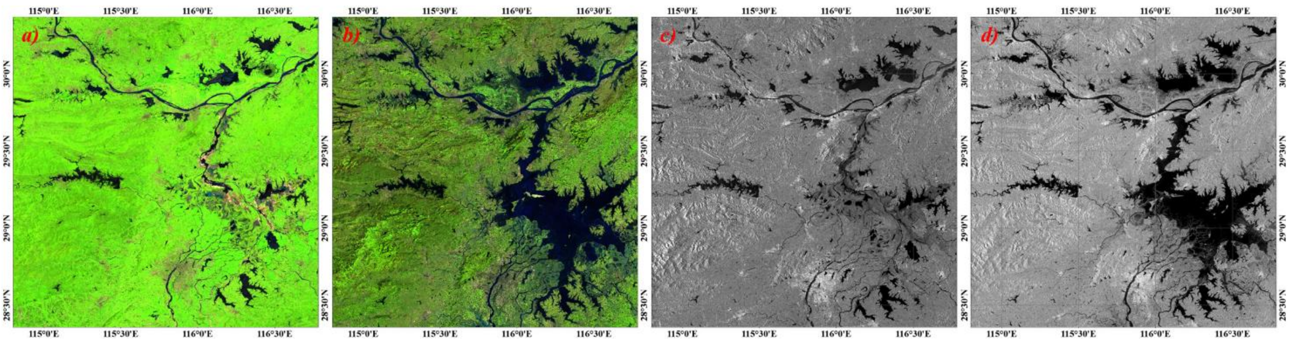

Figure ~~5~~4. The lowest and highest water-level features derived from (a-b) time-series Landsat optical reflectance data and (c-d) the Sentinel-1 SAR imagery using the time-series compositing method in Poyang Lake, China.

Many studies also demonstrated that a multi-temporal phenology was also essential for classifying the vegetated wetlands and excluding these non-wetland land-cover types (Li et al., 2020; Ludwig et al., 2019). There were usually two options for capturing phenological features from time-series Landsat imagery. These included seasonal-based compositing (Zhang et al., 2021a; Zhang et al., 2022a) and percentile-based compositing (Hansen et al., 2014; Zhang and Roy, 2017; Zhang et al., 2021b). The former used the phenological calendar for selecting time-matched imagery. It then adopted the compositing rule to capture the seasonal features, while the latter directly used the statistical distributions to select various percentiles. Azzari and Lobell (2017) quantitatively analyzed the performance of two compositing methods and found that both of them had similar mapping accuracy for land-cover mapping. Meanwhile, the seasonal-based compositing method needed the prior phenological calendar, while the percentile compositing method did not require any prior knowledge or explicit assumptions regarding the timing of the season; therefore, the percentile compositing method was more suitable to generate phenological features. This study composited time-series Landsat reflectance bands and four spectral indexes into five percentiles (15th, 30th, 50th, 70th and 85th) because we wanted to capture as much of the phenological changes in wetlands as possible when comparing to the four seasonal composites (Zhang and Roy, 2017). It should be noted that the minimum and maximum percentiles were excluded because they were usually affected by residual clouds, shadows, and saturated observations.

Lastly, the topographical variables were also important factors for determining the spatial distribution of wetlands (Ludwig et al., 2019; Tootchi et al., 2019). For example, the widely used topographical wetness index (TWI) uses the local slope to reveal soil wetness, which improves wetland classification performance and reduces commission errors within upland areas (Ludwig et al., 2019). Therefore, the elevation, aspect, and slope, calculated from the ASTER GDEM dataset, were included in the multi-sourced features. In summary, a total of 77 multisourced training features (listed in Table 3), including 70 optical features from Landsat imagery, 4 SAR features from Sentinel-1 imagery and 3 topographical features from ASTER GDEM.

Table 3. The multisourced and multitemporal training features for wetland mapping.

Data	**Derived training features from multisource remote sensing imagery**
Landsat	**Water-level features**: the lowest and highest composites with Blue, Green, Red, NIR, SWIR1, SWIR2, LSWI, NDWI, NDVI and EVI bands **Phenological features:** 15th, 30th, 50th, 70th and 85th percentiles with Blue, Green, Red, NIR, SWIR1, SWIR2, LSWI, NDWI, NDVI and EVI bands
Sentinel-1 SAR	**Water-level features**: the lowest and highest composites using 5th and 95th percentiles for VV and VH bands.
ASTER GDEM	**Topographical features**: elevation, slope and aspect.

4.2 The stratified classification strategy for wetland mapping

Since we have simultaneously extracted the maximum coastal and inland wetland extents when deriving training samples from prior wetland datasets, the stratified classification strategy was adopted to fully use the maximum extent constraint. I~~Namely, i~~f a pixel was classified as a ~~coastal wetland~~coastal tidal wetland outside the maximum ~~coastal wetland~~coastal tidal wetland extents, it would be identified as a misclassification~~. ~~. Furthermore, there were two ~~approaches~~ideas for~~,~~ the large-area land-cover mapping~~, which included~~ including global classification modeling (using one universal model for the whole areas) and local adaptive modeling (using various models for different local zones) (Zhang et al., 2020). For example, Zhang and Roy (2017) demonstrated that local adaptive modeling outperformed the global classification modeling strategy. Therefore, the global land surface was first divided into 961 5° × 5° geographical tiles illustrated in Figure 5, which were inherited from the global 30 m land-cover mapping by (Zhang et al., 2021b).~~,~~ ~~and~~ T~~t~~hen, ~~independently trained the local adaption models using training samples from adjacent 3×3 tiles for ensuring the classification consistency across neighboring geographical tiles.~~we trained the local adaptive classification models using derived training samples in Section 3 and multisource and multitemporal features (the highest, lowest water-level and phenological composites and topographical variables) at each 5° × 5° geographical tile. It should be noted that we used the training samples from neighboring 3 × 3 geographical tiles to train the classification model and classify the central tile for guaranteeing the spatially continuous transition over adjacent regional wetland maps. Namely, we trained 961 local adaptive classification models and then produced 961 5° × 5° wetland maps. Finally, we spatially mosaiced these 961 regional wetland maps into the global 30 m wetland map in 2020.

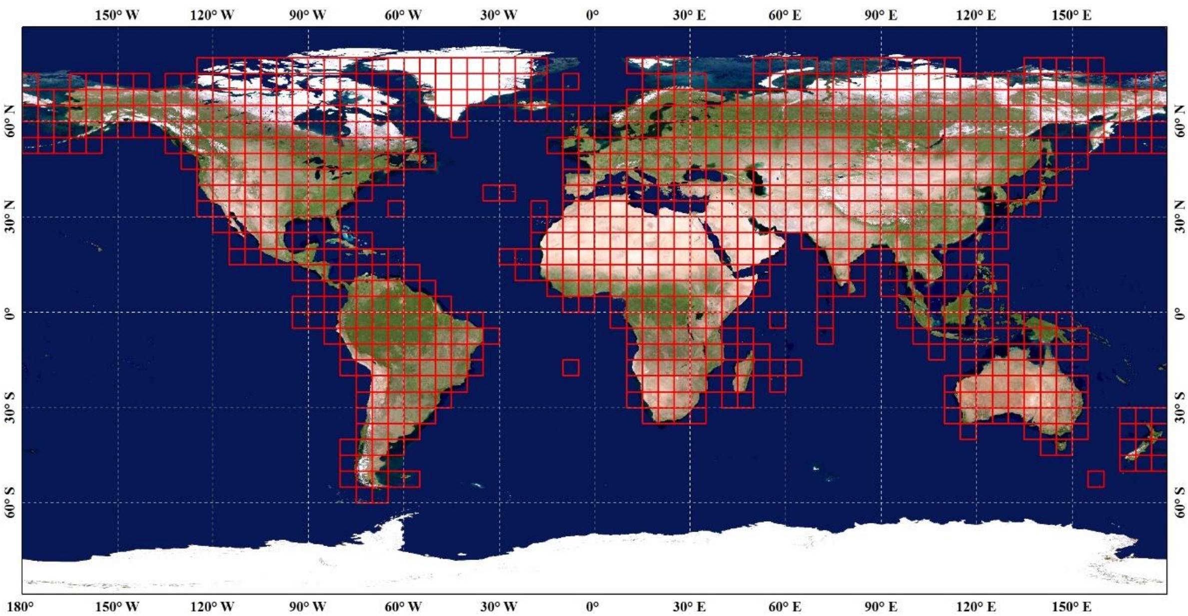

Figure 5. The spatial distribution of 961 5° × 5° geographical tiles used for local adaptive modeling, which was inherited from the global 30 m land-cover mapping by (Zhang et al., 2021b). The background imagery came from the National Aeronautics and Space Administration (https://visibleearth.nasa.gov, last access: 10 Nov 2022).

Afterward, ~~as~~ the random forest (RF) classifier was demonstrated to have obvious advantages including: dealing with high-dimensional data, robustness for training noise and feature selection, as well as achieving higher classification when compared to other widely used machine learning classifiers (e.g., support vector machines, neural networks, decision trees, etc.) (Belgiu and Drăguţ, 2016; Gislason et al., 2006)~~.~~; Therefore, the RF classifier was selected for mapping inland and coastal tidal wetlands using multi-sourced features on the GEE platform. It should be noted that the RF classifier had two key parameters: the number of selected prediction variables (Mtry) and the number of decision trees (Ntree). Belgiu and Drăguţ (2016) and Zhang et al. (2022b) have demonstrated the quantitative relationship of Ntree against classification accuracy and found that the classification accuracy stabilized when Ntree was greater than 100. Meanwhile, Belgiu and Drăguţ (2016) suggested that the Mtry should take its default value of the square root of the number of all input features. Therefore, the Ntree and Mtry took 100 and the square root of the number of all input features, respectively.

The inland and coastal tidal wetland maps were produced by combining water-label and phenological features, the stratified classification strategy, local adaptive modeling, and the derived wetland and non-wetland training samples. As the inland and ~~coastal wetland~~coastal tidal wetlands were independently produced, some pixels in the overlapping area of maximum inland and ~~coastal wetland~~coastal tidal wetland extents were simultaneously labeled as inland wetlands and ~~coastal wetland~~coastal tidal wetlands. However, as the final global wetland map was a hard classification, these pixels should be post-processed into one label. As the random forest classifier could provide the posterior probability for each pixel, we determined the labels of the confused pixels by comparing the posterior probabilities. In addition, as the tidal flats were demonstrated to overestimate some coastal pones as the tidal flats, the global lake and reservoir dataset, developed by Khandelwal et al. (2022), was applied to optimize the tidal flat.

4.3 Accuracy assessment

To quantitatively analyze the performance of our GWL_FCS30 wetland map, a total of ~~18,701~~25,709 validation samples (illustrated in Figure 6), including 10,~~346~~ 558 non-wetland points and ~~8,355~~15,151 wetland points, were collected~~ by combining high-resolution imagery, time-series Landsat and Sentinel observations and visual interpretation method~~. Firstly, as the wetland was sparse land-cover type compared to the non-wetlands (forest, cropland, grassland and bare land), the stratified random strategy was applied to randomly derive validation points at each strata. Then, as the wetlands had significant correlation with the water levels (Zhang et al., 2022b), the time-series optical observations archived on the GEE cloud platform were used as the auxiliary dataset to interpret these water-level sensitive wetlands such as: tidal flat and flooded flat. It should be noted that the visual interpretation was implemented on the GEE cloud platform because it archives a large amount of satellites imagery with various time spans and spatiotemporal resolution (Zhang et al., 2022a). Meanwhile, each validation point is independently interpreted by five experts for minimizing the effect of expert's subjective knowledge, and only these complete agreement points were retained otherwise they were discarded. ~~Figure 2 intuitively illustrated the spatial distribution of global wetland validation points, it can be found that the distribution of wetland points accurately revealed the spatial patterns of global wetlands.~~Then, we employed four metrics typically used to evaluate accuracy, which include the kappa coefficient, overall accuracy, user's accuracy (measuring the commission error), and producer's accuracy (measuring the omission error) (Gómez et al., 2016; Olofsson et al., 2014), were calculated using 25709 global wetland validation samples.

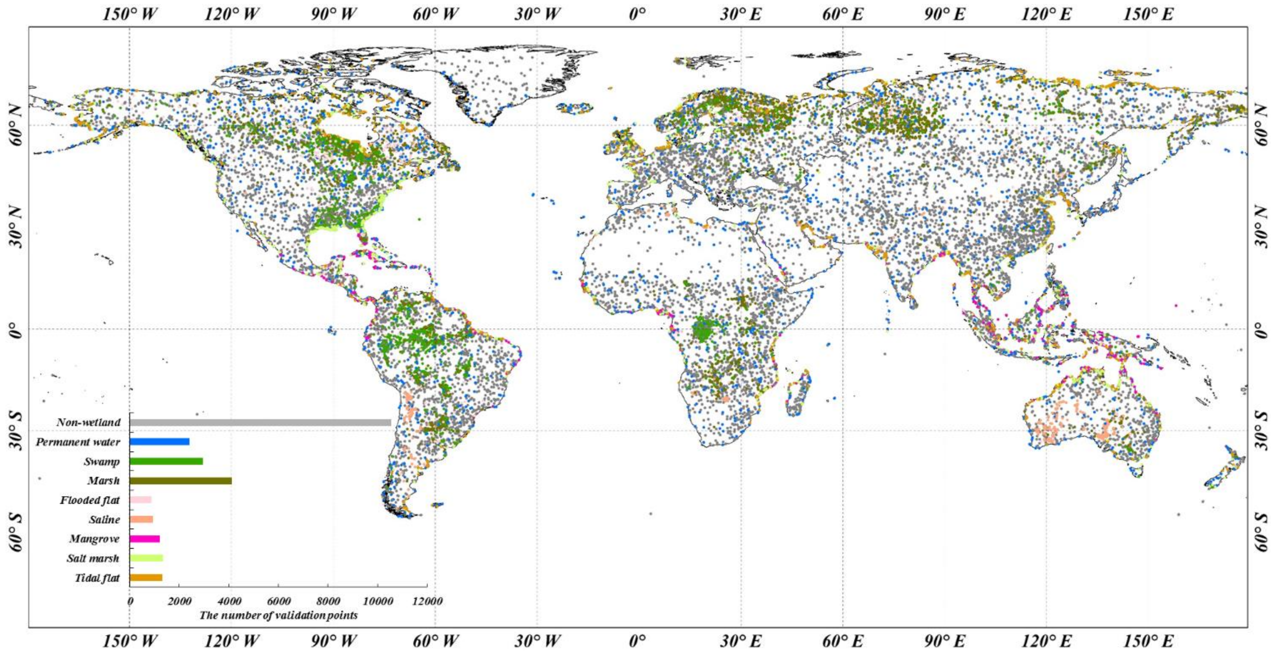

Figure ~~2~~6. The spatial distribution of ~~18,701~~25,709 global wetland validation samples using stratified sampling strategy.

~~5. To quantitatively analyze the accuracy of the proposed method and corresponding GWL_FCS30 wetland maps, we employed four metrics typically used to evaluate accuracy, which include the kappa coefficient, overall accuracy, user's accuracy (measuring the commission error), and producer's accuracy (measuring the omission error) (Gómez et al., 2016; Olofsson et al., 2014), were calculated using 18,701 global wetland validation samples in Section 2.4. Further, to intuitively understand the performance of the produced map, four existing global wetland products (GlobeLand30 wetland layer (Chen et al., 2015), GLC_FCS30-2020 wetland layer, CCI LC wetland layer (Defourny et al., 2018) and GLWD dataset) were collected to analyze the over-estimation and under-estimation problems in the inland regions, and three widely used mangrove forest datasets (Atlas mangrove, Global Mangrove Watch, and USGS Mangrove, 1isted in Table 1) were imported to assess the performance of the developed GWL_FCS30 wetland map in coastal areas.~~

5. Results

5.1 The reliability analysis of derived training samples

~~Previous studies found that the confidence of training samples directly affected the final classification accuracy (Mellor et al., 2015; Radoux et al., 2014). However, collecting global training samples via visual interpretation was highly time-consuming and involved a large amount of manual work, so it was impossible to use the visual interpretation for collecting global wetland samples.~~ This study proposed combining multi-sourced pre-existing wetland products, refinement rules, and expert knowledge to automatically derive these massive inland and ~~coastal wetland~~coastal tidal wetland training samples globally. To demonstrate the reliability of the derived training samples for wetland mapping, we randomly selected approximately 10,000 points from the sample pool and checked their confidence using visual interpretation. It should be noted that we cannot check all the training samples because the number of derived samples was massive (exceeding 20 million training samples in Section 3). After a point-to-point inspection, these selected training samples achieved an overall accuracy of 91.53% in 2020. Meanwhile, we also used 10,000 selected wetland training samples and many non-wetland samples to analyze overall and producer's accuracies of coastal and inland wetlands versus number of erroneous training samples. Specifically, we gradually increased the “contaminated” samples by randomly altering the label of a certain percentage of training samples in steps of 0.01, and then used these “contaminated” samples to build the RF classification model. After repeating the process 100 times, the quantitative relationship between mapping accuracies and erroneous samples is illustrated in Fig. ~~14~~7. Obviously, the overall accuracy and producer’s accuracy of wetlands (merging seven sub-categories into one wetland) was insensitive to the erroneous training samples when the percentage of erroneous samples was controlled within 20%. Beyond this threshold, the accuracies slowly decreased along with the increase of erroneous training samples. Similarly, previous studies by Zhang et al. (2021b) and Zhang et al. (2022a) quantitatively analyzed the relationship between overall accuracy and the erroneous training samples size. They found that the overall accuracy stabilized when the percentage of erroneous training samples was controlled within the threshold and then rapidly decreased after exceeding the threshold. ~~Gong et al. (2019) also demonstrated the random forest classification model was resistant to the erroneous training samples when the percentage of erroneous training samples remained below 20%.~~ Therefore, the derived training samples in Section 3 were accurate enough to support large-area fine wetland mapping.

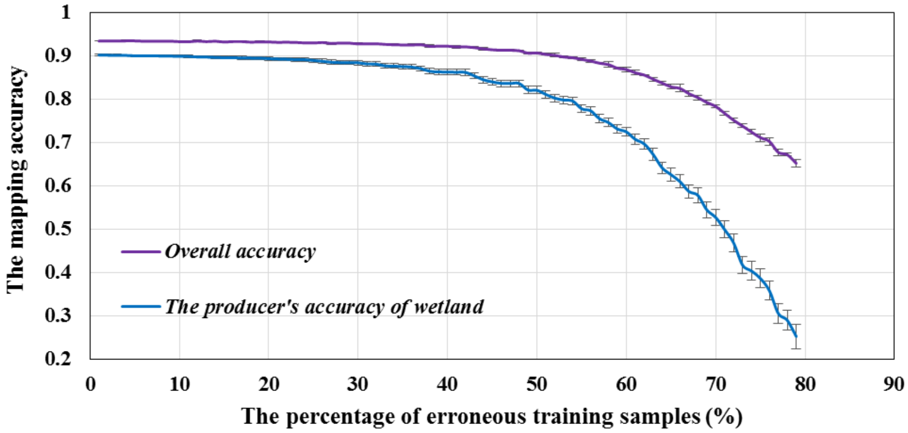

~~6.~~ **Figure ~~14~~7**. The relationship between mapping accuracies with the percentage of erroneous training samples with a step of 1%.

~~5.1~~5.2 The importance of multi-sourced phenological features for wetland mapping

The complicated temporal dynamics and spectral heterogeneity caused great uncertainties in wetland mapping because their spectral characteristics quickly changed with the seasonal or daily water levels of the underlying surface (Ludwig et al., 2019). ~~Single-date optical or SAR observations often failed to capture the spatiotemporal variability of wetlands, which led to the commission and omission errors in wetland mapping, so many studies have demonstrated that using multi-temporal data was an effective way to achieve high-precision wetland mapping, especially for the water-sensitive sub-categories (tidal flat and marsh) (Jia et al., 2020; Zhang et al., 2022b). This study combined the time-series Landsat reflectance and Sentinel-1 SAR products to capture the various water levels and phenological features for comprehensively depicting their temporal dynamics and spectral characteristics, as discussed in Section 4.1.~~ To quantitatively analyze the importance of these multi-sourced and multi-temporal features, we used the random forest classification model, which calculated the increased mean squared error by permuting the out-of-bag data of a variable while keeping remaining variables constant (Breiman, 2001; Zhang et al., 2020), in an effort to compute their importance. Figure ~~15~~ 8 ~~illustrates~~ illustrated the importance of all multi-sourced and phenological features, and it can be found that the phenological features which made the most significant contribution mainly did so because they used the multi-temporal percentiles to comprehensively capture vegetation phenology (EVI and NDVI) and water-level dynamics (NDWI and LSWI) for the various land-cover types. Then, the combination of optical and Sentinel-1 SAR water-level features ranked as the second-most important role in distinguishing the fine wetlands and non-wetlands. Based on the lowest and highest water-level features in Fig. ~~5~~4, the highest and lowest water-level features greatly contributed to determining these water-sensitive wetlands (marsh, tidal flat, and flooded flat). For example, Zhang et al. (2022b) quantitatively analyzed the contribution of multi-sourced features to mapping accuracy. They found that importing water-level features significantly improved the ability to separate tidal flats from non-wetlands. Lastly, three topographical variables also contributed to wetland mapping because the spatial distribution of wetlands had a significant relationship with topography and was mainly distributed in low-lying areas (Zhu and Gong, 2014).

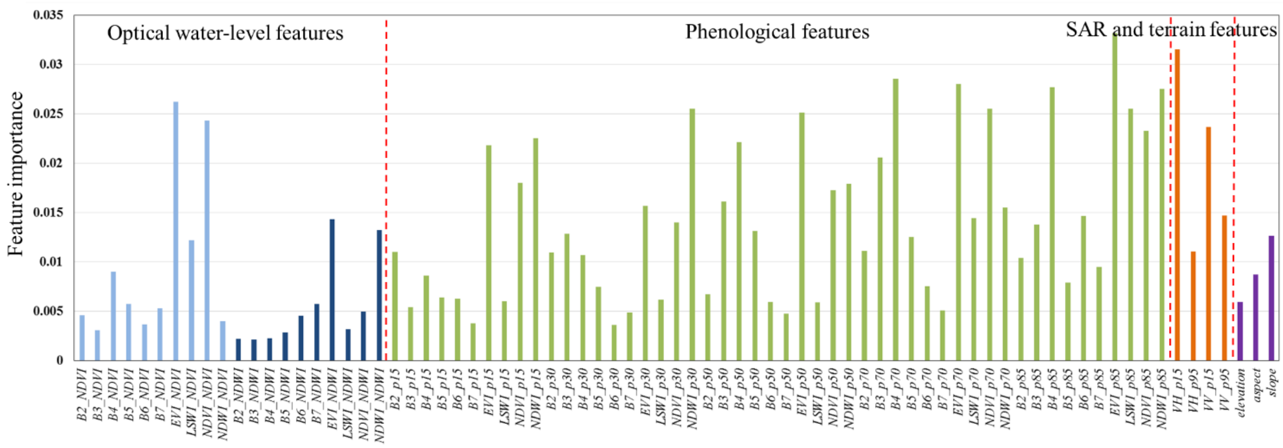

Figure ~~15~~8. The importance of multi-sourced and multi-temporal features derived from the random forest classification model.

~~5.2~~5.3 The spatial pattern of global wetlands in 2020

Figure ~~6~~ 9 illustrates the spatial distributions of our GWL_FCS30 wetland map and their area statistics in latitudinal and longitudinal directions in 2020. Overall, the GWL_FCS30 map accurately captured the spatial patterns of wetlands. It mainly concentrated on the high latitude areas in North Hemisphere and the rainforest areas (Congo Basin and Amazon rainforest in South America). Quantitatively, according to the latitudinal statistics, approximately ~~62~~72.96~~3~~% of wetlands were distributed poleward of 40°N (a large number of wetlands are located in Canada and Russia), and 1~~9.9~~0.6% of wetlands were located in equatorial areas, between 10°S~10°N, within which the Congo and Amazon rainforest wetlands are located. As for the longitudinal direction, there were mainly four statistical peak intervals: ~~100~~120°W~ ~~80~~50°W (Canada wetlands and Amazon wetlands), ~~75°W~50°W (Amazon wetlands),~~ 15°E~25°E (Congo wetlands), 40°E~55°E (the Caspian Sea), and 60°E~90°E (Russia wetlands). Afterward, to more intuitively understand the performance of our GWL_FCS30 wetland map, four local enlargements in Florida, the Congo Basin, Sundarbans, and Poyang Lake were also illustrated. All of them comprehensively captured the wetland patterns in these local areas. For example, there was significant consistency between our results and Hansen's regional wetland maps in the Congo Basin (Bwangoy et al., 2010)~~.~~; both results indicated that the wetlands occurred closer to major rivers and floodplains. Next, according to the lowest and highest water-level features derived from Sentinel-1 SAR and Landsat optical imagery in Figure ~~5~~4, the inland wetlands, varied with the water-levels, ~~having various water levels~~ were also comprehensively identified in the Poyang wetland map (Figure ~~6d~~9d). Figure ~~6c~~ 9c illustrates the spatial distributions of the world's largest mangrove forest in the Sundarbans (Figure ~~6c~~9c), and the cross-comparison in Figure ~~11~~ 14 also demonstrates the great performance of the GWL_FCS30 dataset. Lastly, the Florida wetlands simultaneously contained ~~five~~ six sub-categories (mangrove, tidal flat, salt marsh, marsh, permanent water and swamp). These were distributed along the coastlines and rivers and are accurately captured in Figure 9~~6~~a.

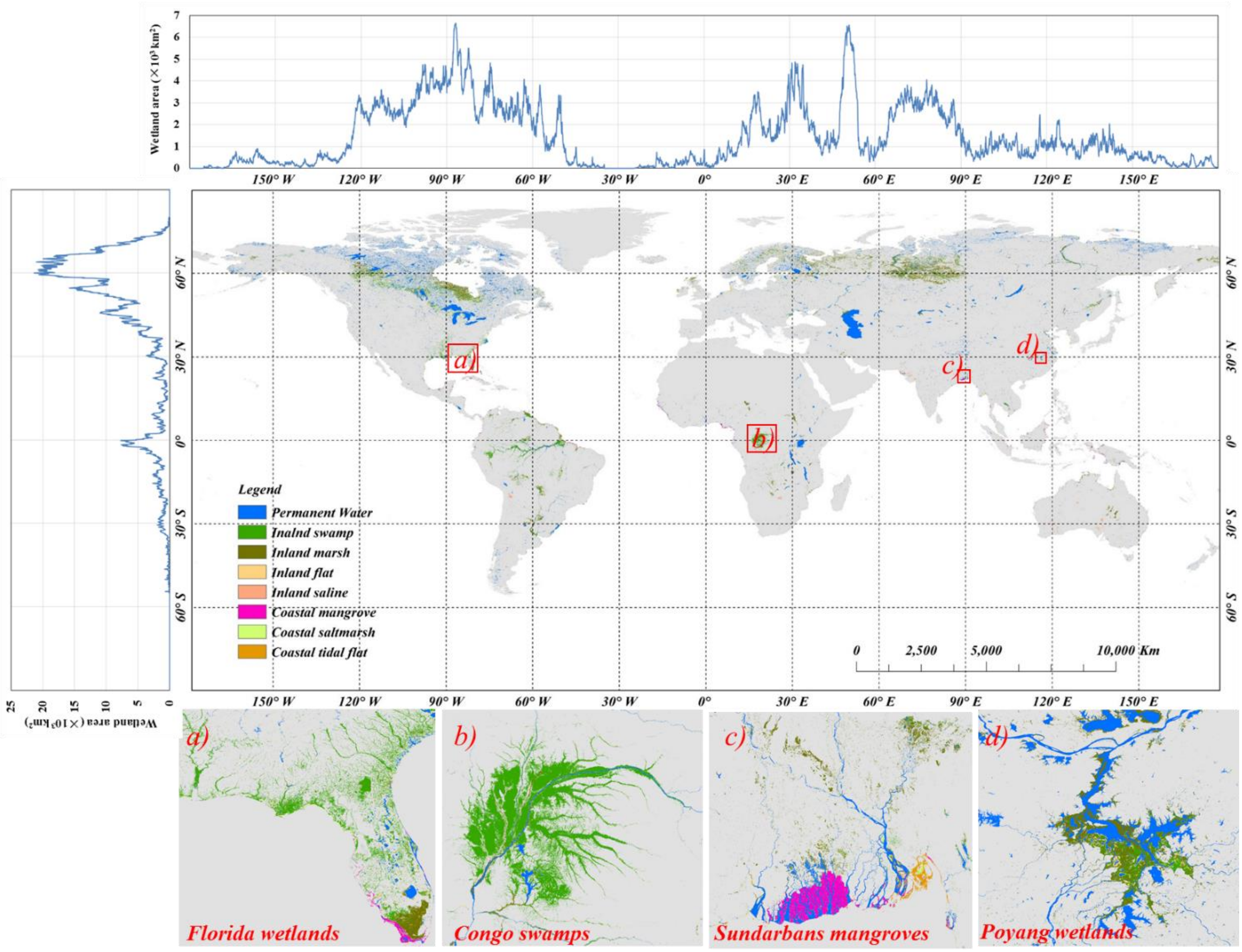

Figure ~~6~~9. The overview of global 30-m fine wetland maps and their area statistics in latitudinal and longitudinal directions in 2020. Four local enlargements in (a) Florida, (b) Congo Basin, (c) Sundarbans, and (d) Poyang Lake were also illustrated.

Figure ~~7~~ 10 illustrates the spatial distribution of ~~seven~~ eight wetland sub-categories after aggregating to the 0.5° × 0.5° grid cell. Intuitively, permanent water body, swamp and marsh accounted for most inland wetlands, while the flooded tidal and inland saline wetlands had obviously lower proportions and the later was only distributed along the surroundings of several saline lakes. In terms of the spatial distribution, it can be found that: 1) the swamp wetlands mainly were concentrated in the Congo and Amazon rainforests, Southern United States, and Northern Canada; 2) most marsh wetlands were located in high latitude areas in the Northern Hemisphere including Northern Canada, Russia, and Sweden; 3) there were significant coexistent relationships between flooded flat, permanent water, swamp, and marsh wetlands~~, and flooded flat wetlands were sparse land~~

~~cover types compared to the other three wetlands~~. Then, as for three coastal tidal wetlands, the mangrove forests were only found in coastal areas below 30°N and were mainly concentrated in regions between 30°N ~ 30°S, including Southeast Asia, West Africa, and the east coast of South America. The salt marshes and tidal flats shared similar spatial distributions. They were widely distributed globally and can be observed along most coastlines. In addition, the tidal flat distributions were closely related to the slope of coastlines, tidal ranges, and sediment inflows. For example, the tidal flats in Asia and Europe usually were located in the tide-dominated estuaries and deltas. Similarly, Murray et al. (2019) also demonstrated that there were often more tidal flats where the river flowed into the sea.

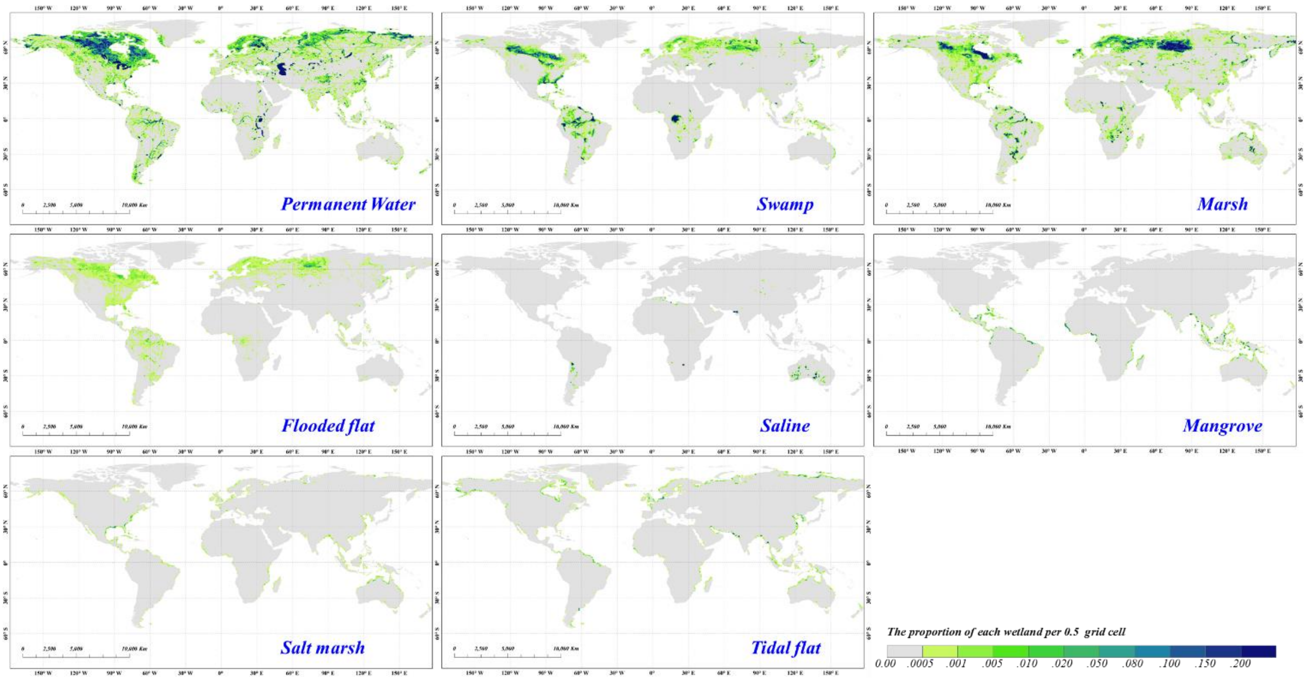

Figure ~~7~~10. The spatial distributions of the ~~seven~~ eight wetland sub-categories after aggregating them to a resolution of 0.5° × 0.5°.

To quantitatively summarize the distribution of the eight sub-category wetlands, the total area and area percentages of eight fine wetland sub-categories over each continent were calculated in Figure ~~8~~ 11 and Table ~~3~~4. The total wetland area was ~~3.57~~6.38 million km^2, including ~~3.10~~6.03 million km^2 of inland wetlands and 0.~~47~~35 million km^2 of coastal tidal wetlands, and the distribution of wetlands varied across different continents. Intuitively, approximately 60% of coastal tidal wetlands (tidal flat, salt marsh, and mangrove) and 70% of permanent water, flooded flat and marsh wetlands were distributed in the Northern Hemisphere, especially in the Asian and North American continents. Comparatively, more than 85% of saline wetlands were located in the Southern Hemisphere, especially the Oceania continent. Then, in terms of specific wetland sub-categories, most permanent water concentrated on the Northern Hemisphere especially in North America (nearly 50% of the world's permanent water bodies). The swamp ~~was~~was mainly distributed on the North American, African, and South American continents, which contained many rainforest wetlands, with corresponding swamp areas of 0.~~35~~39, 0.18, and 0.32 million km^2, respectively. Swamp areas in the Oceania continent were the smallest, covering only ~~6599~~ 6572 km^2, mainly because the forest cover in Oceania was smaller than in other continents. The marsh and flooded flats shared similar areal proportions in all six continents and were mainly concentrated in the North Hemisphere (exceeding 70%), where many lakes and rivers were distributed. Next, as the mangrove forests only covered regions south of 30°N and were mostly concentrated in tropical regions near the equator, such as Southeast Asia, East Africa, and Central America, ~~so~~ this sub-category was absent in the Europe continent and sparse in the Oceania.

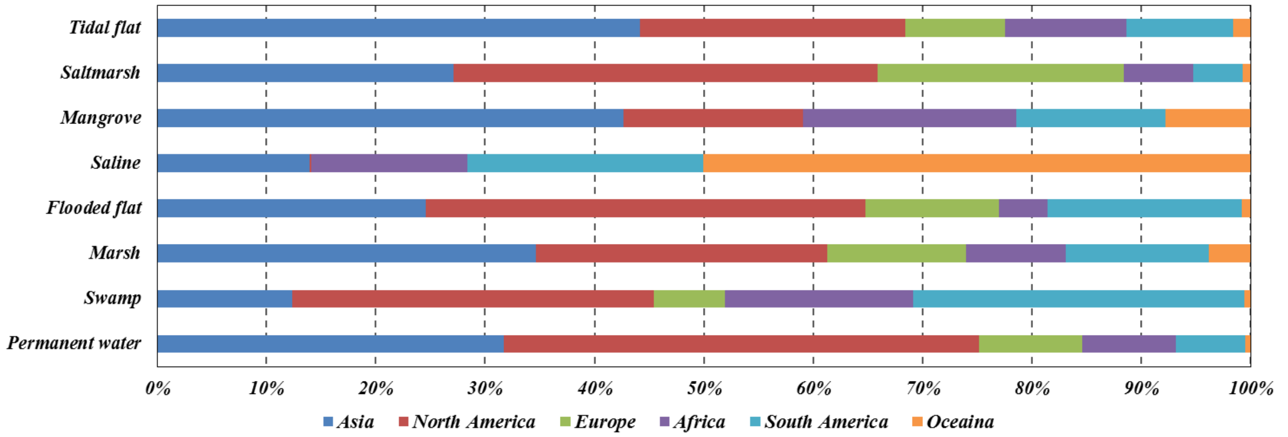

Figure ~~8~~11. The area proportions of ~~seven~~ eight wetland sub-categories over each continent.

Table ~~3~~4. The total wetland area (unit: $10^4 \times km^2$) of ~~seven~~ eight wetland sub-categories at six continents and globe.

	Permanent water	*Swamp*	*Marsh*	*Flooded flat*	*Saline*	*Mangrove*	*Saltmarsh*	*Tidal flat*
Asia	90.529	13.227	58.229	7.244	1.215	6.636	1.852	5.347
North America	123.754	39.314	45.350	11.867	0.008	2.590	2.619	2.697
Europe	27.111	7.010	22.513	3.601	0.005	0.000	0.717	1.408
Africa	24.214	18.393	14.926	1.318	1.248	3.105	0.688	0.731
South America	18.310	32.337	21.640	5.242	1.888	2.175	0.520	1.238
Oceania	1.330	0.657	6.151	0.233	4.355	1.219	1.094	0.875
Total	285.247	110.938	168.810	29.504	8.719	15.725	7.491	12.296

~~5.3~~5.4 Accuracy assessment of global 30 m fine wetland map

Using ~~18,701~~25,709 global validation samples, the confusion matrix of the novel GMW_FCS30 wetland map was calculated in Table ~~4~~5. Overall, our wetland map achieved an overall accuracy of ~~87~~86.~~7~~44% and a kappa coefficient of 0.~~810~~ 82 across the fine wetland classification system. In terms of the producer's and user's accuracies, the non-wetlands achieved the highest ~~performance with a~~ producer's accuracy of ~~93~~94.~~1~~24%~~ and a user's accuracy of 96.1%~~, mainly because we combined multi-sourced pre-existing wetland datasets to determine the maximum wetland boundary and further used multi-sourced and time-series imagery to distinguish between wetlands and non-wetlands. The permanent water achieved the highest user's accuracy of 95.99% because the permanent water had unique and stable spectra characteristics and the training samples were directly from the JRC_GSW database (Pekel et al., 2016). Then, a~~A~~s for the ~~coastal wetland~~coastal tidal wetlands, mangrove forest and tidal flat achieved higher accuracies than ~~other sub-categories~~salt marsh, with producer's accuracies of ~~84.3~~91.43% and ~~83.1~~88.12% and user's accuracies of 95.69% and 94.81%, respectively. ~~The misclassification of mangrove mainly focused on the confusion between mangrove, swamp, and salt marsh because they all shared similar vegetation spectral characteristics. The tidal flat also suffered from confusion with the salt marsh, flooded flat, and the non-wetlands, especially for the water bodies, because~~

~~this land-surface type reflected complicated temporal dynamics at various water levels.~~ The salt marsh had a lower producer accuracy of 7~~5.4~~4.09% ~~than mangrove and tidal flat~~ because its reflectance spectra were affected by both water levels and vegetation cover with considerable spatiotemporal heterogeneity and the sparser prior saltmarsh products were adopted. ~~Furthermore~~Next, ~~in terms of the four~~ as for inland sub-categories, the swamp and marsh obviously performed better than the flooded flat~~ and saline wetland~~, with producer's accuracies of ~~82.6~~72.03% and ~~85.9~~78.09%, respectively. It can be seen that the confusion between swamp and marsh was the main source of the misclassification error of swamp and that the marsh was simultaneously confused with non-wetland, swamp, and flooded flat because the spectra of marsh changed along with the water levels. For example, the marsh in Poyang Lake, shown in Figure ~~5b~~4b, was flooded at its highest water levels. Then, the flooded flat achieved a low producer accuracy of ~~51.1~~65.83% because it usually coexisted with the marsh and shared similar spectral characteristics, so approximately ~~24.3~~10.89% of flooded flat points were labeled as the marsh in our wetland map. The saline wetland was mainly concentrated along the edge of salt lakes and demonstrated great performance in our mapping, with producer's and user's accuracies of ~~74.7~~91.96% and 9~~2.5~~1.66%, respectively.

Table ~~4~~5. The confusion matrix of the global 30 m fine wetland map using ~~18701~~ 25,709 validation points.

	NWT	PW	SWP	MSH	FFT	SAL	MGV	SMH	TFT	Total	P.A.
NWT	99509~~9627~~	17	254~~246~~	2243~~13~~	39~~65~~	3~~0~~	12~~44~~	33~~11~~	26~~40~~	~~103461~~10588	9~~3.1~~4.24
PW	69	2251	4	15	63	0	0	8	9	2419	93.06
SWP	272~~24~~	5	2127~~1950~~	452~~306~~	74~~73~~	11~~3~~	3~~1~~	9~~5~~	0~~0~~	2953~~2362~~	72.03~~82.6~~
MSH	546~~122~~	18	135~~172~~	3218~~2856~~	149~~172~~	18~~1~~	2~~0~~	34~~1~~	1~~0~~	4121~~3324~~	78.09~~85.9~~
FFT	145~~89~~	21	26~~50~~	95~~149~~	574~~312~~	3~~1~~	1~~6~~	5~~1~~	2~~3~~	872~~611~~	65.83~~51.1~~
SAL	26~~30~~	1	0~~13~~	43~~37~~	5~~2~~	846~~271~~	0~~3~~	0~~0~~	0~~7~~	921~~363~~	91.86~~74.7~~
MGV	65~~61~~	4	11~~4~~	2~~3~~	2~~23~~	1~~0~~	1109~~356~~	15~~13~~	3~~12~~	1213~~472~~	91.43~~75.4~~
SMH	157~~39~~	15	6~~32~~	85~~1~~	9~~1~~	30~~0~~	26~~16~~	998~~498~~	22~~4~~	1347~~591~~	74.09~~84.3~~
TFT	78~~28~~	13	0~~22~~	11~~11~~	7~~11~~	11~~17~~	6~~17~~	29~~1~~	1150~~525~~	1305~~632~~	88.12~~83.1~~
Total	11308~~10020~~	2345	2563~~2489~~	4145~~3676~~	922~~659~~	923~~293~~	1159~~443~~	1131~~530~~	1213~~591~~	25709~~18701~~	
U.A.	87.99~~96.1~~	95.99	82.99~~78.3~~	79.56~~77.7~~	62.26~~47.3~~	91.66~~92.5~~	95.69~~80.4~~	88.24~~94.0~~	94.81~~88.8~~		
O.A.						8~~7.7~~6.44					
Kappa						0.~~810~~ 822					

Note: **NWT**: non-wetlands, **PW:** permanent water, **SWP**: swamp, **MSH**: marsh, **FFT**: flooded flat, **SAL**: saline, **SMH**: salt marsh, **MGV**: mangrove forest, **TFT**: tidal flat, **O.A.**: overall accuracy, **P.A.**: producer's accuracy, **U.A.**: user's accuracy.

~~6.~~

6. Discussion

6.1 Cross-comparisons with other global wetland maps

To comprehensively understand the performance of the GWL_FCS30 wetland maps, four existing global wetland datasets (GLC_FCS30, GlobeLand30, CCI_LC, and GLWD), listed in Table 1, were selected. Figure 12 quantitatively illustrates the total wetland area of five products over each continent. ~~Notably, the total wetland area of four existing wetland datasets estimated from our study differed from previous studies because we excluded the water bodies when calculating the total wetland area. Specifically, the estimated total wetland area in this study was more reasonable because permanent water bodies with depths of more than six meters were not considered wetlands, according to the RAMSAR Convention.~~

Specifically, the total wetland area of different wetland products varied. The GLWD obviously overestimated the wetland area on each continent mainly because it was derived from the compilation model instead of actual remote sensing observations (Lehner and Döll, 2004). Namely, the GLWD classified a large amount of non-wetlands as potential wetlands. The remaining four wetland products, derived from the Landsat and PROBE-V remote sensing imagery, shared a ~~similar~~ total wetland area of ~~approximately 3.0~~4.128~7.364 million km^2, and our GWL_FCS30 wetland dataset had the ~~largest~~ total area of ~~3.574~~6.347 million km^2 among these datasets. The CCI LC wetland layer contained the smallest wetland area of ~~2.955~~4.128 million km^{2,} and the estimated area in North America was profoundly lower than the other datasets, mainly because the CCI LC heavily underestimated the wetland distribution in Canada after a comparison with the Canadian Wetland Inventory (Amani et al., 2019). Next, the total wetland area in GlobeLand30 and GLC_FCS30 wetland layer was ~~lower~~ higher than the developed GWL_FCS30 wetland dataset because some water-level sensitive non-wetlands (such as: irrigated cropland) were also ~~cannot be comprehensively~~ captured in these two datasets ~~(Figure 10)~~.

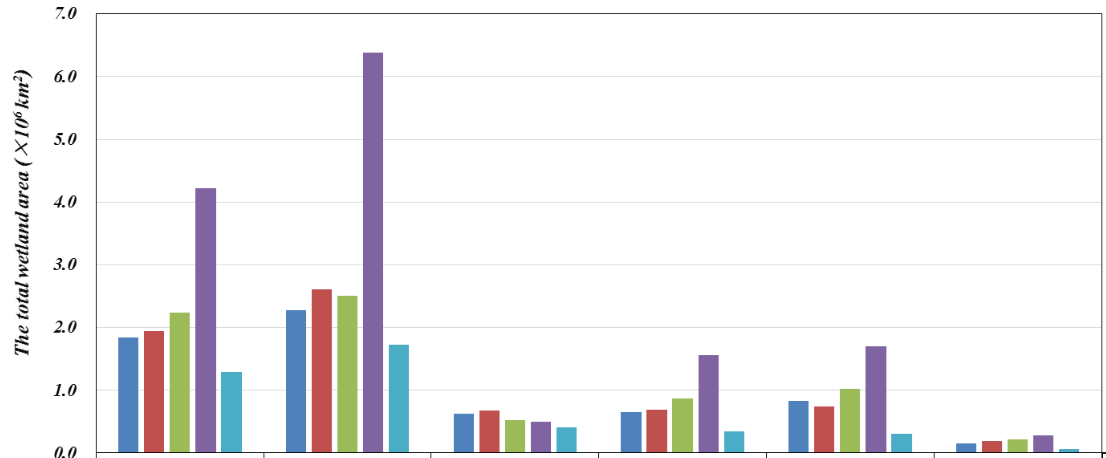

	Asia	North America	Europe	Africa	South America	Oceaina	Total
GWL_FCS30	1.843	2.282	0.624	0.646	0.833	0.159	6.387
GLC_FCS30	1.943	2.609	0.681	0.694	0.738	0.196	6.862
GlobeLand30	2.241	2.503	0.523	0.869	1.017	0.211	7.364
GLWD	4.219	6.376	0.500	1.558	1.706	0.282	14.642
CCI_LC	1.286	1.721	0.405	0.344	0.307	0.065	4.128

Figure ~~9~~12. The total wetland area (unit: million km^2) of five global wetland products on six continents.

Figure 13 illustrates the performances of five wetland products for two typical wetland regions (Poyang Lake in China and Pantanal wetland in Brazil). The reasons for choosing these two regions were that the wetlands in Poyang Lake quickly changed with water levels, and the Pantanal wetland was the largest wetland in the world. Intuitively, the GWL_FCS30 wetland maps had the greatest performance in capturing the spatial patterns of various wetland sub-categories. Comparatively, the GLC_FCS30 wetland layer suffered serious~~ly~~ underestimat~~ed the wetland area in both~~ion and misclassification problems in these two regions, which obviously ~~overestimated~~ misclassified many water-sensitive wetlands (swamp and marsh) as water bodies in Poyang Lake and also missed a large number of marsh and swamp wetlands in the Pantanal wetland. Zhang et al. (2021b) also stated that the wetland in the GLC_FCS30 suffered from low accuracy because of a lack of enough wetland samples and multi-sourced wetland sensitive features. Then, the GlobeLand30 wetland layer performed better in the Pantanal wetland than in Poyang Lake, which also obviously misclassified many ~~water-sensitive~~marsh wetlands as water bodies in the Poyang Lake mainly because the low water-level features were not captured during the development of the GlobeLand30 (Chen et al., 2015). In addition, the wetland layer of GlobeLand30 in Pantanal still suffered from the over-estimation problem, and some non-wetlands in Pantanal Wetland Park were mislabeled as wetland, so the wetland layer in the GlobeLand30 only achieved a user's accuracy of 74.87% (Chen et al., 2015). The CCI LC was highly consistent with the GWL_FCS30 wetland maps in spatial distribution when comparing with GLC_FCS30 and Globeland30, however,~~.~~ ~~Details~~ details show that the wetlands in the CCI LC were still underestimated in the Poyang Lake wetland and overestimated in the Pantanal wetland based on the highest and lowest water-level composites. Lastly, the GLWD dataset significantly overestimated the wetlands in two regions, namely, the mapped marsh area was obviously greater than its actual area and it also misclassified these water-sensitive wetlands as water bodies near Poyang Lake.

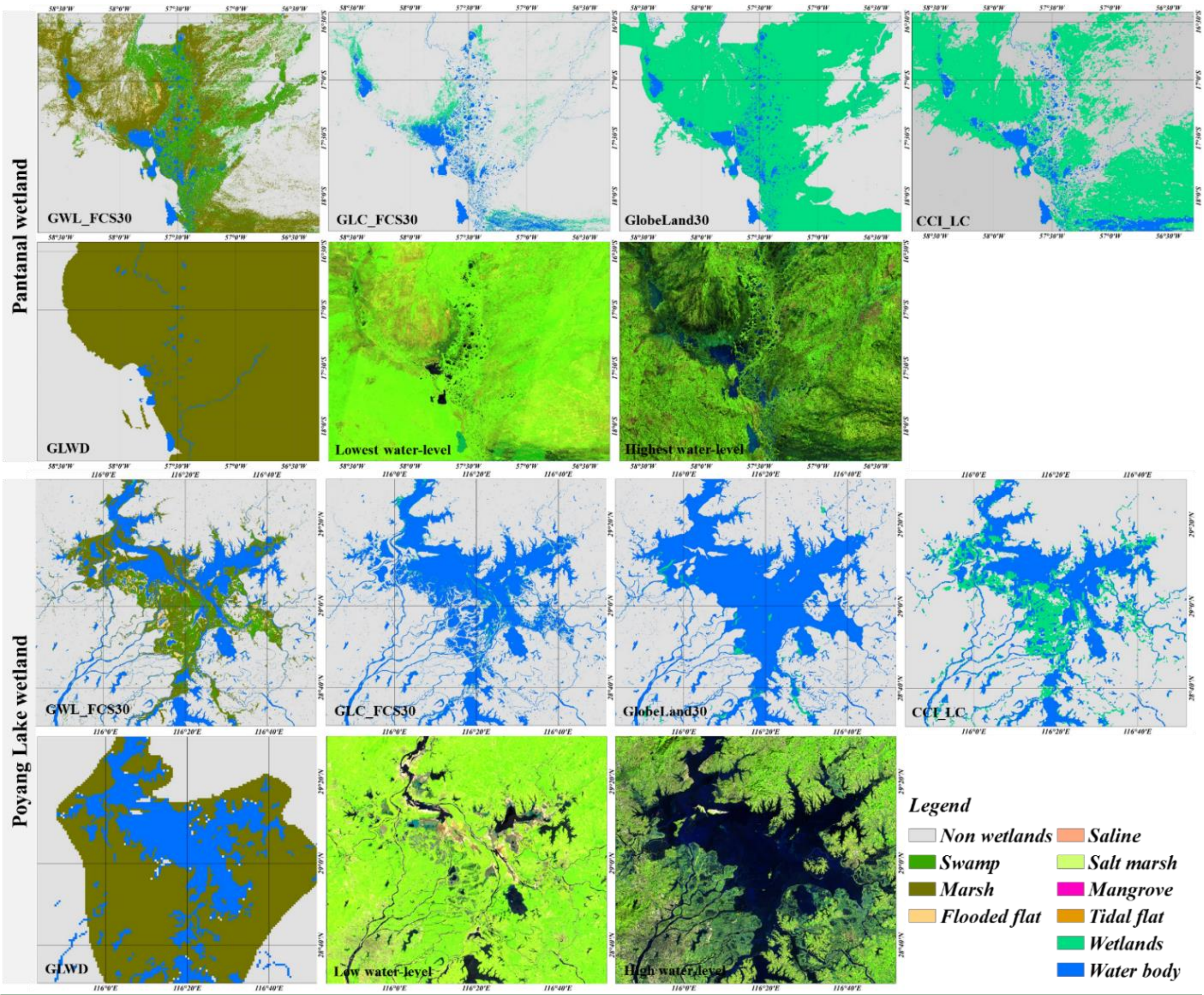

Figure ~~10~~13. The cross-comparisons between our GWL_FCS30 wetland maps with four existing wetland products: GLC_FCS30 generated by Zhang et al. (2021b), GlobeLand30 generated by Chen et al. (2015), CCI LC generated by Defourny et al. (2018) and GLWD generated by Lehner and Döll (2004) at Pantanal and Poyang Lake wetland. The false-color composited Landsat imagery (SWIR1, NIR, and Red bands) at the highest and lowest water levels were also illustrated.

Figure ~~11~~ 14 illustrates the comparisons between ~~our fine wetland~~the GWL_FCS30 map~~s~~ with three widely used global mangrove forest products (Atlas mangrove, GMW_V3 (Global Mangrove Watch Version3), and USGS Mangrove) listed in Table 1 in two typical mangrove regions (coastal Indonesia and Sundarbans). ~~Intuitively~~Overall, there was great consistency over four mangrove datasets because the mangrove forest reflected obvious and strong vegetation reflectance characteristics and was easier to identify than other wetland sub-categories. ~~Specifically~~Detailedly, the Atlas mangrove dataset suffers from the underestimation problem; namely, the mangrove area in the Atlas mangrove dataset was obviously lower than the other three products, especially in coastal Indonesia (~~black rectangles~~local enlargements). The USGS mangrove product can comprehensively and accurately capture the spatial distribution of mangroves over two regions. Still, it missed small and isolated fragments of mangrove forests in ~~the Sundarbans~~two regions (~~black~~ green rectangle) based on high-resolution imagery. The GMW_V3 dataset was validated to achieve an overall accuracy of 95.25%, with user and producer accuracies of mangrove forests of 97.5% and 94.0%, respectively (Bunting et al., 2018;

Thomas et al., 2017), which shows the greatest agreement with our ~~fine wetland maps~~GWL_FCS30 maps in this two regions and enlargements. ~~and confirms~~Using the high resolution imagery, it can be found that ~~this dataset~~GWL_FCS30 and GWM_V3 accurately identified the spatial patterns of mangrove forest in both regions.

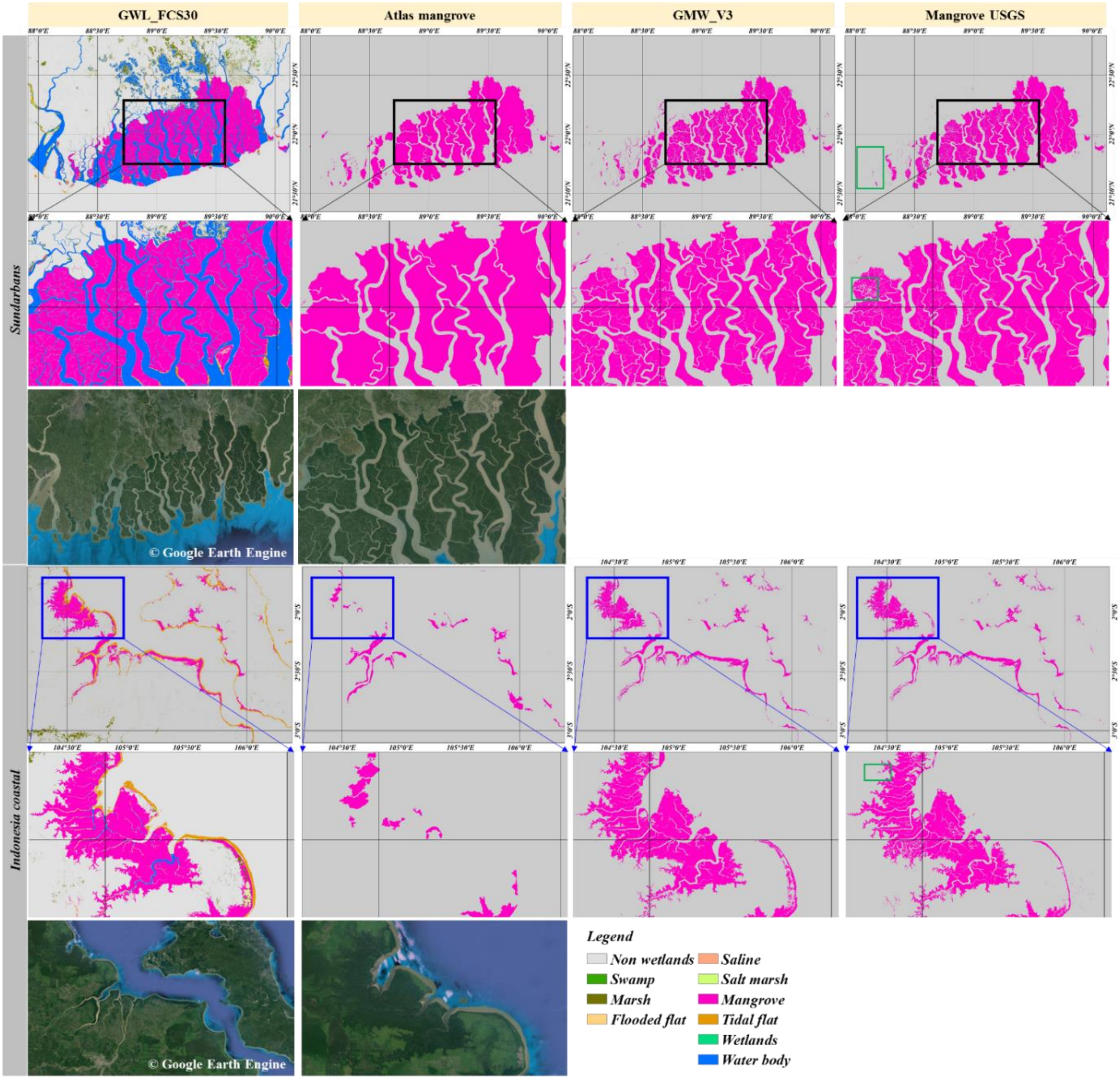

Figure ~~11~~14. The cross-comparisons between our GWL_FCS30 wetland maps with three mangrove products (Atlas mangrove developed by Spalding (2010), GMW_V3 ~~(Global mangrove watch)~~ developed by Bunting et al. (2022) and Mangrove USGS developed by Giri et al. (2011)) in Sundarbans and coastal Indonesia. The high-resolution imagery came from the Google Earth Engine platform (https://earthengine.google.com; last access: 16 May 2022).

Figure 15 illustrated the comparisons between GWLF_CS30 tidal flat layer with the Murray's tidal flat V1.1 in 2016 (Murray et al., 2019) and the updated Murray's tidal flat V1.2 in 2019 (Murray et al., 2022) in two local regions, and the corresponding highest and lowest tidal-level composites are also listed. Overall, three products can comprehensively capture the spatial patterns of tidal flats in these two regions, and the GWL_FCS30-2020 and Murray's tidal flat V1.2 performed higher spatial consistency while the Murray's tidal flat V1.1 suffered the obvious omission error in three typical areas (red rectangles). Detailedly, we can find that the Murray's tidal flat products misclassified some coastal ponds and lakes into the tidal flats especially in the first region while the GWL_FCS30-2020 achieved the best performance and accurately excluded these coastal ponds and lakes. In addition, the GWL_FCS30 also distinguished the salt marshes and tidal flats especially in the Yellow River estuary while the Murray's tidal flat V1.2 database misclassified a lot of salt marshes into the tidal flats.

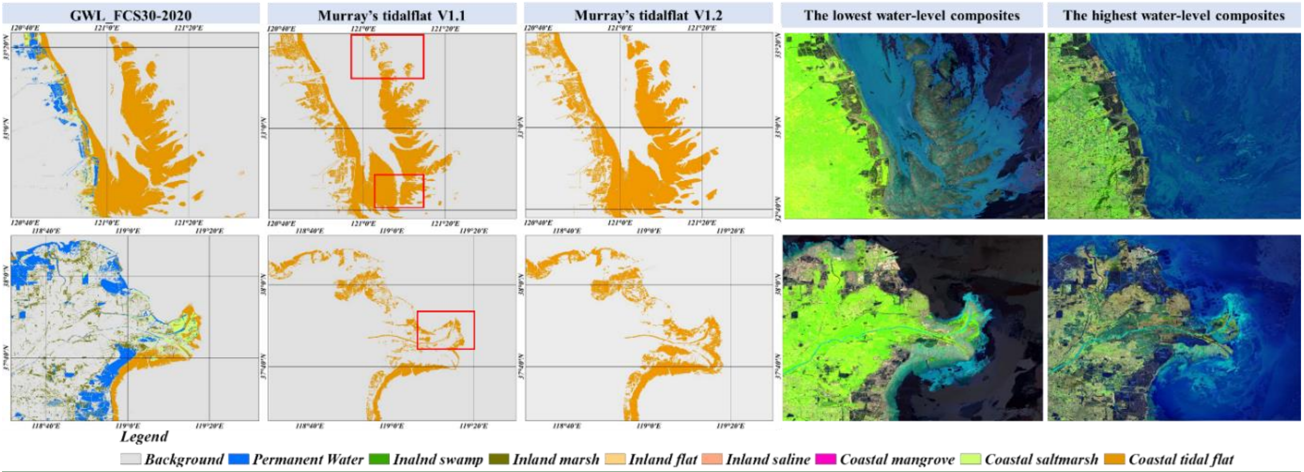

Figure ~~13~~15. The comparisons between the tidal flat of GWL_FCS30 in 2020, ~~and~~ Murray's tidal flat V1.1 in 2016 (Murray et al., 2019) , and Murray's tidal flat V1.2 in 2019 (Murray et al., 2022) for two local regions. In each case, the highest and lowest tidal-level composites, composited by SWIR1, NIR, and red bands, are illustrated.

6.2 Comparisons with the national wetland products

Using 1835 validation points (from the global validation points in Section 4.3) over the continuous United States, we quantitatively assessed the accuracy metrics of NLCD (National Land Cover Database) with GWL_FCS30 after merging the wetland subcategories into 4 classes in Table 6. Overall, the GWL_FCS30 achieved a higher performance than that of the NLCD mainly because a lot of herbaceous wetlands were misclassified into the open water in the NLCD, so the user's accuracy of herbaceous wetland and producer's accuracy of open water in NLCD was lower than that of GWL_FCS30. Then, as the NWI (National Wetlands Inventory) had different wetland system with the NLCD and GWL_FCS30, we also analyzed the metrics of NWI with GWL_FCS30 after merging into 5 classes. It can be found that the NWI shared similar performances with GWL_FCS30 on the non-wetlands and marine wetlands, but the user's accuracies of forest wetland and herbaceous wetland of NWI were lower than that of GWL_FCS30 mainly because some non-wetlands and open water were overestimated as the wetland in NWI. Similarly, Gage et al. (2020) also demonstrated that the NWI was easier to overestimate the wetland areas.

Table 6. The accuracy metrics of NLCD, NWI and GWL_FCS30 using 1835 validation points over the continuous United States

(a) NLCD vs GWL_FCS30

		NWT	Open water	Woody wetland	Emergent herbaceous wetland	O.A.	Kappa
NLCD	U.A.	96.46	93.98	77.92	61.97	83.58	0.756
	P.A.	88.80	53.65	85.96	87.61		
GWL_FCS30		NWT	PW FFT TFT	SWP MGV	MSH SMH	O.A.	Kappa

	U.A.	90.55	94.81	69.87		87.61	85.76	0.786
	P.A.	85.99	95.52	77.97		88.36		
(b) NWI vs GWL_FCS30								
NWI		NWT	FPD EMD RVR LKE	FSSW	FEW	EMW	O.A.	Kappa
	U.A.	94.45	94.74	67.58	60.25	85.71	83.49	0.762
	P.A.	84.93	63.32	86.62	82.76	91.53		
GWL_FCS30		NWT	PW	SWP	MSH TFT	MGV SMH TFT	O.A.	Kappa
	U.A.	90.55	94.74	68.96	80.75	90.08	85.23	0.789
	P.A.	85.99	95.45	76.76	78.78	94.98		

Note: NWT: non-wetlands, PW: permanent water, SWP: swamp, MSH: marsh, FFT: flooded flat, SMH: salt marsh, MGV: mangrove forest, TFT: tidal flat, FPD: Freshwater Pond, EMD: Estuarine and Marine Deepwater, RVR: Riverine, LKE: Lake, FSSW: Freshwater Forested/Shrub Wetland, FEW: Freshwater Emergent Wetland, EMW: Estuarine and Marine Wetland, O.A.: overall accuracy, P.A.: producer's accuracy, U.A.: user's accuracy.

Figure 16 illustrated the comparisons between our GWL_FCS30-2020, NLCD wetland layer and NWI in San Francisco and Florida. It should be noted that the ocean was excluded in the GWL_FCS30-2020 while NLCD and NWI still retained. Overall, three wetland products performed great spatial consistency and accurately captured the spatial patterns of wetlands over two regions. From the perspective of diversity of wetland sub-category, the GWL_FCS30 and NWI had obvious advantages over the NLCD which simply divided the wetlands into open water, woody wetlands and emergent herbaceous wetlands. Afterwards, the NWI had the largest wetland areas in the San Francisco because it included the irrigated cropland (red color) while the other two datasets excluded irrigated cropland. Then, the local enlargement showed that the GWL_FCS30 and NWI also had better performance than NLCD, because they comprehensively captured the coastal tidal wetlands, and our GWL_FCS30 further distinguished the tidal flats and salt marshes which also demonstrated that GWL_FCS30 performed better than NWI over the coastal tidal wetlands. In the Florida, the NWI and GWL_FCS30 accurately divided the inland and coastal tidal wetlands and the GWL_FCS30 further identified the coastal tidal wetlands into the mangrove forest. Meanwhile, the local enlargement also demonstrated the great consistency of three wetland products. However, it can be found that there was obvious difference between GWL_FCS30 and NWI over the wetland categories, in which GWL_FCS30 classified most inland wetlands into marshes while NWI classified them as emergent wetlands and forest/shrub wetlands, mainly because of the differences in the definition of the classification system (GWL_FCS30 defined those low shrubs that grown in the freshwater as marsh, in Table 1).

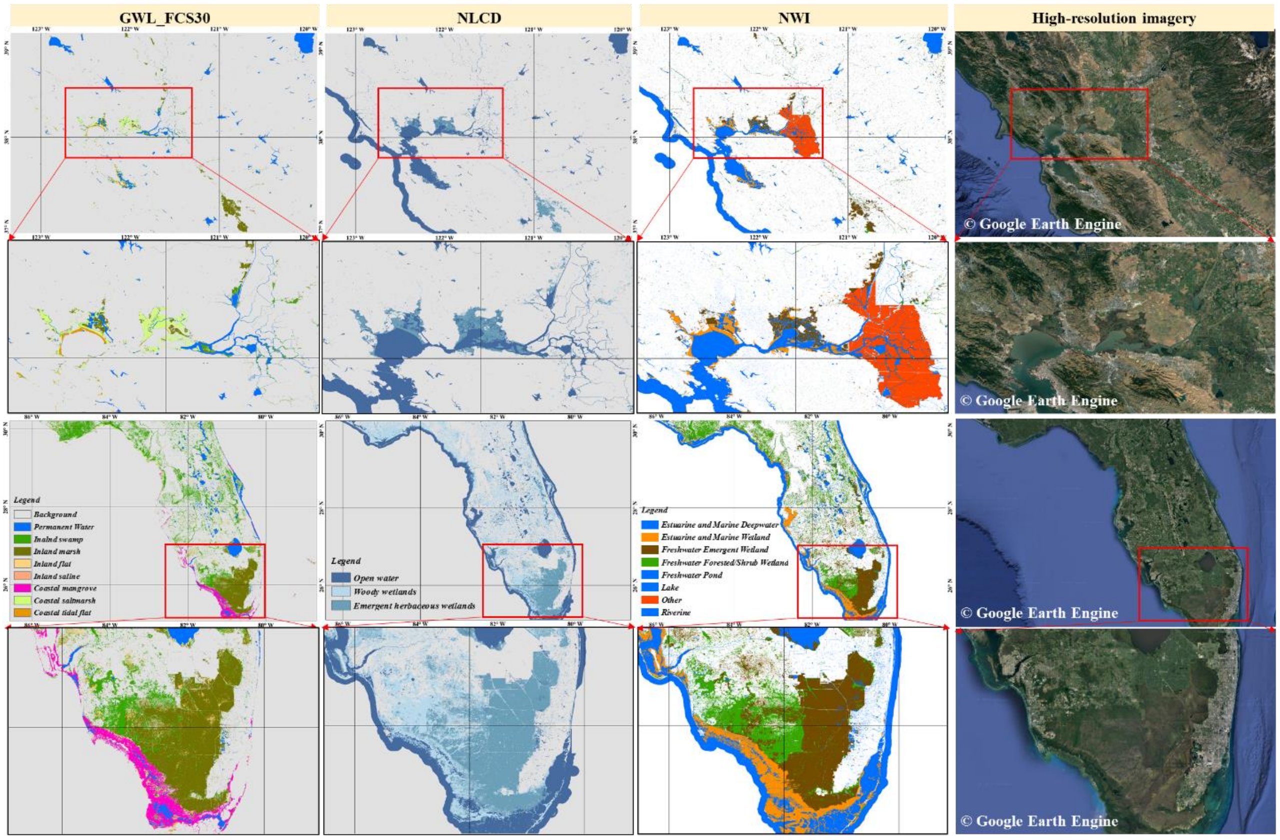

Figure 16. The comparisons between GWL_FCS30 in 2020, National Land Cover Database (NLCD) wetland Layer (Homer et al., 2020) and National Wetlands Inventory (NWI, https://www.fws.gov/program/national-wetlands-inventory, last access: Nov 12, 2022) in San Francisco and Florida. The high-resolution imagery came from the Google Earth Engine platform (https://earthengine.google.com; last access: 12 Nov 2022).

Table 7 illustrated the accuracy metrics of CLC (CORINE Land Cover) and GWL_FCS30 after merging the wetland categories over the European Union area using 1996 validation points from the global validation points in Section 4.3. Overall, the GWL_FCS30 performed better than the CLC and the former mainly had lower commission errors than that of the CLC for salt marsh and tidal flat. To intuitively understand the overestimation of tidal flat, Figure 17 illustrated the comparison between our GWL_FCS30-2020 and CLC wetland layer in 2018 over the Nordic, in which mainly distributed in tidal flats and open water, and these tidal flats gathered around the coastline. In term of specific wetland subcategory, it can be found that the CLC database had larger tidal flat area than that of the GWL_FCS30, however, the lowest tidal-level composite from time-series Landsat imagery indicated that the CLC overestimated the tidal flats in the region. For example, the local enlargement showed that a lot of permanent ocean pixels were wrongly labelled as the tidal flats in CLC and accurately identified as ocean in the GWL_FCS30. The comparison also demonstrated why the CLC had low user's accuracy of 62.90% for tidal flat and producer's accuracy of 57.76% for water bodies. Then, the local enlargement also indicated that the total area of salt marsh in CLC was lower than that of GWL_FCS30 (green rectangles), namely, some salt marshes were wrongly labelled as tidal flat and water body, so the accuracy metrics in Table 7 showed the user's accuracy of salt marsh in CLC was 35.86%.

Table 7. The accuracy metrics between CLC and GWL_FCS30 after merging the wetland categories

CLC	NWT	WC	WB	CL	ET	SO	Peat bogs & Inland marshes	SMH	TFT	O.A.	Kappa

		NWT	PW	SWP	MSH	FFT	SMH	TFT	O.A.	Kappa
	U.A.	92.94	94.81		68.63		35.86	62.90	80.75	0.706
	P.A.	82.80	57.76		83.93		91.23	75.00		
		NWT	PW	SWP	MSH	FFT	SMH	TFT	O.A.	Kappa
GWL_FCS30	U.A.	91.22	88.02		80.98		86.21	94.35	88.10	0.816
	P.A.	88.54	97.69		80.82		91.91	97.50		

Note: NWT: non-wetlands, WC: water courses, WB: water bodies, CL: coastal lagoons, ET: estuaries, SO: sea and ocean, PW: permanent water, SWP: swamp, MSH: marsh, FFT: flooded flat, SAL: saline, SMH: salt marsh, MGV: mangrove forest, TFT: tidal flat, O.A.: overall accuracy, P.A.: producer's accuracy, U.A.: user's accuracy.

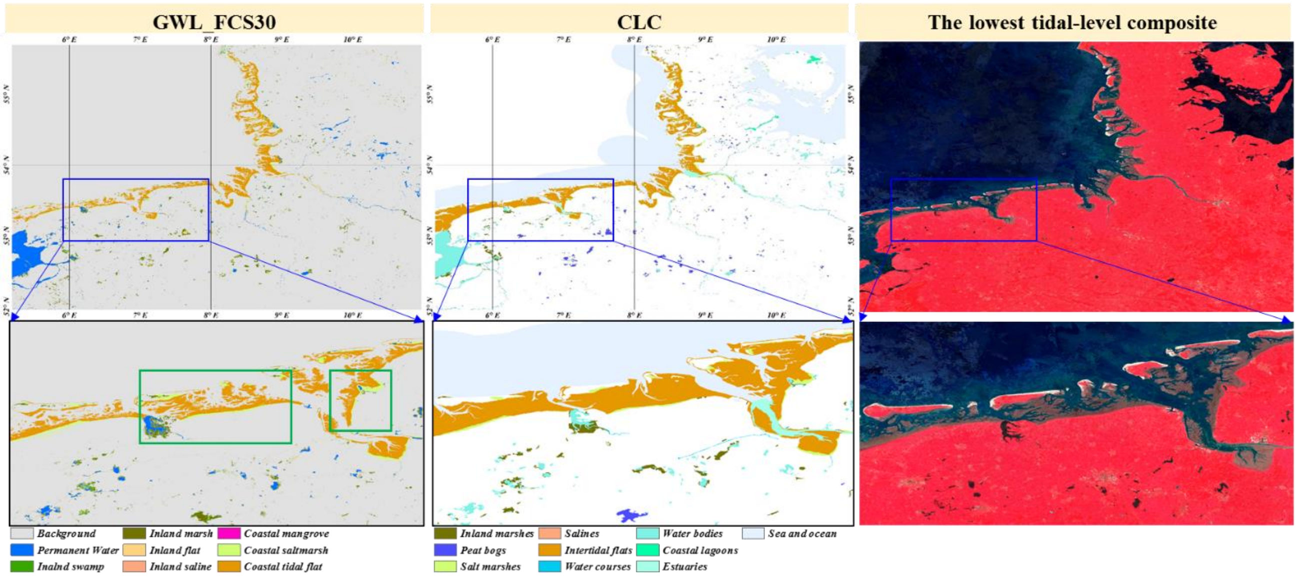

Figure 17. The comparisons between GWL_FCS30 and CORINE Land Cover (CLC) wetland layer in 2018 (https://land.copernicus.eu/pan-european/corine-land-cover/ clc2018?tab=metadata, last access: Nov 22, 2022). The lowest tidal-level Landsat composite, composited by NIR, red, and green bands, was illustrated.

~~6.2~~6.3 The limitations and prospects of our global fine wetland map

~~Using pre-existing global wetland products, multi-sourced and time-series remote sensing imagery, stratified classification strategy, and local adaptive classification methods, the first global 30-m fine wetland maps were produced with an overall accuracy of 85.5% and a kappa coefficient of 0.776. Meanwhile, the training sample reliability analysis and multi-sourced feature importance evaluation also demonstrated that the proposed method was suitable for large-area fine wetland mapping. However, i~~It should be noted there were still many uncertainties and limitations to the proposed method and global wetland maps. First, the proposed method used continuous Landsat reflectance and Sentinel-1 SAR imagery to capture various water-level information. Still, it might fail when the available Landsat observations were sparse and lacked the aid of Sentinel-1 SAR data, especially before 2000. Thus, our future work would focus on combining a richer multi-sourced data source, including MODIS, Sentinel-2, SPOT, and PALSAR imagery, to develop a more robust wetland mapping method. For example, Chen et al. (2018) integrated Landsat and MODIS observations to successfully monitor the wetland dynamics from 2000 to 2014 using a spatiotemporal adaptive fusion model. Then, in this study, we combined the multisourced wetland products and their practical use for ecosystem management to define a fine wetland classification system containing eight sub-categories, however, there are still many wetland sub-categories, such as: submergent vegetation (nymphaea), groundwater-dependent wetlands (karst and cave systems) and seagrass beds (Richardson et al., 2022), cannot be captured because remote sensing observations usually had poor performance on penetrating water body and then capturing underwater characteristics, and there was currently no prior dataset for global underwater wetlands. So, our further work would pay attention to combine multisourced auxiliary datasets, such as hydrological data, bathymetry depth and climate data, for targeted monitoring these special wetland sub-categories.

We ~~then~~ combined the pre-existing global wetland products to derive the training samples and maximum extents; however, the salt marsh and saline samples still used the visual interpretation method to ensure their reliability because of lacking sufficient pre-existing global products. Additionally, it was found that the producer's accuracy of salt marsh and saline in Table 4 was relatively poor compared with other sub-categories mainly because visual interpretation cannot provide massive and geographically distributed salt marsh and saline training samples. Namely, this study cannot comprehensively capture the regional adaptive reflectance characteristics of salt marsh and saline. Fortunately, many studies have built expert knowledge of these sub-categories over recent years. For example Mao et al. (2020) combined multi-scale segmentation, multiple normalized indices, and rule-based classification methods to develop a wetland map of China with an overall classification accuracy of 95.1%. Similarly, Wang et al. (2020) used the four widely used spectral indices to successfully identify three sub-categories within ~~coastal wetland~~coastal tidal wetlands. Thence, our further work would attach more effort on the spectral characteristics of salt marsh and saline wetlands and build expert knowledge of them for automatically deriving their training samples.

In addition, we used the derived maximum extents as the boundary for identifying inland and coastal tidal wetlands, in other words, we assumed that the derived maximum extents contained all inland and coastal tidal wetlands with zero omission error. Actually, the inland maximum extents in Eq. (3) fulfilled the assumption of zero omission error, because the GLWD and TROP-SUBTROP products, produced by the compilation and model simulation method (Gumbricht, 2015; Lehner and Döll, 2004), can capture most wetland areas at the expense of a higher commission error. For example, the Figure 13 illustrated the cross-comparisons between our GWL_FCS30 wetland maps with four existing wetland products, and the GLWD obviously overestimated the inland wetlands. On the other hand, the union of five global wetland datasets in Eq. (3) also minimized the omission error of each dataset for inland wetland sub-categories. Next, as for the maximum mangrove forest extents (Eq. (1)), as the high producer's and user's accuracies were achieved by five prior mangrove products (explained in Section 2.2) and the time-series mangrove products were integrated that these missed mangroves may be complemented by other products or time-series products, the derived maximum extents also can be considered as zero omission error and covered almost all mangrove forests. Recently, Bunting et al. (2022) developed the newest mangrove products covering 1996-2020, it can be used as another important prior dataset in our further works for deriving the maximum mangrove extents. Lastly, the maximum tidal flat extents, derived from time-series Murray's products from 1985~2016 by using the union operation (Eq. (2)), can also contain almost all tidal flats because previous studies demonstrated that they suffered higher commission error than the omission error (Jia et al., 2021; Zhang et al., 2022b).The missed tidal flats would concentrate on these newly increased tidal flats during 2016-2020, fortunately, the new time-series global tidal flat products during 1999-2019 was developed (Murray et al., 2022) and can be used as an important supplement in our further work for deriving the maximum tidal flat extent with zero omission error.

7. Data availability

The GWL_FCS30 wetland dataset in 2020 was freely available at https://doi.org/10.5281/zenodo.7340516~~https://doi.org/10.5281/zenodo.6575731~~ (Liu et al. 2022). It was composed of 961 5°×5° geographical grid tiled files, and each tiled file was stored using the geographical projection system with a spatial resolution of 30-meter in the GeoTIFF format. The fine wetland subcategory information was labeled as 0, 180, 181, 182, 183, 184, 185 186 and 187, representing the non-wetland, permanent water, swamp, marsh, flooded flat, saline, mangrove forest, salt marsh and tidal flat, respectively. The validation samples are available upon request.

8. Conclusions

Over the past few decades, many global and regional wetland products have been developed; however, an accurate global 30-m wetland dataset, with fine wetland categories and coverage of both inland and coastal zones, is still lacking. In this study, the time-series Landsat reflectance and Sentinel-1 SAR imagery, together with the stratified classification strategy and local adaptive random forest classification algorithm, were successfully integrated to produce the first global 30-m wetland product with a fine classification system in 2020. The wetlands were classified into four inland wetlands (swamp, marsh, flooded flat, and saline) and three ~~coastal wetland~~coastal tidal wetlands (mangrove, salt marsh, and tidal flat). The produced wetland dataset, GWL_FCS30, accurately captured the spatial patterns of seven wetland sub-categories with an overall accuracy of ~~87~~86.~~7~~44% and a kappa coefficient of 0.~~810~~ 822 for the fine wetland classification system with lower omission and commission errors compared to other global products. The quantitative statistical analysis showed that the global wetland area reached ~~3.57~~6.38 million km^2, including ~~3.10~~6.03 million km^2 of inland wetlands and 0.~~47~~ 35 million km^2 of ~~coastal wetland~~coastal tidal wetlands. Approximately ~~62.3~~72.96% of wetlands were distributed poleward of 40°N. Therefore, the proposed method is suitable for large-area fine wetland mapping, and the GWL_FCS30 dataset can serve as an accurate wetland map that could potentially provide vital support for wetland management.

Acknowledgements

This research has been supported by the Innovative Research Program of the International Research Center of Big Data for Sustainable Development Goals (Grant No. CBAS2022ORP03), the National Natural Science Foundation of China (grant no. 41825002) and National Earth System Science Data Sharing Infrastructure (grant no. 2005DKA32300).

References

Amani, M., Mahdavi, S., Afshar, M., Brisco, B., Huang, W., Mohammad Javad Mirzadeh, S., White, L., Banks, S., Montgomery, J., and Hopkinson, C.: Canadian Wetland Inventory using Google Earth Engine: The First Map and Preliminary Results, Remote Sensing, 11, 842, https://doi.org/10.3390/rs11070842, 2019.

Azzari, G. and Lobell, D. B.: Landsat-based classification in the cloud: An opportunity for a paradigm shift in land cover monitoring, Remote Sensing of Environment, 202, 64-74, https://doi.org/10.1016/j.rse.2017.05.025, 2017.

Büttner, G.: CORINE land cover and land cover change products. In: Land use and land cover mapping in Europe, Springer, 2014.

Belgiu, M. and Drăguţ, L.: Random forest in remote sensing: A review of applications and future directions, ISPRS Journal of Photogrammetry and Remote Sensing, 114, 24-31, https://doi.org/10.1016/j.isprsjprs.2016.01.011, 2016.

Breiman, L.: Random Forests, Machine Learning, 45, 5-32, https://doi.org/10.1023/a:1010933404324, 2001.

Brown, C. F., Brumby, S. P., Guzder-Williams, B., Birch, T., Hyde, S. B., Mazzariello, J., Czerwinski, W., Pasquarella, V. J., Haertel, R., Ilyushchenko, S., Schwehr, K., Weisse, M., Stolle, F., Hanson, C., Guinan, O., Moore, R., and Tait, A. M.: Dynamic World, Near real-time global 10 m land use land cover mapping, Scientific Data, 9, https://doi.org/10.1038/s41597-022-01307-4, 2022.

Bunting, P., Rosenqvist, A., Hilarides, L., Lucas, R. M., Thomas, N., Tadono, T., Worthington, T. A., Spalding, M., Murray, N. J., and Rebelo, L.-M.: Global Mangrove Extent Change 1996–2020: Global Mangrove Watch Version 3.0, Remote Sensing, 14, 3657, https://doi.org/10.3390/rs14153657, 2022.

Bunting, P., Rosenqvist, A., Lucas, R., Rebelo, L.-M., Hilarides, L., Thomas, N., Hardy, A., Itoh, T., Shimada, M., and Finlayson, C.: The Global Mangrove Watch—A New 2010 Global Baseline of Mangrove Extent, Remote Sensing, 10, 1669, https://doi.org/10.3390/rs10101669, 2018.

Bwangoy, J.-R. B., Hansen, M. C., Roy, D. P., Grandi, G. D., and Justice, C. O.: Wetland mapping in the Congo Basin using optical and radar remotely sensed data and derived topographical indices, Remote Sensing of Environment, 114, 73-86, https://doi.org/10.1016/j.rse.2009.08.004, 2010.

Cao, W., Zhou, Y., Li, R., and Li, X.: Mapping changes in coastlines and tidal flats in developing islands using the full time series of Landsat images, Remote Sensing of Environment, 239, 111665, https://doi.org/10.1016/j.rse.2020.111665, 2020.

Chen, B., Chen, L., Huang, B., Michishita, R., and Xu, B.: Dynamic monitoring of the Poyang Lake wetland by integrating Landsat and MODIS observations, ISPRS Journal of Photogrammetry and Remote Sensing, 139, 75-87, https://doi.org/10.1016/j.isprsjprs.2018.02.021, 2018.

Chen, G., Jin, R., Ye, Z., Li, Q., Gu, J., Luo, M., Luo, Y., Christakos, G., Morris, J., He, J., Li, D., Wang, H., Song, L., Wang, Q., and Wu, J.: Spatiotemporal Mapping of Salt Marshes in the Intertidal Zone of China during 1985–2019, Journal of Remote Sensing, 2022, 1-15, https://doi.org/10.34133/2022/9793626, 2022.

Chen, J., Chen, J., Liao, A., Cao, X., Chen, L., Chen, X., He, C., Han, G., Peng, S., Lu, M., Zhang, W., Tong, X., and Mills, J.: Global land cover mapping at 30m resolution: A POK-based operational approach, ISPRS Journal of Photogrammetry and Remote Sensing, 103, 7-27, https://doi.org/10.1016/j.isprsjprs.2014.09.002, 2015.

Davidson, N. C.: How much wetland has the world lost? Long-term and recent trends in global wetland area, Marine and Freshwater Research, 65, 934, https://doi.org/10.1071/mf14173, 2014.

Defourny, P., Kirches, G., Brockmann, C., Boettcher, M., Peters, M., Bontemps, S., Lamarche, C., Schlerf, M., and M., S.: Land Cover CCI: Product User Guide Version 2, available at: https://www.esa-landcover-cci.org/?q=webfm_send/84 (last access: 22 Nov 2022), 2018.

DeVries, B., Huang, C., Armston, J., Huang, W., Jones, J. W., and Lang, M. W.: Rapid and robust monitoring of flood events using Sentinel-1 and Landsat data on the Google Earth Engine, Remote Sensing of Environment, 240, 111664, https://doi.org/10.1016/j.rse.2020.111664, 2020.

Dixon, M. J. R., Loh, J., Davidson, N. C., Beltrame, C., Freeman, R., and Walpole, M.: Tracking global change in ecosystem area: The Wetland Extent Trends index, Biological Conservation, 193, 27-35, https://doi.org/10.1016/j.biocon.2015.10.023, 2016.

Gómez, C., White, J. C., and Wulder, M. A.: Optical remotely sensed time series data for land cover classification: A review, ISPRS Journal of Photogrammetry and Remote Sensing, 116, 55-72, https://doi.org/10.1016/j.isprsjprs.2016.03.008, 2016.

Gage, E., Cooper, D. J., and Lichvar, R.: Comparison of USACE three-factor wetland delineations to national wetland inventory maps, Wetlands, 40, 1097-1105, https://doi.org/10.1007/s13157-019-01234-y, 2020.

Gardner, R. C. and Davidson, N. C.: The ramsar convention. In: Wetlands, Springer, https://doi.org/10.1007/978-94-007-0551-7_11, 2011.

Giri, C., Ochieng, E., Tieszen, L. L., Zhu, Z., Singh, A., Loveland, T., Masek, J., and Duke, N.: Status and distribution of mangrove forests of the world using earth observation satellite data, Global Ecology and Biogeography, 20, 154-159, https://doi.org/10.1111/j.1466-8238.2010.00584.x, 2011.

Gislason, P. O., Benediktsson, J. A., and Sveinsson, J. R.: Random Forests for land cover classification, Pattern Recognition Letters, 27, 294-300, https://doi.org/10.1016/j.patrec.2005.08.011, 2006.

Gong, P., Liu, H., Zhang, M., Li, C., Wang, J., Huang, H., Clinton, N., Ji, L., Li, W., Bai, Y., Chen, B., Xu, B., Zhu, Z., Yuan, C., Ping Suen, H., Guo, J., Xu, N., Li, W., Zhao, Y., Yang, J., Yu, C., Wang, X., Fu, H., Yu, L., Dronova, I., Hui, F., Cheng, X., Shi, X., Xiao, F., Liu, Q., and Song, L.: Stable classification with limited sample: transferring a 30-m resolution sample set collected in 2015 to mapping 10-m resolution global land cover in 2017, Science Bulletin, 64, 370-373, https://doi.org/10.1016/j.scib.2019.03.002, 2019.

Gong, P., Wang, J., Yu, L., Zhao, Y., Zhao, Y., Liang, L., Niu, Z., Huang, X., Fu, H., Liu, S., Li, C., Li, X., Fu, W., Liu, C., Xu, Y., Wang, X., Cheng, Q., Hu, L., Yao, W., Zhang, H., Zhu, P., Zhao, Z., Zhang, H., Zheng, Y., Ji, L., Zhang, Y., Chen, H., Yan, A., Guo, J., Yu, L., Wang, L., Liu, X., Shi, T., Zhu, M., Chen, Y., Yang, G., Tang, P., Xu, B., Giri, C., Clinton, N., Zhu, Z., Chen, J., and Chen, J.: Finer resolution observation and monitoring of global land cover: first mapping results with Landsat TM and ETM+ data, International Journal of Remote Sensing, 34, 2607-2654, https://doi.org/10.1080/01431161.2012.748992, 2013.

Gumbricht, T.: Hybrid mapping of pantropical wetlands from optical satellite images, hydrology, and geomorphology, Remote sensing of wetlands, 2015. 435-454, https://doi.org/10.1201/b18210, 2015.

Gumbricht, T., Roman‐Cuesta, R. M., Verchot, L., Herold, M., Wittmann, F., Householder, E., Herold, N., and Murdiyarso, D.: An expert system model for mapping tropical wetlands and peatlands reveals South America as the largest contributor, Global change biology, 23, 3581-3599, https://doi.org/10.1111/gcb.13689, 2017.

Guo, M., Li, J., Sheng, C., Xu, J., and Wu, L.: A Review of Wetland Remote Sensing, Sensors, 17, https://doi.org/10.3390/s17040777, 2017.

Hamilton, S. E. and Casey, D.: Creation of a high spatio-temporal resolution global database of continuous mangrove forest cover for the 21st century (CGMFC-21), Global Ecology and Biogeography, 25, 729-738, https://doi.org/10.1111/geb.12449, 2016.

Hansen, M. C., Egorov, A., Potapov, P. V., Stehman, S. V., Tyukavina, A., Turubanova, S. A., Roy, D. P., Goetz, S. J., Loveland, T. R., Ju, J., Kommareddy, A., Kovalskyy, V., Forsyth, C., and Bents, T.: Monitoring conterminous United States (CONUS) land cover change with Web-Enabled Landsat Data (WELD), Remote Sensing of Environment, 140, 466-484, https://doi.org/10.1016/j.rse.2013.08.014, 2014.

Hansen, M. C., Potapov, P. V., Moore, R., Hancher, M., Turubanova, S. A., Tyukavina, A., Thau, D., Stehman, S. V., Goetz, S. J., Loveland, T. R., Kommareddy, A., Egorov, A., Chini, L., Justice, C. O., and Townshend, J. R.: High-resolution global maps of 21st-century forest cover change, Science, 342, 850-853, https://doi.org/10.1126/science.1244693, 2013.

Homer, C., Dewitz, J., Jin, S., Xian, G., Costello, C., Danielson, P., Gass, L., Funk, M., Wickham, J., Stehman, S., Auch, R., and Riitters, K.: Conterminous United States land cover change patterns 2001–2016 from the 2016 National Land Cover Database, ISPRS Journal of Photogrammetry and Remote Sensing, 162, 184-199, https://doi.org/10.1016/j.isprsjprs.2020.02.019, 2020.

Hu, S., Niu, Z., and Chen, Y.: Global Wetland Datasets: a Review, Wetlands, 37, 807-817, https://doi.org/10.1007/s13157-017-0927-z, 2017a.

Hu, S., Niu, Z., Chen, Y., Li, L., and Zhang, H.: Global wetlands: Potential distribution, wetland loss, and status, Sci Total Environ, 586, 319-327, https://doi.org/10.1016/j.scitotenv.2017.02.001, 2017b.

Huang, X., Li, J., Yang, J., Zhang, Z., Li, D., and Liu, X.: 30 m global impervious surface area dynamics and urban expansion pattern observed by Landsat satellites: From 1972 to 2019, Science China Earth Sciences, https://doi.org/10.1007/s11430-020-9797-9, 2021.

Jia, M., Mao, D., Wang, Z., Ren, C., Zhu, Q., Li, X., and Zhang, Y.: Tracking long-term floodplain wetland changes: A case study in the China side of the Amur River Basin, International Journal of Applied Earth Observation and Geoinformation, 92, 102185, https://doi.org/10.1016/j.jag.2020.102185, 2020.

Jia, M., Wang, Z., Mao, D., Ren, C., Wang, C., and Wang, Y.: Rapid, robust, and automated mapping of tidal flats in China using time series Sentinel-2 images and Google Earth Engine, Remote Sensing of Environment, 255, 112285, https://doi.org/10.1016/j.rse.2021.112285, 2021.

Jin, H., Stehman, S. V., and Mountrakis, G.: Assessing the impact of training sample selection on accuracy of an urban classification: a case study in Denver, Colorado, International Journal of Remote Sensing, 35, 2067-2081, https://doi.org/10.1080/01431161.2014.885152, 2014.

Khandelwal, A., Karpatne, A., Ravirathinam, P., Ghosh, R., Wei, Z., Dugan, H. A., Hanson, P. C., and Kumar, V.: ReaLSAT, a global dataset of reservoir and lake surface area variations, Scientific Data, 9, https://doi.org/10.1038/s41597-022-01449-5, 2022.

LaRocque, A., Phiri, C., Leblon, B., Pirotti, F., Connor, K., and Hanson, A.: Wetland Mapping with Landsat 8 OLI, Sentinel-1, ALOS-1 PALSAR, and LiDAR Data in Southern New Brunswick, Canada, Remote Sensing, 12, 2095, https://doi.org/10.3390/rs12132095, 2020.

Lehner, B. and Döll, P.: Development and validation of a global database of lakes, reservoirs and wetlands, Journal of hydrology, 296, 1-22, https://doi.org/10.1016/j.jhydrol.2004.03.028, 2004.

Li, Z., Chen, H., White, J. C., Wulder, M. A., and Hermosilla, T.: Discriminating treed and non-treed wetlands in boreal ecosystems using time series Sentinel-1 data, International Journal of Applied Earth Observation and Geoinformation, 85, 102007, https://doi.org/10.1016/j.jag.2019.102007, 2020.

Liu, L., Zhang, X., Gao, Y., Chen, X., Shuai, X., and Mi, J.: Finer-Resolution Mapping of Global Land Cover: Recent Developments, Consistency Analysis, and Prospects, Journal of Remote Sensing, 2021, 1-38, https://doi.org/10.34133/2021/5289697, 2021.

Lu, Y. and Wang, L.: How to automate timely large-scale mangrove mapping with remote sensing, Remote Sensing of Environment, 264, 112584, https://doi.org/10.1016/j.rse.2021.112584, 2021.

Ludwig, C., Walli, A., Schleicher, C., Weichselbaum, J., and Riffler, M.: A highly automated algorithm for wetland detection using multi-temporal optical satellite data, Remote Sensing of Environment, 224, 333-351, https://doi.org/10.1016/j.rse.2019.01.017, 2019.

Mahdianpari, M., Jafarzadeh, H., Granger, J. E., Mohammadimanesh, F., Brisco, B., Salehi, B., Homayouni, S., and Weng, Q.: A large-scale change monitoring of wetlands using time series Landsat imagery on Google Earth

Engine: a case study in Newfoundland, GIScience & Remote Sensing, 57, 1102-1124, https://doi.org/10.1080/15481603.2020.1846948, 2020.

Mahdianpari, M., Salehi, B., Mohammadimanesh, F., Homayouni, S., and Gill, E.: The First Wetland Inventory Map of Newfoundland at a Spatial Resolution of 10 m Using Sentinel-1 and Sentinel-2 Data on the Google Earth Engine Cloud Computing Platform, Remote Sensing, 11, 43, https://doi.org/10.3390/rs11010043, 2018.

Mao, D., Wang, Z., Du, B., Li, L., Tian, Y., Jia, M., Zeng, Y., Song, K., Jiang, M., and Wang, Y.: National wetland mapping in China: A new product resulting from object-based and hierarchical classification of Landsat 8 OLI images, ISPRS Journal of Photogrammetry and Remote Sensing, 164, 11-25, https://doi.org/10.1016/j.isprsjprs.2020.03.020, 2020.

Mao, D., Wang, Z., Wang, Y., Choi, C. Y., Jia, M., Jackson, M. V., and Fuller, R. A.: Remote Observations in China's Ramsar Sites: Wetland Dynamics, Anthropogenic Threats, and Implications for Sustainable Development Goals, Journal of Remote Sensing, 2021, 1-13, https://doi.org/10.34133/2021/9849343, 2021.

Matthews, E. and Fung, I.: Methane emission from natural wetlands: Global distribution, area, and environmental characteristics of sources, Global biogeochemical cycles, 1, 61-86, https://doi.org/10.1029/GB001i001p00061, 1987.

McCarthy, M. J., Radabaugh, K. R., Moyer, R. P., and Muller-Karger, F. E.: Enabling efficient, large-scale high-spatial resolution wetland mapping using satellites, Remote Sensing of Environment, 208, 189-201, https://doi.org/10.1016/j.rse.2018.02.021, 2018.

McOwen, C. J., Weatherdon, L. V., Bochove, J. V., Sullivan, E., Blyth, S., Zockler, C., Stanwell-Smith, D., Kingston, N., Martin, C. S., Spalding, M., and Fletcher, S.: A global map of saltmarshes, Biodivers Data J, https://doi.org/10.3897/BDJ.5.e11764, 2017.

Murray, N. J., Phinn, S. R., DeWitt, M., Ferrari, R., Johnston, R., Lyons, M. B., Clinton, N., Thau, D., and Fuller, R. A.: The global distribution and trajectory of tidal flats, Nature, 565, 222-225, https://doi.org/10.1038/s41586-018-0805-8, 2019.

Murray, N. J., Worthington, T. A., Bunting, P., Duce, S., Hagger, V., Lovelock, C. E., Lucas, R., Saunders, M. I., Sheaves, M., and Spalding, M.: High-resolution mapping of losses and gains of Earth's tidal wetlands, Science, 376, 744-749, https://doi.org/10.1126/science.abm9583, 2022.

Olofsson, P., Foody, G. M., Herold, M., Stehman, S. V., Woodcock, C. E., and Wulder, M. A.: Good practices for estimating area and assessing accuracy of land change, Remote Sensing of Environment, 148, 42-57, https://doi.org/10.1016/j.rse.2014.02.015, 2014.

Pekel, J. F., Cottam, A., Gorelick, N., and Belward, A. S.: High-resolution mapping of global surface water and its long-term changes, Nature, 540, 418-422, https://doi.org/10.1038/nature20584, 2016.

Radoux, J., Lamarche, C., Van Bogaert, E., Bontemps, S., Brockmann, C., and Defourny, P.: Automated Training Sample Extraction for Global Land Cover Mapping, Remote Sensing, 6, 3965-3987, https://doi.org/10.3390/rs6053965, 2014.

Richardson, D. C., Holgerson, M. A., Farragher, M. J., Hoffman, K. K., King, K. B. S., Alfonso, M. B., Andersen, M. R., Cheruveil, K. S., Coleman, K. A., Farruggia, M. J., Fernandez, R. L., Hondula, K. L., Lopez Moreira Mazacotte, G. A., Paul, K., Peierls, B. L., Rabaey, J. S., Sadro, S., Sanchez, M. L., Smyth, R. L., and Sweetman, J. N.: A functional definition to distinguish ponds from lakes and wetlands, Sci Rep, 12, 10472, https://doi.org/10.1038/s41598-022-14569-0, 2022.

Sexton, J., Feng, M., Channan, S., Song, X., Kim, D., Noojipady, P., Song, D., Huanga, C., Annand, A., and Collins, K.: Earth Science Data Records of Global Forest Cover and Change, User guide, 38, available at: https://lpdaac.usgs.gov/documents/1370/GFCC_ATBD.pdf (last access: 22 Nov 2022), 2016.

Sexton, J. O., Song, X.-P., Feng, M., Noojipady, P., Anand, A., Huang, C., Kim, D.-H., Collins, K. M., Channan, S., DiMiceli, C., and Townshend, J. R.: Global, 30-m resolution continuous fields of tree cover: Landsat-based rescaling of MODIS vegetation continuous fields with lidar-based estimates of error, International Journal of Digital Earth, 6, 427-448, https://doi.org/10.1080/17538947.2013.786146, 2013.

Slagter, B., Tsendbazar, N.-E., Vollrath, A., and Reiche, J.: Mapping wetland characteristics using temporally dense Sentinel-1 and Sentinel-2 data: A case study in the St. Lucia wetlands, South Africa, International Journal of Applied Earth Observation and Geoinformation, 86, 102009, https://doi.org/10.1016/j.jag.2019.102009, 2020.

Spalding, M.: World atlas of mangroves, Routledge, A collaborative project of ITTO, ISME, FAO, UNEP-WCMC, UNESCO-MAB, UNU-INWEH and TNC. London (UK): Earthscan, London, https://doi.org/10.34892/w2ew-m835, 2010.

Tachikawa, T., Hato, M., Kaku, M., and Iwasaki, A.: Characteristics of ASTER GDEM Version 2, Geoscience and Remote Sensing Symposium (IGARSS), 3657-3660, https://doi.org/10.1109/IGARSS.2011.6050017, 2011a.

Tachikawa, T., Kaku, M., Iwasaki, A., Gesch, D. B., Oimoen, M. J., Zhang, Z., Danielson, J., Krieger, T., Curtis, B., and Haase, J.: ASTER Global Digital Elevation Model Version 2 – Summary of validation results, Kim Fakultas Sastra Dan Budaya, https://doi.org/10.1093/oxfordjournals.pubmed.a024792, 2011b.

Thomas, N., Lucas, R., Bunting, P., Hardy, A., Rosenqvist, A., and Simard, M.: Distribution and drivers of global mangrove forest change, 1996–2010, PloS one, 12, https://doi.org/10.1371/journal.pone.0179302, 2017.

Tootchi, A., Jost, A., and Ducharne, A.: Multi-source global wetland maps combining surface water imagery and groundwater constraints, Earth Syst. Sci. Data, 11, 189-220, https://doi.org/10.5194/essd-11-189-2019, 2019.

Torres, R., Snoeij, P., Geudtner, D., Bibby, D., Davidson, M., Attema, E., Potin, P., Rommen, B., Floury, N., Brown, M., Traver, I. N., Deghaye, P., Duesmann, B., Rosich, B., Miranda, N., Bruno, C., L'Abbate, M., Croci, R., Pietropaolo, A., Huchler, M., and Rostan, F.: GMES Sentinel-1 mission, Remote Sensing of Environment, 120, 9-24, https://doi.org/10.1016/j.rse.2011.05.028, 2012.

Townshend, J. R., Masek, J. G., Huang, C., Vermote, E. F., Gao, F., Channan, S., Sexton, J. O., Feng, M., Narasimhan, R., Kim, D., Song, K., Song, D., Song, X.-P., Noojipady, P., Tan, B., Hansen, M. C., Li, M., and Wolfe, R. E.: Global characterization and monitoring of forest cover using Landsat data: opportunities and challenges, International Journal of Digital Earth, 5, 373-397, https://doi.org/10.1080/17538947.2012.713190, 2012.

Veci, L., Prats-Iraola, P., Scheiber, R., Collard, F., Fomferra, N., and Engdahl, M.: The sentinel-1 toolbox, available at: https://sentinels.copernicus.eu/web/sentinel/toolboxes/sentinel-1 (last access: 25 May 2022), 2014.

Vermote, E., Justice, C., Claverie, M., and Franch, B.: Preliminary analysis of the performance of the Landsat 8/OLI land surface reflectance product, Remote Sensing of Environment, 185, 46-56, https://doi.org/10.1016/j.rse.2016.04.008, 2016.

Wang, X., Xiao, X., Xu, X., Zou, Z., Chen, B., Qin, Y., Zhang, X., Dong, J., Liu, D., Pan, L., and Li, B.: Rebound in China's coastal wetlands following conservation and restoration, Nature Sustainability, https://doi.org/10.1038/s41893-021-00793-5, 2021.

Wang, X., Xiao, X., Zou, Z., Hou, L., Qin, Y., Dong, J., Doughty, R. B., Chen, B., Zhang, X., Chen, Y., Ma, J., Zhao, B., and Li, B.: Mapping coastal wetlands of China using time series Landsat images in 2018 and Google Earth Engine, ISPRS J Photogramm Remote Sens, 163, 312-326, https://doi.org/10.1016/j.isprsjprs.2020.03.014, 2020.

Wilen, B. O. and Bates, M.: The US fish and wildlife service's national wetlands inventory project. In: Classification and inventory of the world's wetlands, Springer, 1995.

Worthington, T. A., Zu Ermgassen, P. S., Friess, D. A., Krauss, K. W., Lovelock, C. E., Thorley, J., Tingey, R., Woodroffe, C. D., Bunting, P., and Cormier, N.: A global biophysical typology of mangroves and its relevance for ecosystem structure and deforestation, Scientific reports, 10, 1-11, https://doi.org/10.1038/s41598-020-71194-5, 2020.

Xi, Y., Peng, S., Ciais, P., and Chen, Y.: Future impacts of climate change on inland Ramsar wetlands, Nature Climate Change, 11, 45-51, https://doi.org/10.1038/s41558-020-00942-2, 2020.

Zanaga, D., Van De Kerchove, R., De Keersmaecker, W., Souverijns, N., Brockmann, C., Quast, R., Wevers, J., Grosu, A., Paccini, A., and Vergnaud, S.: ESA WorldCover 10 m 2020 v100, Zenodo: Geneve, Switzerland, https://doi.org/10.5281/zenodo.5571936, 2021.

Zhang, H., Wang, T., Liu, M., Jia, M., Lin, H., Chu, L. M., and Devlin, A.: Potential of Combining Optical and Dual Polarimetric SAR Data for Improving Mangrove Species Discrimination Using Rotation Forest, Remote Sensing, 10, 467, https://doi.org/10.3390/rs10030467, 2018.

Zhang, H. K. and Roy, D. P.: Using the 500 m MODIS land cover product to derive a consistent continental scale 30 m Landsat land cover classification, Remote Sensing of Environment, 197, 15-34, https://doi.org/10.1016/j.rse.2017.05.024, 2017.

Zhang, X., Liu, L., Chen, X., Gao, Y., and Jiang, M.: Automatically Monitoring Impervious Surfaces Using Spectral Generalization and Time Series Landsat Imagery from 1985 to 2020 in the Yangtze River Delta, Journal of Remote Sensing, 2021, 1-16, https://doi.org/10.34133/2021/9873816, 2021a.

Zhang, X., Liu, L., Chen, X., Gao, Y., Xie, S., and Mi, J.: GLC_FCS30: global land-cover product with fine classification system at 30 m using time-series Landsat imagery, Earth Syst. Sci. Data, 13, 2753-2776, https://doi.org/10.5194/essd-13-2753-2021, 2021b.

Zhang, X., Liu, L., Chen, X., Gao, Y., Xie, S., and Mi, J.: GLC_FCS30: global land-cover product with fine classification system at 30 m using time-series Landsat imagery, Earth Syst. Sci. Data, 13, 2753-2776, https://doi.org/10.5194/essd-13-2753-2021, 2021c.

Zhang, X., Liu, L., Wu, C., Chen, X., Gao, Y., Xie, S., and Zhang, B.: Development of a global 30 m impervious surface map using multisource and multitemporal remote sensing datasets with the Google Earth Engine platform, Earth Syst. Sci. Data, 12, 1625-1648, https://doi.org/10.5194/essd-12-1625-2020, 2020.

Zhang, X., Liu, L., Zhao, T., Gao, Y., Chen, X., and Mi, J.: GISD30: global 30 m impervious-surface dynamic dataset from 1985 to 2020 using time-series Landsat imagery on the Google Earth Engine platform, Earth Syst. Sci. Data, 14, 1831-1856, https://doi.org/10.5194/essd-14-1831-2022, 2022a.

Zhang, Z., Xu, N., Li, Y., and Li, Y.: Sub-continental-scale mapping of tidal wetland composition for East Asia: A novel algorithm integrating satellite tide-level and phenological features, Remote Sensing of Environment, 269, 112799, https://doi.org/10.1016/j.rse.2021.112799, 2022b.

Zhu, P. and Gong, P.: Suitability mapping of global wetland areas and validation with remotely sensed data, Science China Earth Sciences, 57, 2283-2292, https://doi.org/10.1007/s11430-014-4925-1, 2014.

Zhu, Z., Gallant, A. L., Woodcock, C. E., Pengra, B., Olofsson, P., Loveland, T. R., Jin, S., Dahal, D., Yang, L., and Auch, R. F.: Optimizing selection of training and auxiliary data for operational land cover classification for the LCMAP initiative, ISPRS Journal of Photogrammetry and Remote Sensing, 122, 206-221, https://doi.org/10.1016/j.isprsjprs.2016.11.004, 2016.

Zhu, Z., Wang, S. X., and Woodcock, C. E.: Improvement and expansion of the Fmask algorithm: cloud, cloud shadow, and snow detection for Landsats 4-7, 8, and Sentinel 2 images, Remote Sensing of Environment, 159, 269-277, https://doi.org/10.1016/j.rse.2014.12.014, 2015.

Zhu, Z. and Woodcock, C. E.: Object-based cloud and cloud shadow detection in Landsat imagery, Remote Sensing of Environment, 118, 83-94, https://doi.org/10.1016/j.rse.2011.10.028, 2012.